REPORT DOCUMENTATION PAGE

AD-A231 676 FILE COPY

1a. RESTRICTIVE MARKINGS

2

3. DISTRIBUTION / AVAILABILITY OF REPORT
Approved for public release; distribution unlimited

2b. DECLASSIFICATION / DOWNGRADING SCHEDULE

DTIC ELECTE FEB 04 1991 S E

4. PERFORMING ORGANIZATION REPORT NUMBER(S)
Technical ; Report #55

5. MONITORING ORGANIZATION REPORT NUMBER(S)

6a. NAME OF PERFORMING ORGANIZATION
Dept. of Chemistry
George Washington Univ.

6b. OFFICE SYMBOL (If applicable)

7a. NAME OF MONITORING ORGANIZATION
Office of Naval Research (Code 418)

6c. ADDRESS (City, State, and ZIP Code)
Washington, DC 20052

7b. ADDRESS (City, State, and ZIP Code)
Chemistry Program
800 N. Quincy Street
Arlington, VA 22217

8a. NAME OF FUNDING / SPONSORING ORGANIZATION
Office of Naval Research

8b. OFFICE SYMBOL (If applicable)

9. PROCUREMENT INSTRUMENT IDENTIFICATION NUMBER
Contract N00014-89-J-1103

8c. ADDRESS (City, State, and ZIP Code)
Chemistry Program
800 Nth, Quincy, Arlington, VA 22217

10. SOURCE OF FUNDING NUMBERS

PROGRAM ELEMENT NO.	PROJECT NO.	TASK NO.	WORK UNIT ACCESSION NO.
		R & T 4134043-01	

11. TITLE (Include Security Classification)
The Past, Present, and Future of Auger Lineshape Analysis (Unclassified)

12. PERSONAL AUTHOR(S) David E. Ramaker

13a. TYPE OF REPORT	13b. TIME COVERED	14. DATE OF REPORT (Year, Month, Day)	15. PAGE COUNT
Interim Technical	FROM ____ TO ____	January 1991	165

16. SUPPLEMENTARY NOTATION
Prepared for publication in Critical Reviews in Solid State and Materials Science

17. COSATI CODES		
FIELD	GROUP	SUB-GROUP

18. SUBJECT TERMS (Continue on reverse if necessary and identify by block number)
Auger Spectroscopy
Spectral Lineshapes
Charge Transform
Electron Screening

19. ABSTRACT (Continue on reverse if necessary and identify by block number)
This review critically evaluates the suitability of Auger spectral line shape analysis as a source of electronic structure information. Methods for extracting the true Auger line shape from the raw data and a theoretical framework for semiquantitative interpretation of that line shape are presented. A wide range of recent applications, concentrating on the line shapes of the low Z metals (Be, Li, Na, Mg, and Al), the line shapes of C and Si, the transition metals, and finally those of the metal oxides and halides, are considered. Spectra for gas phase molecules, adsorbed molecules, and solids are examined. Finally, new methods for controlling the background, the initial state, the spin polarization, and the angle of escape are discussed, along with requirements for improving the theory. Over 350 references are included.

91 2 04 094

20. DISTRIBUTION / AVAILABILITY OF ABSTRACT
☒ UNCLASSIFIED/UNLIMITED ☒ SAME AS RPT. ☐ DTIC USERS

21. ABSTRACT SECURITY CLASSIFICATION
Unclassified

22a. NAME OF RESPONSIBLE INDIVIDUAL
Dr. Mark Ross

22b. TELEPHONE (Include Area Code)
(202) 696-4409

22c. OFFICE SYMBOL

DD FORM 1473, 84 MAR

83 APR edition may be used until exhausted.
All other editions are obsolete.

SECURITY CLASSIFICATION OF THIS PAGE
Unclassified

OFFICE OF NAVAL RESEARCH

Contract N00014-89-J-1103

R & T Code 4134043-01

Technical Report No. 55

The Past, Present, And Future of Auger Lineshape Analysis

By

DAVID E. RAMAKER

Prepared for Publication

in

Critical Reviews in Solid State and Materials Science

George Washington University
Department of Chemistry
Washington, D.C.

January, 1991

OUTLINE

I. FOCUS AND SCOPE

II. THE PAST - PROVIDING THE FOUNDATION

- A. Extracting the Line Shape
  - 1. Removing the Background
    - a. Recording the Derivative Signal
    - b. Numerical Removal from N(E)
    - c. Experimental techniques
  - 2. Removing the Distortion due to Energy Loss
- B. Basic concepts
  - 1. The Basic Energy Expression
  - 2. The Nature of the DOS Sampled
  - 3. The Importance of Widths
  - 4. The Importance of Satellites
  - 5. The Importance of Correlation
- C. Theoretical Framework
  - 1. The Principal kvv Line Shape
  - 2. Atomic Auger Matrix Elements
  - 3. Correlation Effects - the Cini-Sawatzky Model
    - a. Localization in Elemental solids - Metals
    - b. Localization in Multi-element Covalent Systems

III. THE PRESENT - RECENT APPLICATIONS

- A. Metals and Alloys
  - 1. CCV Line Shapes
  - 2. CVV Line Shapes
- B. Silicon and Second Row Metals

C. Gas Phase Molecules

D. Molecular Adsorbates

E. Extended Covalent Solids

F. Metal Silicides and Carbides

G. Metal Chalcogenides and Halides

H. High Temperature Superconductors

IV. THE FUTURE - NEW DIRECTIONS

A. Controlling the Background and Inelastic Loss

B. Controlling the Initial State

1. The APECS Technique

2. The DES Technique

C. Controlling the Spin Polarization

D. Controlling the Angle of Escape

E. Extending the Theory

1. Atomic Auger Matrix Elements

2. Vibrational Widths

3. Satellites

4. Correlation: Application of the Cini expression

a. Materials with unfilled bands

b. Materials with degenerate bands

c. Molecules

F. Expanding the Applications

Acknowledgements

References

I. FOCUS AND SCOPE

Auger electron spectroscopy (AES) has been utilized as a technique for elemental identification and trace analysis at the surface of solids for many years.[1] Indeed, AES has become a widely available and almost indispensable technique for determining surface cleanliness, surface coverage, and sputter depth profiles. AES has also been recognized as a source of chemical information. Usually this is in the form of spectral "finger prints" to identify the chemical nature of various atoms. This has become so common that many surface chemists can recognize on sight the C KVV derivative Auger spectra (i.e. $dN(E)/dE$, where $N(E)$ is the Auger intensity at electron kinetic energy, E) for graphite, metal carbides or diamond,[2,3] or the Si $L_{23}VV$ Auger spectra for Si, SiO_x, or metal silicides.[4] Another source of chemical information is from the Auger chemical shifts.[5,6,7,8,9,10,11,12]

AES has however the potential to provide much more information, namely, detailed electronic structure information, such as orbital hybridization, electron delocalization and correlation, screening effects, charge transfer, bonding, and covalency. Such information can be obtained from a thorough understanding of the factors contributing to the Auger spectral line shape, and a quantitative interpretation of the line shape. AES has not realized its full potential because these are formidable tasks, but significant progress has been made in recent years.

Our focus is to critically evaluate the suitability of Auger spectral line shape analysis as a source of electronic structure information. This significantly narrows the scope of this review. The nature of this article is not to review the extensive literature on Auger spectroscopy. That is a task much too big to do adequately here. Three whole books on Auger spectroscopy have recently appeared which trace the development of AES and summarize the proceedings of

a recent international conference on AES.[13,14,15] A number of review articles on AES have also appeared over the last 10 years, making a literature review unnecessary and unwise.[16,17,18,19,20,21,22,23,24,25,26,27,28,29,30,31] Further, we do not intend to examine more qualitative techniques for gaining chemical information, such as Auger chemical shifts or fingerprinting, nor do we examine the area known as "quantitative" AES, which deals with the absolute intensity of the Auger signal and provides for elemental analysis of surfaces.[32,33,34] Thus we are concerned primarily with spectral line shape or profile in the N(E) mode, not the absolute intensity, nor even the absolute energy, although the latter is often considered as part of the line shape.

I am writing this review with two aims in mind. First, it is written for the novice or beginner who wants a quick primer in Auger spectroscopy. Thus it is written from an intuitive point of view. The number of equations is kept to a minimum. Second, in this review I hope to survey the recent work, say within the last 10 years, and offer suggestions where Auger line shape analysis is headed in the future, both experimentally and theoretically.

In the section on the "Past", the foundations of Auger line shape analysis are described. To obtain chemical or electronic structure information from AES requires two major efforts; first one must extract a true Auger line shape, $A_t(E)$ (in the N(E) mode rather than in the dN(E)/dE mode), from the raw Auger spectrum, and second, one must derive a theoretical framework for semi-quantitative interpretation of that line shape. We summarize current methods for extracting the line shape, examine basic concepts for understanding the line shape, and summarize a theoretical framework for extracting electronic structure from the line shape.

In the section describing the "Present", we review a wide range of recent applications, each with a view toward understanding and appreciating phenomena

important for interpreting the line shape in that system. The line shapes most heavily studied over the years include those of the low Z metals (e.g. Be, Li, Na, Mg, and Al), those of C and Si, and of various other metals and their oxides and halides. We shall emphasize these elements. We examine spectra for gas phase molecules, adsorbed molecules, and solids (metals, semiconductors, and insulators).

In the section on the "Future", we examine new directions, and attempt to encourage work in areas which I feel have promise for providing interesting and enlightening new results.

II. THE PAST - PROVIDING THE FOUNDATION

A. Extracting the Line Shape

The difficulty with obtaining a quantitative Auger line shape is well known, particularly with electron beam excitation.[35] It exists because the relatively small Auger signal sits on top of a large background, consisting of the backscattered (redistributed primaries) and secondary electrons arising from the electron beam which initiated the Auger decay. In addition, the Auger signal itself is distorted due to the inelastic losses which the Auger electrons suffer on their way out of the solid.

1. Removing the background

Several techniques exists for removing the large background. These can be itemized as follows.

a. Recording the Derivative Signal

The most common technique in practice, especially in the early years of using AES for surface analysis, is to record the derivative, $dN(E)/dE \equiv N'(E)$, spectrum. Since the background is normally slowly varying with energy relative to the Auger signal, N'(E) suppresses the background and emphasizes the Auger signal. Although N'(E) is very useful for spectral "finger printing" as discussed

above, a quantitative removal of the background from N'(E) is difficult. It is generally more problematic to quantitatively remove the background from N'(E) than from N(E).[Ramext]

b. Numerical Removal from N(E)

The most helpful technique for removal of the background from N(E) is to utilize some analytical expression to approximate the background function, and numerically remove the background by fitting this expression to the upper and lower energy wings of the Auger signal.[Ramext] At energies above 200 eV, often a simple linear background is sufficient. Below 200 eV, the Sickafus function, $A*(E+\varphi)^{-m}$ has been found to be a reasonably good approximation to the secondary spectral distribution, where φ is the work function of the sample material.[36] Recently, some theoretical justification for this power law behavior has been obtained.[37] The coefficient, A, appears to be related to the number density of valence band electrons. The exponent, m, is seen to depend upon the balance between the elastic scattering strength and the energy dependence of the inelastic mean free path. The exponent m is found to be around 0.8 - 1.0 for a large number of metallic elements, with only a slight dependence on Auger peak energy.[38] Ramaker et al. have previously used a variation of the Sickafus function for the secondaries, and a Bethe function for the redistributed primaries.[Ramext]

Figure 1 illustrates the extraction of the S $L_{23}VV$ line shape from a powdered sample of Li_2SO_4 pressed onto an In substrate. This case truly tests the capability to extract the line shape because the Auger electrons around 100-150 eV lie in the region where the redistributed primary and secondary electrons contribute about equally to the background. To account for this, the analytical expression

$$B(E) = A\,E/[(E+E_0)(E+\varphi)^m] + B\,\ln(E_{th})/E_{th}^{\,n} + C. \qquad (1)$$

was utilized where $E_{th} = (E_p\text{-}E)/E_p$. The terms primary and secondary refer to the source of the electron (i.e. primaries originate from the initial excitation beam, secondaries originate from the solid). Of course the indistinguishability of the electrons precludes this distinction; nevertheless, this terminology is often used in the literature.

The first term in eq. 1, the secondary contribution, is essentially the Sickafus expression $(E+\varphi)^{-m}$ multiplied by an escape factor $E/(E+E_0)$, where φ and E_0 are the work function and the escape probability parameter respectively (here $E_0 \approx 0.35$). In the second term, the redistributed primary function, E_p and E_b are the primary electron beam energy and the binding energy of the largest loss contribution just above the Auger energy. The exponents m and n are nonlinear parameters found to range experimentally from 1.5-3.0 and 0.8-1.5 respectively (their theoretical values are 1.5-2 and 2 respectively[Ramext]). The linear coefficients A, B, C are obtained from a least squares fit of eq. 1 to the high energy wing of the N(E) spectrum and some estimate of the low energy wing as pictured in Fig. 1a. The actual low energy wing can not be used since as Fig. 1b shows, the distorted (experimental) Auger line shape tails off slowly to lower energy.

c. Experimental Techniques

Conventional electron-excited AES not only creates a large background of backscattered and secondary electrons, the intense primary beam can cause sample damage, sample charging problems in insulators, and desorption of adsorbed layers. X-ray induced AES (XAES) has become far more popular in recent years, because it utilizes much lower beam fluxes reducing sample charging and damage, and the magnitude of the background signal.[fuggle]

Two new experimental approaches almost completely eliminate the

background. In one method, low energy positrons are used to remove core electrons by matter-antimatter annihilation, which then allows the core excitation to relax via the Auger process.[39] Positron induced AES (PAES) essentially removes all problems with background removal, since the low energy (< 10 eV) positrons do not produce any secondary electrons above 10 eV. The second method, the technique of Auger photoelectron coincidence spectroscopy (APECS) utilizes the simultaneous detection of a core photoelectron and an associated Auger electron to eliminate the background. The background is eliminated because only those electrons originating from the same excitation event are counted in the spectrum. Although originally proposed over 10 years ago by Haak et al. [40], the increasing availability of synchrotron sources makes this technique much more feasible today.[41,42] Since the latter two techniques will be more important in the future, these two techniques will be discussed further in the section on new directions, Sec. IV.B.

2. Removal of Distortion due to Energy Loss

Removal of the distortion effects due to electron energy loss of the Auger electrons as they escape from the solid is accomplished by deconvolution with a backscattered spectrum, L(E), with primary energy at or near the principal Auger energy as shown in Fig. 1b.[43] Mathematically this can be written

$$A(E) = \int A_t(\epsilon)L(E-\epsilon)d\epsilon, \qquad (2)$$

where A and A_t are the "experimental" and "true" Auger line shapes. In practice $A_t(E)$ is obtained by an iterative deconvolution procedure due to Van Cittert[44], modifications of this approach.[45] or by some filtered Fourier transform approach[46,47]. The deconvolution also removes experimental resolution effects of the analyzer since the elastic peak of L(E) has been broadened by this same amount. The relative intensities of the loss and elastic contributions to L(E) must be weighted differently to account for the different geometrical relationships of

the Auger and backscattered electrons; i.e. the internally created Auger electrons traverse the solid escape region once, the backscattered electrons twice. In practice this is accomplished Madden by weighting the loss contributions such that A(E) has zero intensity at the low energy wing of the spectrum as shown in Fig. 1c. Several papers on background and inelastic loss removal have been published recently.contini,48,49,50,51

The extraction of the Auger line shape from the experimental data is unfortunately not a straightforward and simple procedure. Often greater differences exist between A(E) obtained by different authors, than existed between the original N'(E) or N(E) data, indicating that different choices for the background or deconvolution procedure introduce the wide variations, rather than the recording of the experimental data or preparation of the sample.Ramext Fig. 1c shows two final results obtained from two different background estimates and gives some estimate of the uncertainties involved. We cannot overemphasize the importance of recording the Auger spectrum over a sufficiently wide energy range and then forcing the low energy wing of A(E) to be zero and flat over a 20 to 50 eV energy range, such as in Fig. 1c. Although this is not always trivial to accomplish, it can be obtained by taking several iterations on the background estimate. This is the only way of assuring that one is obtaining a reasonable result for A(E).Ramext

B. Basic Concepts

1. <u>The Basic Energy Expression</u>

Before providing a general theoretical framework for quantitatively interpreting Auger line shapes, we discuss some basic concepts.

The Auger electron has a kinetic energy, $E_{kvv'}$, equal to the difference between the initial core hole state, E_c, and the final two-hole state, $E_v + E_{v'} + U_{vv'}$, thus.[52]

$$E_{kvv} = E_c - E_v - E_{v'} - U_{vv'}. \quad (3)$$

In eq. 3, the E's are the corresponding binding energies relative to the Fermi or vacuum level. [It makes no difference as long as all binding energies and the kinetic energy is defined relative to the same reference. Often E_{kvv} is measured relative to the vacuum level of the spectrometer and the E's relative to the Fermi level, in which case the work function of the spectrometer, $\varphi \approx 5$ eV, must be subtracted from the right hand side of eq. 3. Unfortunately, in the literature it is often not made clear what the reference is for E_{kvv}.] U_{vv} is the hole-hole repulsion energy between the final-state holes. U_{vv} can also be referred to as the difference between the first and second ionization potentials.

2. The Nature of the DOS Sampled

A basic concept in AES concerns the nature of the density of states (DOS) reflected in the line shape and the localization of the final state holes. Fig. 2 helps illustrate some of these concepts for several gas phase hydrocarbons.[53] The sensitivity of AES to local hybridization (sp^3, sp^2, sp) is clearly demonstrated by the CH_4, C_2H_4, and C_2H_2 line shapes. Recently a very simple 4-level model was used to qualitatively show that the changes reflect the different energy splitting of the 2p orbitals (i.e. the 2p orbitals split into 1, 3, or 2 different 2p energy levels, respectively) under the different local symmetries or hybridizations.[54] The insensitivity to substituent effects is demonstrated by the CH_4, CH_3OH, and $(CH_3)_2O$ (all sp^3) line shapes. The normal alkanes show a broadened sp^3 line shape. The cyclic alkanes show a progression from the sp^2 to the sp^3 line shape as the bond angle strain decreases. These trends indicate that AES samples a site specific DOS, i.e. the DOS specific to that atom with the initial core hole.

Fig. 2 also shows that the principal peak energy for the alkanes is unchanged in spite of the increasing size of the molecules. This suggests that the final-state holes are not completely delocalized about the molecule in these systems, otherwise U_{VV} should decrease as the molecule size increases and increase the kinetic energy.[Ryealk] However, if the holes were completely localized on the methyl group having the initial core hole, we would expect the line shapes to be essentially the same for all alkanes, which clearly is not the case either (e.g. the CH_4 and C_3H_8 line shapes are very different in Fig. 2). The holes are apparently delocalized over just a few methyl groups, hence the similarity in the C_nH_{2n+2} line shapes for $n \geq 3$ (see Sec. III.C below).

A self-fold of the appropriate one-electron density of states (DOS), $\rho(E)$,

$$\rho * \rho(E) = \int \rho(E-\epsilon)\rho(\epsilon)\, d\epsilon, \qquad (4)$$

is known to represent a first approximation to the line shape.[55] Hence, almost all line shape analyses start with a determination of the one-electron DOS. Very often an empirical procedure is used to obtain the DOS. Photoelectron spectroscopy (x-ray or ultraviolet, XPS or UPS) is often used independently. Others use a combination of x-ray emission (XES) and XPS, along with theoretical calculations.[56] Fig. 3 illustrates a procedure for obtaining the DOS for cyclohexane. The dipole selection rule in the K_α x-ray emission process means that the XES spectrum[57] reflects the p DOS. The Final State Rule (to be discussed later) also indicates that XES reflects the DOS in the final state (i.e. in the absence of the core hole) and not those of the initial state (i.e., in the presence of a core hole).[58] The Mg K_α XPS spectrum[59] in Fig. 3 reflects primarily the s DOS with a small component of the p DOS (actually s + {1/14}p).[60] This small p component can easily be removed from the XPS spectrum to obtain the s DOS. The XES and XPS spectra are normalized to give the well-known sp^3 electron configuration for all alkanes.

Many of the molecular orbitals (MO's) in the alkanes have primarily either carbon-carbon (C-C) or carbon-hydrogen (C-H) bonding character.[61] In the Auger spectrum, it has been shown previously [62] that final states involving these different MO's have different hole-hole repulsions. Therefore, the p DOS must be separated into the p_{CC} and p_{CH} components. This can be accomplished by identifying each MO as having either C-C and C-H character upon examining the orbital structure as reported by Jorgensen and Salem.[Salem] Four such structures are shown in Fig. 3a, showing for example that the $2a_{1g}$ MO has primarily s character, the $2e_g$ has some s and p_{CH} character, and the $3e_g$ and $1a_{2g}$ MO's have p_{CH} and p_{CC} characters, respectively. Using the appropriate identification for each MO, the relative intensities obtained from a GAUSSIAN 82 calculation[63] shown in Fig. 3, and the widths from the semi-empirical DOS, the s, p_{CC}, and p_{CH} components can be obtained.

3. The Importance of Widths

Several arguments can be given for utilizing semi-empirically derived DOS, even for simple molecules.[Ramhydc] First, most one-electron theoretical calculations do not include electron correlation effects and therefore do not give sufficiently accurate binding energies. Second, the semi-empirical DOS include approximate widths for each orbital feature. Assuming the XES and XPS spectra utilized to obtain the DOS were measured at sufficiently high resolution, these widths primarily reflect broadening due to the vibrational state manifold of the final state which project onto the core initial state in XES, or the ground state in PES. The DOS self-fold, $\rho * \rho(E)$, then has twice the vibrational broadening consistent with the Auger two-hole final state.

Fig. 4 illustrates why the vibrational widths in the Auger profile are expected to be larger than for photoemission.[64] Since the equilibrium bond length shift, $|Q_2\text{-}O|$, is expected to be larger than $|Q_1\text{-}O|$, as shown in Fig.

4, the energy widths are expected to be larger because of the steeper two-hole potential curve near the Franck-Condon region. However, Matthew has determined that if the core lifetime is much less than a vibrational period, and if the electron-phonon coupling and linear dielectric response are linear, then the widths for photoemission and Auger processes are comparable for the case of localized holes in ionic crystals.[Matthew] On the other hand, for rare gases physisorbed on metal surfaces, the Auger width (FWHM) will be about 3 times greater than the PES width. Other accurate calculations for the O_2 molecule indicate that the Auger width is about a factor of 2 greater than the PES width (i.e. that a PES self-fold is a reasonable approximation to the Auger widths).[65] Thus the self-fold of PES or XES data may not accurately reproduce the Auger widths, but it appears to be a good first approximation to them, at least for molecules when vibrational broadening dominates.

Cini and Andrea have determined that in highly electron correlated solids, the broadening is dominated by two-hole resonant hopping, and that phonon broadening is very small in this case.[66] In general it appears that core-hole lifetime broadening is not important. However, there are special cases where the core lifetime can be so short that not only does it introduce broadening consistent with the Heisenberg uncertainty principle, but severe distortions to the line shape. In these rare cases the Auger process cannot be considered as an isolated event occurring after the core-hole excitation, but must be considered in tandem with the initial excitation.[67] These effects often appear as plasma gain satellites resulting from incomplete relaxation of the core-hole prior to the Auger decay.[68,69] If the coupling between the plasmon field and the valence atomic orbital is large compared to the level width, severe distortions may also occur as a result of plasmon interaction in the final state.[70]

It is important to include the vibrational widths of the various orbital states for a quantitative interpretation of experimental spectra, at least for molecules. Often sophisticated techniques are utilized to obtain the one-electron DOS. without considering the vibrational widths. After calculating the energies and intensities by theory, a bar diagram (i.e. zero widths) is then compared with the experimental data. Sometimes a constant broadening of all lines is utilized. Using these procedures, the presence of satellites sometimes has not even been recognized, particularly when the normal kvv line shape accounts for all of the major features.

Fig. 5 gives an example of this problem for ethane. The bars indicate the intensities and energies obtained from a Hartree-Fock, self-consistent-field, configuration interaction (HF-SCF-CI) calculation. Clearly most of the features in the experimental spectrum appear to have a bar under them, suggesting that the kvv line shape can account for the entire experimental spectrum. The curve labelled "THY" was obtained by broadening each bar with a Gaussian of constant width, chosen to provide optimal agreement with the experimental curve (this is not a good approximation because in general the s features are much broader than the p features: e.g. see Fig. 3). Again, it appears that the kvv line shape can account for the entire experimental spectrum; however, now some of the features in the THY curve appear to have been "broadened out" (e.g. the features at 258 and 244 eV no longer appear). In Sec. III.C below (Fig. 18), the feature at 258 is identified as arising from a satellite process. The feature at 244 eV apparently arises from the main kvv line shape, but it is broadened out of the theory because the "optimal" width is now too large. This occurs because of the attempt to account for the entire spectrum by including just the kvv component, when in actuality large satellite components are also present (see Sec. III.C).

4. The Importance of Satellites

The presence of satellite contributions in the Auger spectra of molecules and free atoms has been known for some time, but their importance has been recognized only relatively recently.[71,72,73,74,75,Ramhydc] To illustrate the importance of such satellites, consider Fig. 6, which compares the DOS self-folds with the experimental Auger line shapes. The Auger line shapes in Fig. 6 for the gas phase hydrocarbons are the raw data[Ryealk]; those for the solids are obtained from the data[76,77,ryealk] after background subtraction and deconvolution utilizing the procedures described above (i.e. via numerical background removal from N(E)). Fig. 6 reveals several important points. First, note that the experimental line shape for the gas phase molecules is shifted by about 6-10 eV to higher two-electron binding energy (or lower Auger kinetic energy). The binding energy scale is determined by subtracting the Auger kinetic energy from the C K binding energy [i.e. $E_b = -(E_c - E_{kvv})$]. This shift of the experimental line shape to higher binding energy is due to final state hole-hole repulsion, since the two holes cannot completely delocalize. No shift is seen for the solids, since in this case the holes can completely delocalize. However, hole-hole correlation effects are seen in all of the experimental line shapes, as indicated by the clear distortions from the one-electron self-fold.

The second interesting point concerns the onset or threshold of the spectra. Although the principal peaks of the gas phase experimental spectra are shifted to higher binding energy, the onsets of both the experimental line shape and the DOS self-fold for each case are essentially the same. This suggests that each of the spectra has at least some contribution which arises from a process producing a final state with a much smaller hole-hole repulsion. Furthermore, note that each experimental spectrum extends to much higher binding energy than does the DOS self-fold, indicating a process producing a final state with a higher hole-hole

repulsion. It has been shown that the processes producing these satellite contributions are resonant excitation, initial-state shakoff, and final-state shakeoff.Ramhydc

These satellites have been referred to as the ke-vve, ke-v, kv-vvv and k-vvv satellites, where the notation indicates the particles in the initial and final states before and after the hyphen.ramhydc Here, the "k" refers to the initial 1s core hole, the "e" to the resonantly excited bound electron, and v to a valence hole created either by the "shakeoff" process or by the Auger decay. The principal Auger process is indicated without the hyphen (kvv rather than k-vv) consistent with that used historically. We use kvv to indicate this principal or normal Auger contribution to differentiate it from the total KVV experimental line shape.

In light of the above, the line shape apparently consists of the sum of several intensities, I: namely,

$$N(E) = c_1 I_{kvv}(E) + c_2 I_{ke\text{-}vve}(E) + c_3 I_{ke\text{-}v}(E) + c_4 I_{kv\text{-}vvv}(E) + c_5 I_{k\text{-}vvv}(E). \quad (5)$$

The coefficients in eq. (5) are generally obtained by least squares fit to the experimental spectra.Cinisih4.ramhydc

The process creating each component in eq. 5 is illustrated in Fig. 7. Here the ke-vve term refers to the resonant Auger satellite. It arises when Auger decay occurs in the presence of a localized electron, which was created by resonant excitation into an excitonic or bound state upon creation of the core hole. The ke-v contribution arises when the resonantly excited electron participates in the Auger decay. The kv-vvv term is the initial-state shake Auger term arising when Auger decay occurs in the presence of a localized valence hole, which was created via the shakeoff process during the initial ionization. The shakeoff of a valence

electron is an intrinsic phenomena resulting from the "sudden" change of the core hole potential upon ionization. The k-vvv term denotes the final state shake Auger satellite, which arises when Auger decay occurs simultaneously with shakeoff of a valence hole. These latter two terms arise as a direct result of core hole screening. The ke-vve and ke-v terms arise because the Auger process is generally excited by electron excitation which allows the resonant excitation.

5. The Importance of Correlation

Another very important result is evident from Fig. 6. The chemical effects seen in the various experimental C KVV line shapes in Fig. 6 do not arise from one-electron effects, but rather from many-body correlation effects. This is apparent because the DOS self-folds are very similar to each other, in contrast to the experimental line shapes which reveal significant differences. Thus the differences seen between graphite and diamond result because diamond has just the σ orbitals with a single ΔU, graphite has both σ and π orbitals with different ΔU's for the $\sigma\sigma$, $\sigma\pi$, and $\pi\pi$ holes. On the other hand, we will see below that hole-hole correlation and repulsion effects are much diminished for chemisorbed systems because of metallic screening from the substrate. In the chemisorbed case, and only in this case, the C KVV Auger line shape reflects the DOS self-fold without significant distortion. For the line shapes in Fig. 2, the DOS self-folds are simply shifted by U, the hole-hole repulsion. In this case, the molecular species are so small that correlation effects primarily just shift the line shape to higher two hole bonding energy, but do not dramatically distort the line shape (i.e. the correlation effects are primarily reflected through δ not ΔU in eq. 6 below).

C. Theoretical Framework

1. The Principal kvv Line Shape

A theoretical prescription for generating the kvv term can generally be expressed by the equation,[Ramhydc]

$$I_{kvv}(E) = B \sum_{ll'} [P_{kll'} R_l R_{l'} A(E+\delta_{\lambda\lambda'},\Delta U_{\lambda\lambda'},\rho_l,\rho_{l'})]. \qquad (6)$$

Some published work does not include all of the effects indicated in eq. 6. but most interpretations can be expressed in the general form indicated here. In eq. 6. the function A is the Cini-Sawatzky function,[78,79]

$$A(E.\ \Delta U.\ \rho,\ \rho') = \frac{\rho^*\rho'(E)}{[1-\Delta U\, I(E)]^2 + [\Delta U\, \pi\, \rho^*\rho'(E)]^2} \qquad (7)$$

which introduces hole-hole correlation effects, and distorts the DOS self-fold. ΔU is the effective hole-hole correlation parameter and I(E) is the Hilbert transform.

$$I(E) = \int \rho(E-\epsilon)\rho(\epsilon)/(E-\epsilon)\, d\epsilon. \qquad (8)$$

The Cini function. which distorts the DOS self-fold for treatment of Auger line shapes in solids will be discussed more fully below (Secs. II.C3 and IV.E4). In eq.(6) we have included additional arguments in A to make explicit the point that the total theoretical kvv line shape is a sum of components, with each ll' component (e.g. the ss. sp. and pp components or more appropriately each multiplet ^{2s+1}L) having an energy shift. $\delta_{\lambda\lambda'}$. and a hole-hole correlation parameter. $\Delta U_{\lambda\lambda'}$. and with each component derived from a fold of the ρ_l and $\rho_{l'}$ DOS (e.g. s or p) such as that defined in Fig. 3 for cyclohexane. B is a

normalization constant and the R_l's and $P_{kll'}$'s are core hole screening factors and atomic Auger matrix elements, respectively, to be defined below.

The subscripts $\lambda\lambda'$ in eq. (6) on ΔU and δ are to make explicit that these parameters vary with the nature of the orbital combination or the different multiplets. In general, these parameters are chosen to give optimal agreement with experiment.[Ramhydc.80,81,82] Alternatively, only the ΔU in the dominant multiplet is chosen to give the best fit, with the ΔU's in the remaining multiplets fixed by the relevant Slater integrals, etc. (see further discussion below in Sec. III.A). It should be pointed out that in the extended solids, the δ's are by definition zero, since the delocalized holes have zero hole-hole repulsion. In general from 1 to 3 ΔU parameters have been used depending on the material studied and the investigator reporting the work. In the event the δ's and ΔU's are all zero, the A function reduces to the self-fold of the DOS, $\rho * \rho$ weighted by the appropriate Auger matrix elements.

The factors R_l included in eq. (5) are to make the theory consistent with the final state rule for Auger line shapes.[83] The final state rule indicates that 1) the shape of the individual ll' contributions should reflect the DOS in the final state, and 2) the intensity of each ll' contribution should reflect the electron configuration of the initial state. For the kvv line shape, the final state has no core hole. In general it is assumed that the DOS in the final state and ground state are similar, so that the spectral shape of ρ_l should reflect the ground DOS. However, the initial state in the kvv process has a core hole, therefore the integrated ρ_l should reflect the electron configuration of the initial core hole (CHS) state. The R_l factors are defined,

$$R_l = \int \rho_{CHS,l}(\epsilon)d\epsilon \Big/ \int \rho_l(\epsilon)d\epsilon . \qquad (9)$$

In most systems, the R_l factors are similar so that they are generally ignored. Effectively this ignores the "static" effects of core hole screening. The satellites arising from shakeoff are "dynamic" core hole screening effects which can be included separately. The latter will be discussed further in Sec. III.B. The R_l factors are important only when one orbital momentum component dominates the screening. This apparently occurs in many metals such as in Li and Be, and in the $L_{23}VV$ line shapes for Na, Mg, Al, and Si (see Sec. III.B), where the core-hole screening is dominated by the valence s electrons as opposed to the p electrons. However, considerable disagreement exists as to the dominant screening charge in some systems. For example, Jennison et al.[84] on the basis of a semiempirical theory argue that the core-hole screening involves mainly the s electrons in Be, while recent calculations by Almbladh and Morales[85] argue that the p electrons dominate. Recent results almbladh also indicate that the total Auger rates calculated from wave functions perturbed by a static core hole are a factor of 2-4 larger than those calculated from ground state orbitals. Thus static core hole screening is important for all Auger processes, but it is known to significantly alter the Auger profile just for certain systems. An analysis of the profile can shed some light on the nature of the core hole screening process.

2. Atomic Auger Matrix Elements

The atomic Auger matrix elements have been calculated for much of the periodic table within a one-electron Hartree-Fock-Slater approximation by McGuire[86] and Walters and Bhalla[87], or in a Dirac-Hartree-Slater approximation by Chen and Crasemann[88,89]. A complete review of calculated Auger transition probabilities has been published.[90] Recently the problem of obtaining the proper continuum orbital has been considered.[91]

McGuire's and Walters and Bhalla results for $L_{23}VV$ transitions at low atomic number are compared with experimental data in Fig. 8. The matrix element per filled shell, $A_{cll'}$ (i.e. for s^2, p^6, d^{10}, etc.) is plotted. $A_{cll'}$ is defined by the expressions,[92]

$$A_{cll} = [(4l+2)(4l+1)]/[(4l+2-n)(4l+1-n)]\,(A_{cll})_{act.} \qquad (10)$$
$$A_{cll'} = [(4l+2)]/[(4l+2-n)]\,(A_{cll'})_{act.}\ (l \neq l').$$

where n is the number of holes in the initial l shell and $(A_{cll'})_{act.}$ is the actual Auger matrix element or experimental intensity. Note that it is assumed the l' shell in eq. 10 is filled. Since generally one is only interested in the relative $A_{cll'}$ intensities, they have been normalized such that A_{cpp} is 100 for all Z. The matrix element per electron, $P_{cll'}$, required in eq. 6, can be obtained from $A_{cll'}$ by the simple relationship

$$P_{cll'} = 1/[(4l+2)(4l'+2)]\ A_{cll'}. \qquad (11)$$

Similar results for the KVV transition with Z = 6-18 and for the KL_1V and $KL_{23}V$ transitions with Z = 10-80 have been plotted elsewhere.[93,94]. In both the KVV and $L_{23}VV$ data, the theoretical results of McGuire, and Walters and Bhalla have been scaled to the experimental results of the inert gases. Scale factors (ranging from 0.59 to 2.06) significantly different from one were required. These scale factors reflect the magnitude of the errors in the one-electron results. Electron correlation effects at the atomic level are clearly very important in the two valence hole final states (i.e. VV). The CI calculations of Chen and Crasemann[95] for the KLL transitions[96] and for the LMM transitions[97,98] in Fig. 8 include electron correlation, and their unscaled results agree much better with

experiment. As one would expect, the $KL_{23}V$ and KL_1V one-electron results (not shown here) agree nicely with experiment, indicating the insignificance of correlation effects in these core-valence final states (i.e. CV).[ramsi]

The atomic matrix element data reveal three very important points. (1) the variation of the relative Auger matrix elements with atomic number is rather small. (2) The variation that does exist is predicted remarkably well by scaled one-electron results, indicating that the large correlation error is rather constant with Z. (3) No systematic differences between atomic gas phase, molecular phase, and solid phase experimental data exist. This is true even for the dd, pd, and pp matrix elements of the transition metals, where electron screening in the solid is expected to cause significant changes.

Vayrynen has suggested that the relative atomic matrix elements for solid Mn are very different from those in the gas phase.[99] However, Vayrynen's results are inconclusive, because of an inadequate background removal procedure in the solid phase. Recently the effects of the solid state on the matrix elements has been considered by Cubiotti, but the effects of charge transfer due to core-hole screening were included into the matrix element factors so that this is not a real comparison of matrix elements per electron.[100] The results in Fig. 8 and similar ones like it, still suggest that the gas phase atomic data or the scaled one-electron results can be utilized for the determination of $P_{cll'}$ in the interpretation of Auger line shapes for solids, provided that the individual multiplets are not resolved. If the intensities of individual multiplets are required, the theoretical calculations do indicate that these intensities have much larger variations with Z.

Table 1 gives s/p ratios for the CCV and sl/pp ratios for the CVV line shapes, all obtained from the plots similar to Fig. 8. The results in Table 1 are specifically for Si, but as the plots in Fig. 8 reveal, these ratios are surprisingly constant with atomic number, except for the $L_1L_{23}VV$ s/p ratio which varies

dramatically with Z.[Ramsi] The A's in Table 1 are rates per filled shell, i.e. per two 3s electrons and six 3p electrons. They are in fact close to the ratios of the ss, sp, and pp intensities found experimentally for Ar, which has filled s and p shells. The P's are rates per electron, i.e. per 3s or $3p_x$, etc. The P's are used in eq. 6 because the $\rho(E)$ DOS have **not** been normalized to unity. The areas under the DOS curves utilized in eq. 6 are proportional to the total number of electrons in the s and p shells, i.e. approximately s^1p^3. Thus for Si, $P_{csp}/P_{cpp} = 0.38/3$ and $P_{css}/P_{cpp} = 0.025/9$ (see eq.11). The intensity ratios obtained from actual line shape fits for Si are also indicated in Table 1.[Ramsi] In general, good agreement is obtained except for the $L_{23}VV$ case. This will be discussed more fully in Sec. III.B.

An important difference between molecules or covalent solids vs. metals should be pointed out here. In the former case, the line shape reflects multiplets (and hence the matrix elements) appropriate for the initially filled s and p shell, even if these shells are not filled in the separated free atom. As an example, consider the C and Si systems to be discussed below. These systems, as well as other covalent systems, reflect the $(sp)^{n+2}$ configurations in the Auger line shape, where n is the initial number of holes in the occupied molecular orbitals or bands (e.g. n is zero for diamond, graphite, and silicon, even though a separated C or Si atom has 4 holes in the outer p shell). Thus for these covalently bonded materials, the appropriate $A_{cll'}$ in eq. 11 is for the filled shells even though the separated atoms do not have these shells filled. In contrast, the line shapes for the transition metals apparently exhibit multiplets and hence matrix elements arising from the unfilled d shell, d^{n+2}, where n is indeed the number of d holes in the separated atom as suggested in eq. 10. This difference arises because in covalent systems the filled bonding bands can apparently be treated as isolated from the unfilled bands. In metals, of course this is not the case, since the filled

and unfilled parts of the band must be treated together as one band. As we will see in the next section, this has to do with the relative size of the covalent interaction vs. the hole-hole repulsion (i.e. V and U).

3. Correlation Effects - The Cini-Sawatzky Model

a. Localization in Elemental Solids - Metals

The Cini-Sawatzky model has been the basis for understanding correlation effects in Auger line shapes. In elemental solids, two parameters determine the degree of localization of the CVV (core-valence-valence) two-hole final state. If the effective Coulomb repulsion U_{VV} is large compared to the band width ($U_{VV} > \Gamma$), the line shape will be atomic-like, if $\Gamma < U_{VV}$ the line shape will be band-like. In systems where $U_{VV} \approx \Gamma$, both atomic- and band-like contributions are evident in the line shape (i.e. correlation effects are important).[Cini,Sawatzky]

The results of Cini and Sawatzky were obtained from utilizing the Anderson and Hubbard many-body models. The Cini expression was derived assuming an initially filled single band so that it is not rigorously valid for partially filled bands or degenerate bands (this will discussed much more fully in Sec. IV.E4 below).[Cini] Nevertheless, the Cini-Sawatzky expression, in the absence of a better alternative, has been used for metals, alloys, and insulators, and even molecules [i.e. systems for which the bands are not filled and which have degenerate bands], with apparently satisfactory results.

The Cini-Sawatzky results can be simply understood by considering a cluster AO-CI (e.g. configuration interaction [CI] of atomic orbitals [AO] approach. This can be contrasted with the more familiar LCAO-MO-CI where molecular orbitals [MO's] are first constructed and mixed in a CI).[101] For the moment consider a simple two orbital system which has two holes present resulting from the Auger process in an initially filled state.[102] The holes can be described by one-electron atomic orbitals f_a^2 and f_b^2 with binding energy ϵ (ϵ =

$\langle f_a \mid H \mid f_a \rangle$ where H is the proper Hamiltonian operator) giving the Hamiltonian matrix as follows:

$$\begin{array}{c|ccc} & f_a^2 & f_b^2 & 1/\sqrt{2}(f_af_b+f_bf_a) \\ f_a^2 & 2\epsilon+U_{aa} & 0 & H_{ab} \\ f_b^2 & 0 & 2\epsilon+U_{aa} & H_{ab} \\ 1/\sqrt{2}(f_af_b+f_bf_a) & H_{ab} & H_{ab} & 2\epsilon+U_{ab} \end{array} \quad (12)$$

where $U_{aa} = \langle f_a^2 \mid r_{12}^{-1} \mid f_a^2 \rangle$, $U_{ab} = \langle f_af_b \mid r_{12}^{-1} \mid f_af_b \rangle$, and $H_{ab} = \sqrt{2}\langle f_a \mid H \mid f_b \rangle$ ($H_{ab} = \Gamma$ in the solid). Clearly if $H_{ab} < U_{aa}-U_{ab}$, very little mixing occurs and the hole states f_a and f_b properly describe the localization of the two holes. In this instance the Auger line shape is atomic like probing only the two-electron eigenstate f_a^2 (core hole site). For example see recent result for Ca metal.[103] If $H_{ab} > U_{aa}-U_{ab}$, the mixing of the configurations is complete and the linear combination $f_a \pm f_b$ properly describe the localization of the holes. As such, the line shape is molecular-like (band-like for the solid) and gives Auger intensities reflecting the DOS on the atom with the core-hole. If $H_{ab} \approx U_{aa}-U_{ab}$, of course intermediate mixing occurs giving both contributions.

To the novice, the Cini-Sawatzky model might seem to be counter intuitive. First, the Auger process preferentially creates initially localized holes, because of the atomic matrix element. The more localized, the higher the energy of the system final state, hence the lower the kinetic energy of the Auger electron. Now one's intuition would suggests that the more the holes are localized, the greater the urgency for the holes to fly apart, but this is where conservation of energy comes in. If the holes are to fly apart, the potential energy of the Coulomb repulsion must be converted to kinetic energy of the holes. And if $U >> V$, it is not possible for the holes to gain this kinetic energy, so they are "stuck" in this

uncomfortable position. Of course if the holes are "stuck", the atoms themselves can move, but this occurs on a much slower time scale. Thus the Auger profile reflects a localized final state, but ultimately the atom might "Coulomb explode" or dissociate. This is the essence of the Auger induced desorption or Knotek-Feibelman mechanism that is the basis of much electron or photon stimulated desorption work.[104,105]

As an illustration of these correlation effects, Fig. 9 compares the bandwidth Γ_{nd} with U_{ndnd} for the metals with electron configuration d^6s^2 to $d^{10}s^2p^2$. For all three rows of this series the plots of Γ and U cross in the region d^8s^2 and $d^{10}s$. The Auger line shapes of these "transitional" metals are given in Fig. 10 and are compared with a fold of the DOS, N*N, and in some instances the calculated atomic-like Auger line shape. The line shape for Cu and Ag are clearly atomic-like. The line shape for Au appears to be band-like although shifted down in energy by 5 eV. The Ni and Pd line shapes show atomic-like and band-like contributions separated by 3 to 4 eV, and with some multiplet structure still evident. These line shapes illustrate the rather smooth transition from atomic to band-like character.

The short screening length in metals causes the inter-atomic hole-hole repulsion, U_{ab}, to be negligible so that $\Delta U = U_{aa}$. The magnitude of U_{aa} is determined by the Coulomb Slater integrals F^0(nd,nd), F^2(nd,nd), and F^3(nd,nd) and the spin-orbit coupling ξ_{nd}. The spin-orbit coupling constant is determined by the atomic potential deep inside the atom and is not changed by metallic screening. On the other hand, the value of F^0, generally the largest term, is greatly reduced from its value in the free atom by metallic screening. The non-symmetrical terms, the F^2 and F^4 Slater integrals responsible for the multiplet splittings, are reduced by at most 20% from the free atom values, particularly for those elements with tightly bound d bands and large correlation energies, i.e.

those elements to the right in Fig. 9.[106] In the transition region, such as for Pd and several alloys of Pd, the final-state splittings are reduced more significantly (≈34%) from the free Pd atom values.[107] The splittings do not seem to depend on the nature of the metallic host, indicating that the reduction is a consequence of the metallic state in general and not significantly dependent on the DOS at the Fermi level or the nd band width, for example.[108] In contrast, in alloys involving Mn (e.g. the semi-magnetic alloy $Cd_{1-x}Mn_xTe$), a metal much further to the left of the transition region in Fig. 9, all multiplet splitting effects apparently are absent.[109] Thus, the magnitudes of the higher order F^n terms decrease significantly only after F^0 has been reduced to 3 eV or less. This explains how multiplet structure can still be evident even after U appears to be nearly negligible.

b. Localization in Multi-element Covalent Systems

Dunlap et al. have generalized these concepts to multi-element covalent systems by providing criteria for assessing the nature of localization in covalent systems where intermediate levels of localization can occur.[dunlap] In these systems the localization can occur onto atomic, bond, group, or extended band orbitals (AO,BO,GO, or EBO) such as those schematically illustrated for $LiNO_3$ in Fig. 11. These criteria for localization can be summarized as follows:

$$\begin{aligned} &\text{AO:} && V < \Delta U_{xx}, && \\ &\text{BO:} && V > \Delta U_{xx}, && \gamma < \Delta U_{bb}. \\ &\text{GO:} && \gamma > \Delta U_{bb} && \Gamma < \Delta U_{gg}. \\ &\text{EBO:} && \Gamma > \Delta U_{gg}. && \end{aligned} \qquad (13)$$

Here V is the covalent interaction between nearest neighbor AO's and can be estimated from the bonding-antibonding orbital energy separation. γ is the

covalent interaction between nearest neighbor BO's and can be estimated from the s and p atomic orbital energy separation. Γ is the covalent interaction between neighboring GO's: for example, the GO's are the planer arrangement of three N-O BO's about a single N atom. In metals, the extended band width is determined primarily by V, but more commonly the symbol Γ is used to refer to the extended bandwidth. Consistent with this, Γ is used in the previous section to refer to the bandwidths in metals. U_{xx}, U_{bb}, and U_{gg} are the effective Coulomb interactions between holes localized on a single AO, BO, or GO, respectively, and are schematically defined in Fig. 11.

To intuitively understand this intermediate level localization phenomena, consider diamond. It is well known that the best starting point for considering the occupied DOS in diamond is to consider a linear combination of bond orbitals, since the bonding and antibonding σ bands are so far removed in energy from one another (they are separated by a large band gap). Thus, we can say at the outset that $\Delta U_{xx} < V$ (the AO-AO interaction parameter), and we will not have atomic localization such as that seen in the metals discussed above. What about BO localization? The one-electron DOS for diamond has the s and p dominated peaks separated by more than 10 eV.[110] These s and p DOS arise from the clustering of four bond orbitals about each C atom having s and p symmetry (actually a_1 and t_2 symmetry in the point group for tetrahedral symmetry, T_d). If the s and p bands can be treated as separate bands, i.e. $\Delta U_{bb} < \gamma$ (the BO-BO covalent interaction parameter), then we do not have BO localization. This leaves us with GO localization, which is proposed for diamond. Stated in another way: when the ^{2s+1}L multiplet contributions arising from the GO's are resolved sufficiently so that separate features are visible, we can speak of BO localization, since these separate features then correspond to configurations of holes on the same or different BO's. When the multiplets are not sufficiently resolved we

speak of GO localization.

We can generalize this picture for the hydrocarbons. Examination of the wavefu. tions for most hydrocarbons. such as those pictured in Fig. 3 for cyclohexane. show that the MO's can best be considered as linear combinations of CH_n GO's.[Salem] It follows that for most of the C based systems. GO localization is the best qualitative picture for characterizing the localization.

Further analysis of the Auger profiles and bonding in covalent systems indicates that a correlation exists between the ionic bonding character and the nature of the localization. As the bond orbitals polarize from say atom N to O in an NO_3 type cluster in Fig. 11, U_{bb} increases, and γ decreases. The increase of U_{bb} relative to γ raises the extent of BO localization. We conclude that increasing BO ionicity increases the character of the localization from GO to BO. Thus the more ionic BeO,[111] BN, and B_2O_3[112] solids can best be characterized as exhibiting BO localization. The silicon tetrahalide molecules. SiX_4, exhibit BO localization, consistent with the large Si-X electronegativity difference. in contrast with CF_4, which does not, consistent with the smaller electronegativity difference here.[113] The oxyanions NO_3^-.[114] PO_4^{3-}, and SO_4^{2-}. regardless of cation, exhibit GO localization.[Dunlap] In this latter case. it is expected that the holes can not get off of the oxyanions where they were created by the X $L_{23}VV$ process, so that GO localization is a fait accompli. The Si $L_{23}VV$ profile for SiO_2 exhibits structure similar to that for the SiX_4 molecules. so that it also appears to exhibit some BO localization character.[Ramcorr]

II. THE PRESENT - RECENT APPLICATIONS

We see that many different phenomena can occur which affect the Auger line shape. These include localization. shakeoff. charge transfer. polarization. etc. By understanding these phenomena we obtain the interesting electronic

structure information which motivates the interpretation of the Auger line shape. Below we shall examine a wide range of applications, each with a view toward elucidating the fundamental physical phenomena in that system.

A. Metals and Alloys

1. CCV Line Shapes

Core-core-valence (CCV) line shapes have been shown to exhibit large core-hole screening effects, consistent with the presence of a final-state core hole. This follows from the final state rule (see Sec. II.C1 above), which indicates that the line shape should reflect the DOS in the presence of the core-hole. These effects are very pronounced, and have been studied very extensively in metals, alloys, and also in Si. Some of the early work involved the $L_1L_{23}V$ line shape in Si,[115] and the $KL_{23}V$ line shape in Na.[116] More recent work involves the KL_1V and $KL_{23}V$ line shapes in metals (Na[vonBarth], Mg, Al[117], Mg[118]), metal alloys (AlNi[119], Mg with Ni, Cu, Zn, Pd, Ag, or Al[120,121,122]), and Si.[Ramsi] Finally several studies on the $M_1M_{23}V$ and $M_{23}M_{45}V$ line shapes in GaAs[123,124,125], Ge[126], GeS and GeSe[127] have been reported. These investigations have been very helpful in determining the fundamental properties of the materials under study. For example, the studies on the Mg/metal alloys listed above revealed the strong hybridization of the Mg s and p orbitals with the other metal d orbitals[Mgalloys]. The studies on GaAs upon exposure to O and CO indicated very clearly the relative reactivity of the surface Ga and As atoms.[Lagally] But all of these studies revealed large core-hole screening effects which needed to be understood before detailed interpretations of the line shapes could be carried out.

Perhaps most illustrative of the effects of the core-hole on the valence band DOS in metals is the data of Hannah et al. in Fig. 12, which compares the KL_1V and $KL_{23}V$ line shapes for Mg, Al, and two alloys.[Hannah] These data can best be

understood in terms of ΔZ, the effective charge on the core of the local atom compared with the average of its neighbors. To understand this data, we also use the results in Table 1 which indicates the relative weighting of the s to p DOS in these Auger line shapes. Qualitatively, the $KL_{23}V$ line shape reflects primarily p DOS, the KL_1V reflects about equal s and p. Thus the difference between the two, indicated by the shaded areas in Fig. 12 qualitatively reflects the s DOS. Based on this analysis, the p DOS peaks around 2 eV for $\Delta Z = 0$ or 1, but at 4 eV when $\Delta Z = 2$. This appears to be a general trend in the systems studied; i.e. the p DOS is not strongly altered by the presence of a single core-hole, but apparently it is ultimately strongly affected by two core-holes. On the other hand the s DOS is strongly distorted by a single hole, as revealed by a comparison of the s DOS in Mg and $Al_{85}Mg_{15}$ in Fig. 12 (the s DOS peak is shifted from 4 to 6 eV). A second core-hole pushes the s DOS further to higher binding energy, so that it peaks around 8 eV when $\Delta Z = 2$.

2. CVV Line Shapes

The Cini model for understanding hole-hole correlation effects in metals was based originally on a filled (or nearly filled) band. Treglia et al.[128] developed the formalism for cases where the d band is not filled, but as we will indicate in Sec. IV.E4 below, the results are similar to that for filled bands, except that the apparent ΔU appears to decrease with increasing hole density. This can be seen from the results in Fig. 13 which shows Ni $L_{23}VV$ Auger line shapes for various Ni alloys.[129] Photoemission data reveals that the d band width does not significantly change, but that the DOS shifts down with decreased DOS at the Fermi level for $Ni_{20}Zn_{80}$ and $Ni_{50}Al_{50}$. This decreased density of d-holes limits the ability for electron screening, and hence a larger ΔU for these systems is expected. This is clearly evident in Fig. 13, which shows a line shape that is

narrower and shifted to higher binding energy for $Ni_{20}Zn_{80}$ and $Ni_{50}Al_{50}$. This is exactly as expected by the Cini model for larger ΔU.[andrews]

In contrast to the above case for Ni alloys, a recent study on Cu alloys (Al_2Cu. Mg_2Cu.. and $Ni_{90}Cu_{100}$)[130] revealed that changes in the L_3VV line shape occurred primarily as a result of changing 3d bandwidth. Cu exhibits a nearly atomic-like spectra, revealing individual multiplets. The separation of these multiplets and relative intensities are seen to change just as expected within the Cini theory for changing bandwidth.[Andrew2]

General theoretical treatments of CVV Auger spectra in dilute and disordered alloys have been given by Drchal and Kudrnovsky and Vos et al.[131,vos] In these general theories the importance of U, the covalent interaction. and the energy separation between the impurity (dilute metal) level and bulk level are emphasized. The energy separation is as important as U in understanding the Auger profiles in these alloys. In the latter work the $L_{23}M_{45}M_{45}$ line shape in $CuCd_2$ and Cd_3Cu were considered in detail. Other recent work includes Auger studies on the following alloy systems: Fe-B-P.[132] U-M (M = Fe. Co. Ni) metallic glasses.[133] Au,Ag/Ge.[134] and UPt_3 and UBe_{13}.[135]

We examine more closely the recent Auger work on the Pd/Cu alloy.[136] This work reveals the importance of the effects of local lattice expansion around Pd impurities in Cu.[Pdlattic] This is an excellent example of a "noble-metal-impurity, free-electron-like host, and shows the importance of the impurity-host interaction. Fig. 14 compares the theoretical results obtained for the Pd $M_{45}N_{45}N_{45}$ line shapes in the dilute alloy $Cu_{95}Pd_5$. The important parameter is $t = (T_{CuPd} - T_{CuCu})/T_{CuCu}$, which varies the d-d transfer integral between the host and impurity. When t is -1. the impurity is decoupled from the host and the impurity DOS is a Lorentzian centered around 6 eV (i.e. the feature at 6 eV in the Pd DOS shown in the insets of Fig. 14). When t=0. the impurity-host and host-

host transfer integrals are equal. This corresponds to the usual Clogston-Wolff result, which assumes that the lattice around the impurity has expanded to equalize the hopping integrals. As t is increased above zero, more of the impurity DOS is mixed into the host d band, and for t=0.6 the admixture is comparable to that given by impurity calculations. Fig. 14 compares the Pd DOS and resultant Auger line shape obtained with t = 0.6 and 0.2, indicating that indeed an expansion has occurred to nearly equalize the transfer integrals.[Pdlattic] EXAFS calculations on this same system show similar local lattice expansions around the Pd impurity.[Pdlattic] In contrast to the Cu-Pd alloy, similar Auger line shape studies on the Ag-Pd[137], Cd-Ag[138], Ag-Mn and Cu-Mn[139], and Ni-Fe[140] alloys do not reveal such lattice expansion effects in the CVV Auger line shapes.

B. Silicon and Second Row Metals

The $L_{23}VV$ Auger line shapes of the simple metals (Li, Be, Na, Mg, Al) and Si probably are the most often studied in the literature. This work dates back over nearly 15 years and the references are too numerous to cite all of them here. Recent work by Almbladh and Morales,[141] Vidal et al.,[142] and Ramaker et al[Ramsi] review much of this work. The conclusions reached by all investigators is usually always the same: namely that a simple fold of the bulk DOS including atomic Auger matrix elements does not reproduce the experimental line shapes. Furthermore, dramatically reducing the ss and sp contributions in the line shapes can give excellent agreement. Fig. 15 shows this result.[ramsi] Table 1 indicates the extent to which the ss and sp contributions must be reduced. But how can this be justified?

An early explanation by Jennison[143] indicated that the bonding charge must be excluded from the total charge, since the Auger process samples only the charge local to the atom with the core hole. This reduces the ss and sp

contributions, since the s orbitals are very diffuse in Si, and there is greater overlap (i.e. bonding charge). But the final state rule indicates that the Auger intensities should reflect the initial state, which because of the core-hole, now has s orbitals contracted relative to the ground state. Thus, this explanation generally is no longer accepted.ramsi. a'mbladh2

More recent explanations for the reduction of the ss and sp contributions depend on surface effects or dynamical screening effects. One way to test for surface effects is to compare the KVV and $L_{23}VV$ line shapes. If the ss and sp contributions are fully reflected in the KVV line shape, but not in the LVV line shapes of these elemental solids, then surface effects must be playing an active role. This is because electrons from the LVV transition have kinetic energies of only about 100 eV. Thus, these come primarily from the first 1-3 surface layers, compared with KVV electrons which have kinetic energies well above 1500 eV and come more from the bulk. Table 1 does indeed indicate that the ss and sp contributions in the KVV line shape for Si have the expected intensities, in contrast to that for the LVV line shape in Si. The KVV and LVV line shapes for Mg[144] and Al[145] have also been compared. In contrast, these results suggest that the KVV and LVV line shapes are very similar (or at least that they both reflect similar ss and sp reductions). However, all of these comparisons have difficulties. In general the KVV transition gives a very weak signal, and usually the KVV spectra have been taken with extremely poor resolution because of the high electron kinetic energies. Furthermore in Mg, the ss and pp contributions have similar spectral shapes, so that it is difficult to determine their exact relative size. These problems have been discussed in detail by Ramaker et al. ramsi.

Surface effects have also been considered by performing detailed calculations which explicitly include the effects of the surface. Feibelman et al.[146] and Kunjunny and Ferry[147] have performed such calculations and these

results do indicate that surface effects add intensity to the line shape in the region where it is needed. But inclusion of these surface effects do not solve the problem; indeed, Feibelman's work lead to the discovery of this problem. However, calculations for Al metal have indicated that surface layers have more p-like character than the bulk, and this has been proposed previously to explain the reduction of the ss and sp components in the Al LVV line shape.[148,149] Recent Auger spectra[150] utilizing photon energies near the Si 2p binding energy, namely at two different energies which emphasize either the bulk or surface contributions, indicate that surface effects cause a 4 eV shift to higher kinetic energy in the principal peak of the Si $L_{23}VV$ line shape. A large change in the s/p intensity ratio in the Si line shape with different Ge overlayer coverages also suggest a large surface effect.[151]

On the other hand several arguments can be given suggesting that dynamic screening effects play a dominant role in the reduction of the ss and sp contributions in the LVV line shape. By dynamic screening effects, we mean those effects which arise from the non-orthogonality of the initial and final state orbitals that result because of the initial core-hole and final no-core-hole states. These non-orthogonality effects introduce satellites, such as the initial state and final state shakeoff (kv-vvv and k-vvv) processes discussed in Sec. II.B4 above. No evidence exist for initial state shakeoff satellites in these materials, because the "shake" hole propagates away from the core-hole before the Auger decay. However, final state shakeoff has the effect of redistributing Auger intensity over a large energy range which ultimately causes some intensity to disappear into the background. Thus final state shakeoff can preferentially reduce some components of the total line shape.

Ramaker et al.[ramsi] have suggested that the diffuse 3s orbitals in ground state Si contract in the presence of a core hole. This causes a particularly large

reduction of the ss and sp Auger contributions. The fact that the Si LVV line shape for most metal silicides, where the Si s orbitals are more local, do not exhibit the ss and sp reduction is very suggestive here of the shakeoff mechanism (see Sec. III.F and Figs. 22 and 23). Furthermore, dynamical calculations of core-hole effects by Schulman and Dow[152] for Li indicate that accounting for dynamic screening significantly improves the agreement with experiment.

Davis and Dow indicate that the L23VV line shapes of Al, Mg and KVV of Be and Li when plotted as a function of the reduced energy E/2k (where k is the free-electron Fermi energy), are all nearly the same. From this they conclude that the Auger profiles of simple metals depend primarily on the electron gas density and are almost independent of the details of the band structure.

Very recently, Almbladh and Morales [almbladh2] performed extensive calculations which included dynamical screening and surface effects on the CVV line shapes for Li, Be, Na, Mg, and Al. These results for Li and Al are shown in Fig. 16. Their results still provide no clear picture, indeed they cloud the situation still more because their conclusions are so different from previously cited work. They conclude that the final state rule result accounting for just static screening provides good agreement with experiment for Li and Be. They indicate that dynamical effects worsen the agreement in Li, Mg and Al, but improve it in Na. They further conclude that surface effects are critical for Mg and Al.

Obviously further work will be required here before any definite conclusions can be reached about this important and long term problem. In spite of this, recent analysis of the $L_{23}VV$ line shape has provided some information on the surface density of states,[154] and on silicon-hydrogen bonding in hydrogenated amorphous Si.[155]

C. Gas Phase Molecules

Detailed interpretations of the Auger line shapes for gas phase molecules have been reported for around 50 or more different molecules (see Ref Ramrev1 for a partial list with original references). More recent work has been on the following molecules: CH_3CN,[156] $ZnCl_2$ and $CuCl_3$ vapors.[157] F_2,[158] CO,[159] C_2H_4,[160] Neopantane ($C(CH_3)_4$)Jennneop, $Co(CO)_3NO$ and $Fe(CO)_5$,[161] CX_4(X = F. Cl. Br) and SiF_4,[162] NH_3 radical,[163] CH_n (carbynes),[164] ROCSSNa (xanthates),[165] HBr,[166] $(HF)_n$,[167] OCS[168] and NO_2.[169] Such ab initio theories as Hartree Fock-self-consistent field theory (HF-SCF)[170,171,172], local density function (e.g. LCAO-MO-X_a)Dunlap, configuration interaction (CI)[173,174,175,176] or Green's functions theories[Ohrendorf,177,178] have been used. Recently, semi-empirical calculations (e.g. CNDO or INDO) have also been utilized with good success.[179,180,Larkrev]

In these approaches, the different two-hole final states resulting from the Auger process are described directly as approximate solutions to the Schrodinger equation, $H\psi = E\psi$. The resultant final state energies are utilized to calculate Auger kinetic energies. The wave functions may be utilized to calculate the Auger intensities of each transition, or some empirical procedure may be used. Usually a comparison of the experimental line shape with a "bar" diagram is reported, where the position and height of each bar represents the energy and intensity of each Auger transition. Generally, a bar of significant intensity is found under each feature in the experimental line shape, so that good agreement between theory and experiment is assumed. Rarely has a width for each transition been determined, so that a quantitative comparison between theory and experiment could be made (an exception is ref. Dunlap). Furthermore, the totally different approaches for molecules and solids has generally made it impossible to compare trends in the molecular spectra with those for solids.

In a totally different approach. Hutson and Ramaker[ramhydc] have utilized solid state methods and the Cini expression (eq. 6 and 7) to interpret the Auger line shape of several hydrocarbons. and compared the results with that obtained for graphite. diamond. and polyethylene. The justification for utilizing the Cini-Sawatzky expression for molecules on an empirical DOS self-fold. which includes the vibrational widths is not very clear. However, we have indicated above that the distortions to the DOS self-fold caused by the Cini expression qualitatively mimics the distortions normally occurring within the Ci theory for molecules. Therefore. as long as the correlation effects are relatively small (i.e. $\Delta U <$ the appropriate covalent interaction). this approach appears to work reasonably well (see further discussion in Sec. IV.E4).

Figs. 17 and 18 compare the optimal total theoretical line shape obtained by Hutson and Ramaker with the experimental line shapes for ethylene and ethane.[Ryealk] In general. the theoretical line shapes generated by the formalism described agree nicely with the experimental line shapes. Similarly good agreement is obtained for other gas phase molecules not shown. i.e. for methane. cyclohexane and benzene.[Ramhydc] Table 2 summarizes the results for the satellites and Table 3 summarizes the ΔU and σ parameters for the principal kvv components.

Table 2 reveals that the normal kvv line shape accounts for only about half of the total experimental intensity for the gas phase molecules. The remaining part of the experimental intensity can be attributed to 3 different satellite contributions: namely resonant excitation, initial-state-shake, and final-state shake satellites (i.e. via the ke-vve, kv-vvv, and k-vvv processes). The spectral line shapes for the ke-vve and kv-vvv satellites also were generated by eq. (6) but with different values for $\Delta U_{\lambda\lambda'}$ and $\sigma_{\lambda\lambda'}$ as schematically indicated in Fig. 7.[Ramhydc] The results in Fig. 17 for ethylene and the conclusions concerning the

importance of satellite contributions utilizing the semi-empirical method is totally consistent with recent ab-initio Green's functions results reported by Ohrendorf et al.[Ohrendorf]

The ratio of the resonant satellite intensities, I(ke-v)/I(ke-vve), indicates something about the character of the orbital containing the resonantly excited electron, i.e. the excitonic level. The atomic Auger matrix elements per electron are essentially the same, for the ss, sp and pp contributions in kvv spectra (see Sec. II.C2). Therefore, one can estimate what the ratio of intensities should be, based purely on the ratio of local electron densities, assuming a completely localized excitonic level. With an initial state charge distribution of $\sigma_s\sigma_p{}^2\pi$e, I(ke-v)/I(ke-vve) should be 0.5, compared with $\approx$0.14 for ethylene and other alkenes found experimentally.[ramhydr] This suggests that although the excitonic level may be localized in time, it must be of a more diffuse nature spatially. The factor of two or more reduction from that expected theoretically suggests that the excited electron spends only part of its time on the methyl group with the core hole, the other part of the time presumably on neighboring carbon atoms or methyl groups.

We note that the relative intensities of the kv-vvv satellites for the 6 molecules listed in Table 2 are essentially all around 20% to within experimental error. Methane is isoelectronic with the neon atom. The shakeoff probability for neon has been both measured and calculated to be around 21%. This is in excellent agreement with that found for all of the carbon systems.[181,182] Table 2 shows that the empirically determined intensity for the k-vvv satellite is quite constant around 17%. This intensity was determined by integrating the area under the long tail from E_{th} (the threshold energy for the shakeoff satellite) down to E_{th} + 50 eV.[Ramhydc] This includes most of the final state shake satellite although some intensity exist beyond this region. This could easily introduce an

error of 3%, so that to within experimental error, the initial and final state satellite intensities are similar, as expected.

D. Molecular Adsorbates

Once a molecule is placed on a metal surface, localization of the hole on the molecule is no longer a fait accompli. The hole can escape via electron transfer from the substrate, i.e. charge transfer. It is therefore interesting to compare the Auger spectrum for the free molecule with that for the molecular adsorbate. Either an interpretation of the line shape or comparison with the gas phase has recently been done for several molecular adsorbates including diatomics and hydrocarbons: O_2, H_2O, CH_3OH, HCHO, CO, N_2, CH_3NH_2, and $(CH_3)_2NH$ on Ni, Cu, Pd, and Ag.[183] C_2H_4/W(100).[184] C_2H_2/Cu(100).[185] O_2 and CO/Al,[186] CCl_4/Ni(110),[187] CH_3NO_2 and $C_2H_5NO_2$/Rh(111).[188] CO, C_2H_4, C_2N_2, and C_6H_6/Pt(111),[189] CO/Pd(111).[190] CO/Ni(100).[191,192] CO/Pt(111) and Cu(111).[193] A review of the literature up through 1980 on the use of Auger spectroscopy for the study of molecular adsorbates has been given by Netzer.[194] He noted the presence of additional satellites near the top of the spectra for almost all of the adsorbates and a shift of the spectra to lower energy relative to the gas phase. Cini and D'Andrea have presented a general theory for understanding dynamic screening effects, and Schonhammer and Gunnarsson for many body effects in CVV spectra of molecular adsorbates.[195,196]

Fig. 19 shows C KVV Auger data for ethylene/Ni(100) deposited at 100K, and then heated to higher temperatures as indicated.[197,198] These line shapes result after the data treatment summarized in Sec. IIA.1b. Notice the significant changes in Auger profile and the gradual shift to lower two-hole binding energy with increasing temperature. HREELS, XPS, and UPS data indicate that these line shapes are representative of π-bonded ethylene (C_2H_4)at 100K, σ-bonded vinyl ($CHCH_2$) at 250K, a mixture of di-σ-bonded acetylene (HCCH), ethynyl

(CCH) and methylidyne (CH) at 300K, and carbidic carbon (C) at 600K on the surface.[Ramethyl] Clearly the Auger line shape is sensitive to the adsorbate/substrate bonding changes, suggesting that much can be learned about these systems from Auger line shape interpretations.

We consider in detail here the results for the 100K spectrum. Fig. 17 compares the Auger line shape for gas phase C_2H_4 with the C_2H_4/Ni at 100K (i.e. the p-bonded ethylene).[Ramethyl] The spectrum in Fig. 17b was excited by x-rays, so that no resonant satellites appear. Charge transfer from the substrate into the π^* orbital occurs to screen the holes, in both the core-hole initial state and the two- or three-hole Auger final state. This charge transfer has the affect of decreasing the ΔU and δ parameters; the transferred charge playing the role of the resonantly excited electron in the gas phase.[Ramethyl] Thus the kvv and kv-vvv contributions which comprise the intramolecular component (i.e. termed the VV component) for the chemisorbed state are similar to the ke-vve and kvv in the gas. The $V\pi^*$ component is similar to the ke-v, and the $\pi^*\pi^*$ component is a new contribution unlike that of any in the gas phase, in fact it is approximated in Fig 17b by the Ni L_3VV Auger line shape. Although the latter two components are facilitated through an intra-atomic $V\pi^*$ and $\pi^*\pi^*$ Auger process. respectively, they ultimately appear inter-atomic in character because one or both holes ultimately end up on the substrate.

The relative intensities of the three components can be understood within the final state rule. The electronic configuration per carbon atom in the ground state of the chemisorbed ethylene, assuming charge neutrality, is nominally $\sigma^3\pi^{1-x}\pi^{*x}$, where the x indicates the π bonding and π^* back-bonding charge transfer involved in the interaction with the metal substrate. Upon creation of the core hole, we expect that the valence electronic configuration assuming charge neutrality, becomes $\sigma^3\pi^1\pi^{*y}$ or $V^4\pi^{*y}$, where y is the net charge transfer in

the presence of the initial core hole. The relative intensities of the components. VV: $V\pi^*$: $\pi^*\pi^*$ should then be 16:8y:y^2. or upon including the P_{kll} matrix elements 13:7y:y^2. Best agreement with the results obtained from the fit to the experimental line shapes (56:34:10. total normalized to 100) is obtained when y = 1.3. which gives relative intensities of 55:38:7.[Ramethyl] The 1.3 total electron transfer is consistent with the 1.3 core hole screening electrons found in benzene as determined from ab-initio theoretical calculations.[199]

Similar interpretations of the line shapes in Fig. 19 have been reported by Ramaker et al.[Ramethyl,200] Most interesting of these results is the evidence that the line shape at 600K is not representative of a true carbide. since considerable C-C bonding character is reflected in the line shape. Similar C KVV Auger data reported by Caputi et al. reveal further changes in the line shape around 620K.[201] Quantitative interpretations of these data suggest that the amount of C-C bonding character decreases at this temperature.[Ramcarb] Recently. CEELS data has shown that the C-C bonding below 600K correspond to C_n (n mostly equal to 2) horizontally bonded to the surface, and that above 620K a significant fraction of the C_n dissociates; however. at high coverages. some of [illegible] flip up vertical to the surface.[202] Comparison with theoretical calculations [13] and additional experimental data indicate that these vertical C_2's serve as precursors to the graphite nucleation sites.[RamvertC]

It is interesting to consider at what point in an adsorbate/substrate interaction the charge transfer takes place. Rye et al. have considered this by comparing the C KVV line shape for a free C_2H_6 molecule. to that for a thick condensed layer, a monolayer physisorbed on Ni(111) at 20K. and data taken at higher temperatures similar to Fig. 19.[204] First the effective δ decreases by about 2.5 eV upon condensation of the free molecule (i.e. a decrease from about 10eV as indicate in Table 3 to 7.5 eV). This arises from polarization of the

condensed gas. At 20K, the coupling to a Ni surface is insufficient to delocalize the two-final state holes, so that δ remains essentially at 7.5 eV.

Figure 20 shows what Rye found as the temperature is increased. Here the energy scale, $U_{eff}(T) - 2[IP(20K) - IP(T)]$, which equals $U_{eff}(20K)$ at T = 20K, is essentially the change in two-hole binding energy from the 20K spectrum with increasing T. This includes shifts due to a changing U and a changing ionization potential (IP) with temperature. Rye's U_{eff} is essentially $\Delta U + \delta$ in Table 3, hence $U_{eff} \approx 7.5 + 1 \approx 8.5$ eV at 20K. Rye et al. suggest that the energy shift primarily results from a decreasing U over most of the temperature range, so that U_{eff} does not reach zero until nearly 500-600K. However, Fig. 17b, indicates that already at 100K, both ΔU and δ are zero, so that U_{eff} is already zero at 100K. This difference of opinion obviously arises from experimental energy calibration differences between the data of Rye et al. and Ramaker et al. at 100K.[ryeethyl,ramethyl] The shift beyond 500K in Fig. 20 obviously occurs because of a decreasing IP, since the ethylene is undergoing conversion to metal carbide in this temperature range as discussed above.[Ramethyl] The shift between 100 and 250 eV most likely also arises from a decreasing IP, due to conversion from π-bonded to σ-bonded C_2H_6 in this temperature range, and the increased interaction with the substrate.[Ramethyl] In this picture the charge transfer and dramatic reduction in U occurs upon conversion of physisorbed to chemisorbed ethylene already at 100K, but more experimental work is required here to resolve the absolute energy problem.

AES has also been very useful for studying the decomposition of molecular adsorbates with increasing temperature on many other systems, such as C_2H_2/Cu,[205] CH_3OH/Fe(110),[206] and the ultimate formation of graphite at higher temperatures.[Ramcarb]

E. Extended Covalent Solids

A considerable amount of work on Auger line shape analysis has been published for various covalent solids. Most prevalent of this is the work on Si, SiO_2, SiC, and Si_3N_4 because of there use in the electronics industry. Many studies have also been reported on the covalent solids involving carbon. As mentioned at the beginning of this review, the Auger dN(E)/dE "fingerprints" for these covalently bonded solids are well known. However, the number of detailed quantitative interpretations of these line shapes is somewhat limited, except for Si, which was considered in Sec. II.B and for SiO_2.[ramcorr,ramsio2,207,208,209,210] Several papers on the early oxidation of Si using Auger line shape analysis have also been published recently.[211,212,213] For the C KVV line shape, several studies have appeared for graphite,[Housgrap,cinigrap] diamond,[ramdia] polyethylene,[rampoly,214] SiC,[215] and amorphous carbon.[216,217] We examine some results for diamond and polyethylene here.

Fig. 21 shows an interpretation, utilizing eq. 6, of the line shapes from polyethylene and diamond.[Dayan,218,219,220] Note that in graphite and diamond no initial-state-shake satellites or resonant satellites are observed.[Ramdia,Housgrap] The absence of such satellites in graphite and diamond arises because neither the shake hole nor an excited electron in the initial state of these covalently bonded solids stays localized near the core hole for a time sufficient to "witness" or participate in the Auger decay. In the presence of a core hole, the occupied valence band DOS of diamond indeed does not exhibit any bound states.[Rampoly] On the other hand, the DOS for polyethylene in the presence of a core hole does exhibit narrow peaks indicative of bound-like states, consistent with the kv-vvv satellite observed. Furthermore, polyethylene has an

excitonic level as seen by x-ray absorption (XAS) and electron energy loss (EELS) data.[221,222]

Comparison of the ΔU's for molecules and extended solids in Table 3 indicates something about the nature of the screening processes in these covalent systems. Note that the ΔU for the CC-CC contribution increases in the order cyclohexane < polyethylene < diamond. This can be understood from the definition of $\Delta U = U_{11} - U_{12}$. For very short screening lengths, one might expect both U_{11} and U_{12} to be reduced substantially, so that ΔU would be decreased.[Housgrap] For long screening lengths, one might expect U_{12} to be decreased more than U_{11}, having the effect of increasing ΔU. Apparently the latter is occurring in these materials. The longer chain length in polyethylene and full three dimensional covalency in diamond suggests that the extent of polarization should increase in the order cyclohexane < polyethylene < diamond. This increased polarization then has the effect of increasing ΔU. For the alkenes, the ΔU's are all the same. This suggests that the screening length is much shorter so that "full" screening already occurs in ethylene. This is consistent with the more delocalized π electrons in the alkenes.

The δ parameters in eq. 6 are interpreted as the delocalized hole-hole repulsion.[Ramhydc.dunlap] As the size of the molecule increases, Table 3 shows that δ decreases, reflecting the ability of the two final state holes to stay apart from each other in the delocalized molecular orbitals. Note also that for similar sized molecules, the δ's for the alkenes are smaller than for the alkanes. This may reflect the increased screening due to the π electrons. Note that the δ's are zero for the extended solids, as expected, although a controversy has existed for polyethylene (the problem again arose from energy calibration problems which will not be discussed here).[Ryepoly,223]

F. Metal Silicides and Carbides

In contrast to the extended covalent solids mentioned above, an enormous volume of work has been published on the study of the metal silicides and carbides. This work has been motivated primarily by interfacial-compound formation: i.e. metal/diamond or graphite and metal/Si interfaces. The technological motivations for studying these interfaces start with the observation that the vast majority of microelectronics devices are currently based on Si. and in the future increasingly on diamond for high temperature applications. The thrust to employ new metallurgical schemes for Schottky barrier and for Ohmic contacts to Si and diamond is directed toward improvements in contact stability at high device density and in device performance.[224]

Auger spectroscopy has been of great help in studying these interfaces and for understanding the electronic structure of the metal compounds formed. Theoretical electronic structure calculations indicate a qualitatively similar bonding for almost all of the metal silicides and carbides.[225,226] An example of this is indicated in Fig. 22 (inset 1) for Pd_4Si.[Bader] Generally 3 bands are found in the Si or C DOS: a Si 3s (or C 2s) band at 8-12 eV. the Si 3p- metal (or C 2p-metal) bonding band around 3-7 eV, and the Si 3p-metal (or C 2p-metal) antibonding band around 0-3 eV (the latter two bands are sometimes referred to as the σ and π bonding bands; they are labelled p_1 and p_2 in Fig. 22). The p_1 electrons exist in molecular orbitals with much of their density localized interatomically between the Si or C and metal nuclei. The p_2 electrons exists in comparatively well delocalized molecular orbitals largely responsible for the metallic conductivity exhibited by many of the silicides and carbides.[Neckel] These two bands straddle a large non-bonding metal d band not shown in the inset: although recent calculations for NiSi indicate that this band has extensive metal d-metal d interaction which is also important for the placement of the Si or

C bands.[227] It is this large metal band which obscures the bonding bands in photoemission, and thus makes Auger spectroscopy so uniquely helpful in observing the important bonding features in the DOS.

In the limit of the one-electron approximation (i.e. $\Delta U = 0$), the C KVV or Si $L_{23}VV$ Auger spectra should reflect the DOS self-fold, consisting of the features labelled a'-e' in Fig. 22. These features have been identified as arising from the following: a' - ss, b' - $sp_1 + sp_2$, c' - $p_1p_1 + sp_2$, d' - p_1p_2, and e' - p_2p_2.[bader] All 5 features are seen in the experimental Si $L_{23}VV$ spectrum (Fig. 22), which even has similar intensities as those in the self-fold. This is in sharp contrast to the line shape for elemental Si as discussed above (Sec. III.B) and strongly indicates that the 3s electrons are much more localized in the silicides compared with Si, where they are involved in the bonding.

The localization of the 3s electrons in the silicides is also indicated by the results in Fig. 23 for Ca_2Si and $CaSi_2$.[228] Here again the DOS self-fold are compared with the experimental line shapes. Good agreement is found for $CaSi_2$ but not for the Ca_2Si line shape. The introduction of correlation effects utilizing the Cini expression, eq. 6, with $U_{sp} = U_{ss} = 3$ eV, and $U_{pp} = 0$ gives excellent agreement with experiment. This indicates again the strong localization of the s orbitals, and increasing localization with increased Ca content, as one might expect. Furthermore, comparison with other data suggest similar localization in Mg_2Si[229], and apparently also in Yb/Si.[230,231] In contrast, Si $L_{23}VV$ line shapes from silicides formed with transition metals (e.g. Ti,[232] Ni,[233] Pt,[234] Cu,[235,236,237] Al,[238] Ir,[239] V,[240] and Au[241]) do not show large hole-hole repulsion effects.

These trends in the silicides are remarkably similar to those in the carbides. Fig. 24 shows C KVV dN(E)/dE fingerprints for several metal carbides as indicated.[242] Detailed interpretations of the TiC, NbC,[243, 244] BC,[245]

VC.[246,247] and TaC[248] line shapes reveal that the 5 features arise from the ss, $sp_1 + sp_2$ (singlet) $sp_1 + sp_2$ (triplet), p_1p_1, and $p_1p_2 + p_2p_2$ contributions. Note that the derivative fingerprints show, as one proceeds from the upper left to the lower right, a decreasing singlet-triplet splitting, an increasing intensity of the highest energy feature resulting from the p_2 DOS, and a decreasing ss and sp localization. Perhrsson et al have shown that these changes can be correlated with the enthalpy of formation ($\triangle H$) of the metal carbides.[Pehrsson] The magnitude of the singlet-triplet splitting in the sp contribution is sensitive to the degree of orbital localization, since the more compact the orbitals, the greater the interaction, and hence the greater the splitting. $\triangle H$ is a measure of the ionicity of the C-M bonds in the carbides, so one might expect U to increase with $\triangle H$.

The high energy shoulder seen in the C KVV line shape for the carbides and the Si $L_{23}VV$ line shape for the silicides is similar to the high energy shoulder visible in the O KVV and N KVV Auger line shapes for many other materials.[249,250,251] At least six different mechanisms have been postulated for its presence. These can be summarized as follows:

1) interatomic Auger transitions,

2) hole-hole correlation effects,

3) electron transfer or core-hole screening,

4) shake satellites,

5) band splitting due to covalent interactions, and

6) chemical shifts due to different species present.

The first two of these can be classified as final-state effects, 3) and 4) as initial-state effects, and 5) and 6) as chemical environment effects. Full descriptions of these mechanisms have been given elsewhere previously.[Ramrev]

Of these six mechanisms, the band splitting mechanism for the carbides is currently favored based on the results summarized above. However, we can not

completely eliminate the hole-hole correlation effects mechanism, favored for the transition metal oxides and previously suggested for the carbides.[RamASS] Recent cluster calculations modelling the O KVV line shape for Ag_2O using a Slater-Koster type Hamiltonian (Fig. 25) shows the familiar high energy shoulder.[Tjeng] This broad shoulder from 5 to 11 ev arises from hybridization of the localized state with states having one hole on one oxygen and another on either silver or on a different oxygen atom (i.e. from delocalized states). Cluster calculations modelling the O KVV line shape for SiO_2 produced similar results.[Ramsi] From the Cini perspective, the pp contribution undergoes a large Cini-Sawatzky distortion so that the shoulder reflects the DOS self-fold, and the principal peak results from the more localized states. The correlation of the shoulder intensity with the heat of formation across the carbide series is also consistent with this mechanism.

G. Metal Chalcogenides and Halides

The Auger spectra of metal chalcogenides and halides have been published many times over the years. Recent efforts include work on Cl/Ag,[252] TiO_2.[253,254] Zn_3P_2.[255] γ-Fe_4N.[256] sulfide minerals,[257] SO_2, O_2, and H_2O/Li.[258] O/NiAl.[259] various La compounds,[260] M_xTiS_2 intercalation compounds.[261] Fe_2Ti_4O,[262] and Cu/GaP.[263] Much of this Auger data provides information on coverage at a surface, or stoichiometry in the bulk, and perhaps some bonding information. However, the Auger spectra of these generally ionic materials can provide more fundamental information, such as direct evidence for the ultimate fate of the shake excitations upon creation of the core hole.

Within the sudden approximation, XPS data reflect the core-hole state shortly after its creation, say within 10^{-17} sec.[264] We note that shakeup states with lifetimes significantly shorter than this will not be visible in XPS, because

they relax before the photoemission event is complete. Well after 10^{-15} sec., the core level decays via the AES or XES process, with considerable relaxation occurring in the interim.

Evidence for relaxation of the charge transfer shakeup excitations before Auger decay in CuX_2 and the Cu oxides is clearly evident from Figs. 26. The primary $2p^{-1}d^{10}L^{-1}$ core-hole state produces the principal peak in the Cu L_{23} XPS spectrum (not shown here). The notation indicates that one hole exists on the ligand (L) leaving 10 electrons in the Cu 3d shell. The XPS data also reveal a satellite arising from a $2p^{-1}d^{9}$ "charge transfer" shakeup state. The primary core-hole state decays to a $d^{8}L^{-1}$ Auger final state in the Cu L_3VV case and to a $d^{9}3p^{-1}L^{-1}$ state in the $L_3M_{23}V$ case.[265]

Auger satellites are known to arise from the L_3V-VVV or L_3V-$M_{23}VV$ processes, respectively. the L_3V initial states resulting either from Coster-Kronig decay of the L_1 and L_2 core-holes (L_1-L_3V and L_2L_3V) or from direct shakeoff during the initial L_3 core-hole creation (coincident Auger studies verify these processes. see Fig. 28 and Sec. IV.B1). These processes can account for an Auger satellite with intensity of 0.7 relative to the main peak in the Cu and Cu_2O line shapes.[Ramhtsc1] It has been indicated that the charge transfer shakeup $2p^{-1}d^{9}$ states responsible for the XPS satellites in Cu^{2+} materials decay to d^{7} states and hence will add to the Auger satellite intensity.[266,267,268] However, while the relative intensity of the XPS satellites grows from 0.45 for $CuBr_2$ to 0.8 for CuF_2,[vanderlaan] Fig. 26 shows no change in Auger satellite intensity for the CuX_2, or even between Cu, Cu_2O, and CuO.

The above results indicate that all of the charge transfer shakeup states must relax before the core-hole decay.[269] This is not unexpected within relaxation theories, because the shakeup excitation energy is much larger than the core-level width.[270] In contrast, the additional valence-hole states resulting from

Coster-Kronig decay and shakeoff do not dissipate before decay, because the extra hole is apparently bound on the local CuO_n cluster.[ramhtsc1] However, for CO/Cu(111), Chen et al concluded that all shake excitations (both shake-up and shake-off) relax before the Auger decay.[271] Near a metal surface, the metal to CO charge transfer is apparently much faster than charge exchange between CuO_n clusters in CuO.

H. High Temperature Superconductors

Since the discovery of the copper oxide based high temperature superconductors (HTSC) several years ago, a deluge of electron spectroscopic data on these materials has appeared. Cu L_3VV and O KVV Auger line shapes on $La_{1.85}(SrBa)_{0.15}CuO_4$,[272] $YBa_2Cu_3O_{7-y}$ (commonly called the 123 material)[273,274,275,276,277] and on $Bi_2CaSr_2Cu_2O_{8+d}$ (commonly called the 2122 material)[278,279,280] have been reported. Because of the surface sensitivity of AES, specific care must be taken to maintain sample purity, reduce beam damage, and limit O depletion; indeed, some of the early work had severe problems with O depletion, particularly with the 123 material.[htsc]

Comparison of the HTSC Auger line shape with similar line shapes for CuO and Cu_2O (such as those in Fig. 26) have been very helpful to ascertain something about the electronic structure and about the U parameters in the HTSC materials.[ghijsen,tjeng,281,282] Note the larger satellite in the Cu L_3VV line shape for the Bi 2212 HTSC material compared with CuO and Cu_2O in Fig. 26. These line shape studies reveal:

1) that the local electronic structure around the Cu and O atoms is not dramatically different from the conventional oxides,

2) that Cu^{+3} is not present, but rather the effective valence of Cu is somewhere between Cu^{+1} and Cu^{+2} (i.e. the Cu-O bond is more

covalent in the HTSC's than in CuO), and

3) that some line shape changes can be correlated with T_c.[allhtsc]

One of the parameters that may be critical to the superconducting mechanism is U_{pp}, the Coulomb interaction on the O atom. Values from 4 to 14 have been reported (see reference Ramhtsc2 for a summary of the theoretical and experimental estimates). The O KVV AES line shape rather directly reflects U_{pp} for Cu_2O, since the d_{Cu}-p_O valence band is initially filled in Cu_2O leaving a two-hole final state. Table 4 indicates a value of around 5 eV (4.6 to 5.7 eV) for U_{pp}.[ghijsen,tjeng] The Auger data for CuO and the HTSC's is not so easily interpreted, because now the valence d-p band initially has one hole per CuO unit leaving a three-hole final state after the Auger decay. In this case the Cini expression is not rigorously valid.

In spite of these problems, many interpretations of the O KVV line shape for several transition metal oxides using the Cini model have appeared in the literature. The U_{pp} values obtained are indicated in Table 4.[283,284,285,286,287,288,289] These qualitative U's indicate some very revealing points. First, the d electron count is apparently very important in determining U_{pp}, probably because the d electrons help to screen the hole-hole repulsion on the O atom. Those oxides with no d electrons have U_{pp} values in the range of 10-14 eV. Those oxides with partially filled d-bands have U_{pp} values in the range 3-6 eV, and those with filled d bands have U_{pp} values around 11 eV except for Cu_2O. Obviously the d electrons are very effective screeners of two O p holes when they are more mobile (i.e. when the d band is not filled).

In Cu_2O a different screening mechanism is apparent, as suggested by the much reduced U_{pp} for Cu_2O compared with the other filled d-band oxides. The filled and expanded 3d shells in the Cu^{1+} atoms which surround the oxygen are apparently uniquely polarizable, and thus decrease U_{pp} significantly. O K

XANES data support this interpretation, since exitonic effects are also strongly reduced for Cu_2O compared with CuO.[290] Therefore a larger U_{pp} is anticipated for CuO and the HTSC's, compared with Cu_2O; probably something around 6-8 eV. ramjes

III. THE FUTURE - NEW DIRECTIONS

The review above of several areas where Auger line shape interpretation has provided considerable insight into localization, charge transfer, polarization, and screening processes should convince many readers that the results obtainable from this approach are worth the effort. However, Auger line shape analysis has not realized its full potential because a quantitative interpretation is still a formidable task in view of the many simultaneous processes and the many-body effects reflected in the total line shape. As mentioned above, just the extraction of the line shape (i.e. removal of the background and inelastic losses) is not an easy task. One way to simplify these two tasks is to limit the number of variables or to limit the number of simultaneous processes. I believe this is the direction of the future for AES, and that much progress will be made in this area in the coming years. Below, I will outline several areas, and give several examples, where controlling some of the variables greatly eased the tasks required for quantitative interpretation of the line shape, and in some instance provided significant new insights.

A. Controlling the Background and Inelastic Loss

Sec. II.A.1c. mentioned two ways to experimentally nearly eliminate the magnitude of the background and inelastic loss contributions; namely by positron induced AES (PAES), or by coincident techniques. An example of the former is given here, and coincident techniques are discussed in a different context below.

Fig. 27 compares Cu $M_{23}VV$ Auger data induced by electron (EAES) and positron excitation (PAES).[Weiss1,291,292] It dramatically reveals the strong reduction of the background in PAES. The incident beam energies were 3 KeV and 25 eV for the electron and positron beams, respectively. Secondary electrons cannot be created through collisional processes with energies in excess of the beam energies, hence the secondary electron contribution drops essentially to zero beyond 25 eV in the PAES spectrum. Similar spectra taken with overlayers of S and Cs[Weiss,293] reveal that 95% of the Auger intensity arises from the topmost atomic layer of the Cu surface. This is because the positrons are trapped in the image potential induced at the surface.[294] This surface sensitivity should drastically reduce the extrinsic inelastic loss contribution. The presence of considerable intensity remaining around 40 eV in the PAES spectrum of Fig. 27. may in fact arise from intrinsic loss processes, such as shakeoff. A shift of nearly 6 eV to lower kinetic energy in the PAES data compared to the EAES data may arise from increased hole-hole repulsion near the surface compared with the bulk. Thus PAES data may provide significant new information on intrinsic shakeoff processes and localization near metal and other surfaces.

The relatively high efficiency with which positrons generate low energy Auger lines combined with the low background permit Auger spectra to be obtained with energy doses of 10^{-5} times less than those necessary for EAES. This may allow PAES data to be obtained on systems highly susceptible to beam damage. Finally, recent data suggest that the positrons annihilate core electrons preferentially near surface defects or impurity sites.[295] This may allow new unique studies of the electronic structure occurring near such defect sites, information of great interest in the electronics industry.

B. Controlling the Initial State

We have emphasized in this review the significant contributions due to satellites arising from initial and final state shakeoff, shakeup, resonant processes, and Coster-Kronig transitions. These simultaneous processes make interpretation of the total line shape much more difficult. Controlling the initial state helps to confine some of these processes.

1. The APECS Technique

Auger-photoelectron coincidence spectroscopy (APECS)[Haak] allows one to limit or control the initial state in the Auger process. By counting only those Auger electrons which arrive in coincidence with photoelectrons of specific kinetic energy, the initial state is uniquely determined, thus controlling the magnitude of various satellites.[296] Recent work on Ar,[297] GaAs,[Bartynski] and TaC,[Hulbert] have appeared.

Fig. 28 shows the APECS spectrum for the $L_{23}M_{45}M_{45}$ line shape of Cu in coincidence with the L_1, L_2, and L_3 lines.[298] Also shown is the total Auger spectrum for comparison. Note that the inelastic loss contributions are substantially reduced compared with the AES line shape because in APECS, Auger electrons which have suffered inelastic collisions on their escape from the sample will not arrive in coincidence with the photoelectron. The satellites due to the Coster-Kronig process are uniquely separated from the L_3 Auger contribution, and the L_2 and L_3 Auger contributions are also clearly separated. This separation allows the "delocalized" portion of the L_3 Auger signal around 927 to be clearly visible, as well as the ^1S multiplet around 912 eV in the localized portion.

2. The DES-technique

A second way of controlling the initial state is by utilizing a tunable photon source, such as a synchrotron, to resonantly excite a core electron into a bound state.

$$M \rightarrow M[c^{-1}\phi]. \quad (14)$$

The excited electron can then either participate in the Auger decay

$$M[c^{-1}\phi] \rightarrow M^{+}[v^{-1}] + e^{-} \quad (15)$$

or be a spectator to the Auger decay of the core hole

$$M[c^{-1}\phi] \rightarrow M^{+}[v^{-1}v'^{-1}\phi] + e^{-}. \quad (16)$$

This technique has been called de-excitation electron spectroscopy (DES).[299] The initial state can in fact also be controlled utilizing a coincident electron technique. In this case, the Auger electron is collected coincidentally with the scattered electrons, of fixed energy loss and fixed low scattering angle. In this coincident procedure the electron beam mimics an incoming photon beam.

The DES technique has been used extensively for free molecules[300,301,302,303,304,305] and for small molecules chemisorbed on surfaces.[chendos,306,307] In the free molecule, resonant excitation into a π level generally results in a spectrum reflecting the occupied one-electron DOS of the molecule. For an adsorbate, the excited electron may escape before the Auger decay, resulting in essentially the normal kvv spectrum. The DES technique has also been used in solids, such as in Ni,[308] and recently in Si, where it has been used to emphasize surface effects as opposed to bulk contributions.[Woicik] Excitation into various excitonic levels in insulators also enables one to obtain information on the nature of Z+1 defects sites.

As an example of DES data, Fig.29 shows electron and nonresonant photon (Al K_α x-rays) excited Auger (EAES and XAES) data along with DES data for the O_2 molecule.[309] The DES data in Fig. 29 were obtained utilizing the coincident electron technique; however, recently Lapiano-Smith et al also presented very similar photon excited data for O_2 gas[310], and Chen et al for solid O_2.[311] Detailed interpretations of these data along with calculations have recently been reported for this molecule.[312,313] The normal Auger v^{-2} features actually

extend to much lower kinetic energy than shown. The nonresonant XAES spectrum reveals features resulting from shakeup ($1\pi_g^{-1}1\pi_u$) around 504 and 506.5 eV. The EAES spectrum reveals additional features around 507, 511, and 518 eV resulting from resonant excitations, $1s^{-1}1\pi_g$. These same features may be present, but with much reduced intensities, in the XAES data. There appearance in the XAES data arises because of secondary electrons with energy significantly greater than the 1s binding energy. The features above 509 eV in all three spectra arise from the process in eq. 15: namely when the resonantly excited electron participates in the Auger decay. Those features below 509 eV in the DES spectrum arise predominantly from when the resonantly excited electron is a spectator to the Auger decay (eq. 16).

Sambe and Ramaker have successfully interpreted the resonant contributions above 510 eV by making comparison with PES data on the basis that the separation between peaks in the v^{-1} DES final state and the v^{-1} PES final state should be nearly identical.[sambe] Carrol and Thomas showed that the AES and entire DES profiles are very similar except for a 11.4 eV energy shift.[thomas] Carroll and Thomas argue that the normal AES profile above 498 eV is dominated by $1\pi_g^{-1}v^{-1}$ final states, and that one cannot distinguish between the resonantly excited $1\pi_g$ electron, and the two original $1\pi_g$ electrons. Thus, the entire DES spectrum can be considered as a two-hole, one-electron spectrum. Since the extra electron screens the hole-hole repulsion, the DES spectrum is shifted by 11.4 eV from the AES for O_2 gas, but by only about 2 eV in solid O_2.[Chen] This difference between the gas and solid phase data arises because of large intermolecular screening which reduces the U in the 2-hole AES final state in solid O_2. This intermolecular screening is much less significant in the 2-hole, 1-electron DES final state because of the resonantly excited electron. The separation between the

participator and spectator contributions depends on the binding energy of the electron in the excited bound state.[314]

C. Controlling the Spin Polarization

By measuring the spin polarization of the Auger electrons one gains additional information about the possible process which caused them.[315] Spin polarized AES (SPAES) thus has two aspects; namely it assists in interpreting the the normal N(E) spectra and it has the potential to provide useful information in surface magnetism. Fig. 30 shows an example of the former capability for the $M_{23}M_{45}M_{45}$ Auger line shape from Fe(100).[316] Shown in Fig 30 is the normal Auger signal (here indicated as I) and the effective spin polarization $P_{eff} = P_0 + (P-P_0)I/(I-I_0)$ where the polarization $P = (n\uparrow - n\downarrow)/(n\uparrow + n\downarrow)$ [$n\uparrow$ ($n\downarrow$) is the number of electrons with the spin parallel(opposite) the magnetization of the sample], and P_0 and I_0 are the polarization and Auger intensity in the background region. The leading peak in I around 42 eV is the main line leaving the d^{-2} configuration. The M_{23}e-V satellite around 51eV (see eq. 15) and above the M_{23} threshold, is the well-known autoionization satellite with final d^{-1} configuration. The autoionization emission is strongly polarized. but not as strongly as a very weak satellite around 64 eV. The source of the Auger gain satellite is not known exactly, but its extremely high polarization restricts it source.Allen

SPAES data has been published recently for O/Fe(100),[317] Gd/Fe(100),[318] and Fe/Au(100),[319] providing exciting new data on the magnetic coupling between different metals at a surface. Significant conclusions were reached without detailed understanding of the Auger processes involved. Clearly more theoretical work is required in this area before detailed magnetic applications can be accomplished. I expect much more progress in this area in the near future.

D. Controlling the Angle of Escape

Recently, strong angular variations in the Auger line shapes of adsorbed molecules have been observed.[320,321] These can be explained by applying selection rules derived from simple symmetry considerations. The angular variations are of significant help in determining the correct assignment of some of the fine structure in the line shape. Furthermore, it provides direct evidence for the angular orientation of the molecule on the surface. Recent studies have been reported on CO/Ru(001) and NO/Ni(111).[Umbach,322]

Fig. 31 gives an example of the data for the coadsorbed system, CO + K/Ru(001).[323] Many different models have been suggested to explain the K induced effects on the CO bonding ranging from pure enhanced 2p back donation to the formation of ionic K-CO salts. Some models postulate a lying down π-bonded CO or a strongly tilted CO configuration. The angular dependence of peak 4 arising from the $4e_1 1b_1$ final state, and comparison with model calculations in Fig. 31 indicate quite clearly that the CO is vertically bonded to the surface. Further interpretation indicates that its valence orbitals are rearranged by the presence of coadsorbed K.[wurht,324]

Use of angular variations in Auger line shapes, although quite rare to date, should have considerable potential. Angle resolved Auger data for graphite also showed considerable variation with angle.[325, 326] Recently, initial results have been reported where both the incident angle of the primary electron beam and the collection angle of the Auger electrons are varied independently.[327,328] Both angles strongly influence the surface sensitivity of AES. The angular variation of Auger spectra for K/Si(001),[329] Cu/Ni,[330] and O/Mg[331] were also recently reported, where the data was utilized to determine the adsorbate sites on the surface. These latter studies relate to electron scattering after the Auger event.

but I anticipate more effort in the future on the changes of the intrinsic line shapes with angle as well.

E. Extending the Theory

In this section I want to assess the current theory, it limitations, and areas where further work is urgently needed. It goes without saying, that ones perspective is different than anothers, so that I may be a bit biased in my assessment. My bias leans toward building a balanced, semi-empirical, convenient approach, that can be utilized for a wide variety of materials of technological interest. We know that a complete solution of Schrodinger's equation for a two-hole final state in a molecule or cluster gives an excellent interpretation of the Auger line shape. But this approach is inconvenient, and can only be performed on the simplest of molecules. If the interpretation of Auger line shapes is ever going to provide a convenient and useful means of extracting electronic structure information on a wide range of materials, a theory must be provided which is widely applicable, convenient to use, and balanced with regard to its validity and fundamental justification. Considerable progress has been made, but much remains to be done.

1. Atomic Auger Matrix Elements

A discussion of atomic Auger matrix elements was given in Sec. II.C2. Fig. 8 and similar plots for other Auger transitions clearly indicate that one-electron calculations are not adequate to evaluate these elements. These same figures suggest that the relative values of these matrix elements are surprizingly constant with nuclear charge Z, and that no verifiable difference exists between atoms, molecules, and solids (some investigators may differ particularly on the latter point). Nevertheless, many investigators continue to perform sophisticated calculations to obtain the DOS, and then calculate the matrix elements within the one-electron model. In my opinion, this is an unbalanced approach (i.e. accurate

DOS but widely inaccurate matrix elements) which can easily be corrected by utilizing the semi-empirical matrix elements. Although the paper by Jennison strongly warns against using matrix elements calculated from one basis set along with wavefunctions calculated from another, Jennison was utilizing nonlocal Wannier functions for the wavefunctions and local Slater orbitals for the matrix elements.[JenPRL] Most DOS are obtained utilizing local basis sets, or obtained semiempirically as described above (Sec. II.B2), and experience on a wide variety of systems has indicated that the semi-empirical matrix elements are quite adequate. The apparent problem with the Si $L_{23}VV$ line shape in elemental Si arises from other causes (see Sec. III.B).

2. Vibrational Widths

Vibrational widths are a big problem in molecules; and although not as evident in solids, vibrational broadening certainly is present here also. As discussed in Sec. II.B3, the problem with widths is acute only when they are totally ignored, sometimes causing the presence of satellites to be unrecognized. No simple theory exists for calculating the vibrational widths, but the problem identified above can be eliminated by broadening the "bar" diagrams or utilizing an empirical DOS as describe in Sec. II.B2. They are not a major problem when considering solids.

3. Satellites

The importance of "many-body" satellites has been increasingly recognized, particularly for free molecules but also in extended solids. Nevertheless, many investigators still insist on ignoring them. Although these satellites may complicate the interpretation of the line shape, they provide valuable and unique information on charge transfer, screening, and localization. Better techniques must be developed for generating line shapes for these satellite contributions.

4. Correlation: Application of the Cini expression

The Cini-Sawatzky expression has been the basis for our understanding of correlation in Auger line shapes. It has been utilized with surprising success for metals, insulators, semi-conductors, and for molecules. But its application is only fully justified for completely filled nondegenerate bands. What are its exact limitations?

a. Materials with Unfilled Bands

Some theoretical work has been reported for initially unfilled bands by Treglia et al,[treglia] Cini et al[332,333,334] and Liebsch.[335] We briefly summarize some of this work. According to Treglia et al., the Cini equation is still applicable for nearly filled bands (i.e. low hole density); however, $\sigma(E)$ must now include the self-energy effects. In this prescription, $\sigma(E)$ might be determined from the measured photoemission spectrum which includes static and dynamic screening effects, etc. (the latter introduces satellite contributions).[336] Cubiotti et al. applied the model of Treglia et al. to consider the XVV spectra of several alloys; unfortunately, they did not compare their results with experiment to verify their findings.[337] However, Cini et al. suggest that within the ladder approximation, the undressed or bare one-hole propagator is more appropriate (this has become known as the bare ladder approximation, BLA).[cinverdoz] Cini has concluded for Pd[Cini above] and graphite[338], both possessing unfilled bands, that the Cini expression can satisfactorily be utilized with the undressed DOS, provided ΔU is treated as a parameter to give an optimum fit to experiment, and the correlation effects are small. Apparently, the two holes tend to interact more as bare holes because the size of their screening clouds is larger than the range of hole-hole repulsion. Bennet et al.[bennet] have introduced a procedure which removes any photoemission satellite contributions so that the undressed DOS might be approximated empirically assuming the remaining static screening effects are relatively small.

To understand some of the problems which arise for unfilled bands, Sawatzky has presented a revealing illustration as shown in Fig. 32.[339] Sawatzky considers a lattice of H atoms with $U >> W$ for the 1s electrons. This is then a ferromagnetic system with one electron on each atom in the majority spin configuration and a small number of minority spins added as shown (i.e. the band is slightly greater than half-filled). The schematic dressed (or correlated) DOS and photoelectron spectrum for this system is then shown, along with a self-fold of the PES to approximate the AES profile (this approach is consistent with the theory of Treglia et al.). The expected AES spectrum is also shown assuming that two localized holes can only be produced in those initial states containing two electrons per atom. Therefore nearly all the Auger spectral weight occurs around a binding energy of U, in sharp contrast to the self-fold of the correlated DOS.

Fig. 32 reveals that a straight forward application of the Cini expression to the occupied "dressed" DOS self-fold does not account for the spectrum, and at best gives a negative U value. Perhaps the self-fold of the correlated DOS includes the effects of U twice, and the negative U in the Cini expression is simply undoing this error. Whatever the case, as suggested by Cini's BLA approach, it is better to consider the uncorrelated DOS. The uncorrelated DOS in Fig. 32 would have a band symmetrically situated around E_f, the lower portion occupied, the upper unoccupied. The self-fold of the occupied portion of this uncorrelated DOS would give a spectrum centered just below E_f, and the Cini expression would then shift the spectrum to the left by U. This is a strong argument for using the undressed DOS, or at least eliminating the satellite contributions from the dressed DOS or PES data before the self-fold. However, it does not necessarily settle the issue of whether the correlated (minus satellites) or uncorrelated DOS should be used.

Now consider the two filling limits. As the band fills, the intensity of the

minority spin band at E_f in the PES increases and the majority spin band decreases (i.e. the latter ultimately becomes a "satellite" feature). At the filled band level, only the peak around E_f remains so that the correlated and uncorrelated DOS become the same. If we utilize the idea of Bennet et al.[bennet] mentioned above for removing the satellite, we can self-fold just the "main" peak and obtain a reasonable approximation to the AES profile for nearly filled bands. At the other limit, for substantially less than half-filled bands, the contribution with highest binding energy (previously called the "satellite") becomes the "main" peak, and the Fermi level moves down to it, so that again either of the DOS can still be used in the Cini expression . Furthermore for $U >> W$ and less than half-filled bands, we obtain no Auger intensity because under these circumstances no two electrons exists on the same atom.

We conclude that Cini's bare ladder approximation seems, at last qualitatively, to be able to handle all situations. Treglia's approximation may also be adequate provided the satellite contributions are removed. Which of these approaches is better is however not yet clear.

The existence of negative U's has indeed been observed for the transition metals on the left side of the periodic table, i.e. with less than half-filled 3d bands. Table 4 shows the effective U's obtained utilizing the Cini expression on an empirically derived DOS self-fold for the transition metals (XPS data were used however no distinct satellite features were evident). Indeed, the U becomes increasing negative as the band becomes more unfilled.[340] Negative U's have also been found for some transition compounds, such as $CrSe_2$ and $TiSe_2$.[deboer] Different suggestions have been given for obtaining these negative U's. deBoer et al. suggested that the negative U's were caused by a dynamic bipolaron effect involving the conduction electrons. Others have proposed that these are caused by the potential of the core-hole in the initial state, i.e. due to edge or non-

orthogonality effects.[341,342] Ramaker et al. have argued that for the low electron density limit, i.e. **nearly empty bands**, the negative U values can be interpreted as arising naturally from correlation effects in the initial state.[343,344] Note that all of the above suggestions involve additional complications not even considered yet in discussing Fig. 32, and do not primarily involve the satellite problems discussed above.

To intuitively understand some of these additional complications, consider again the lattice in Fig. 32, but now with just two H atoms, and compare the case when the band is full on the left and when the band is half full on the right.

	Full	Half full	
Initial state	$\varphi_1^2\varphi_2^2$	φ_1^2	
Final state	φ_1^2	empty	(17)
Matrix element	$<1skl]r_{12}^{-1}[\varphi_1\varphi_1>$	$<\varphi_1\varphi_1]r_{12}^{-1}[1skl>$	

In this simple diatomic molecule case, the orbitals φ_1 and φ_2 are the uncorrelated orbitals, such as the $1s_a \pm 1s_b$ bonding and antibonding MO's, and 1s and kl refer to the core and continuum orbitals involved. The Auger matrix can be written in either the hole picture or the electron picture; i.e. we can enumerate the electrons or the holes. Obviously, on the left, it is better to consider the holes, while on the right better to consider the electrons, because in either case we then have an empty band; empty of holes in the initial state on the left, and empty of electrons in the final state on the right. Therefore, we need to worry only about final state hole-hole interaction on the left, and initial state electron-electron interaction on the right. This initial state electron interaction on the right will increase the initial state energy, thus increasing the Auger kinetic energy, and make the conventional U parameter come out negative. For U > W, the two

electrons will remain on separate atoms (antiferromagnetic), and the Auger intensity goes to zero for less than one-half filled bands as discussed above. Thus the electron interaction in the initial state alters both the intensity and the profile. This is to be expected, since by the nature of the sum rules, the initial state must always determine the total intensity.[RamFSR]

These intuitive ideas have been applied by utilizing the Cini expression as depicted in Fig. 33 where the final state and initial state rule prescriptions are compared.[RamISFS] In the initial state prescription, appropriate for less than or equal to half-filled bands, the Cini expression is applied to the entire DOS, occupied and unoccupied portions. As U increases the occupied DOS self-fold is distorted upward by a negative U and the total Auger intensity (shaded area) decreases. This is in contrast to the final state case, where the distortion is downward, and the total intensity is conserved because it is applied only to the occupied part. The upward distortion in the less than half-filled case occurs because the Auger process tends to select those electrons which exist on the same atom in the initial state.

Let us now go back to the illustration in Fig. 32. The initial state rule prescription was not derived for these circumstances: the band is greater than half full, and it is applied here to the self-fold of the correlated (plus satellite) DOS. Thus we should be highly skeptical of the result. Nevertheless, we see that the initial state prescription also qualitatively works on the self-fold of the correlated DOS (with satellite contributions). Note that the actual AES intensity is much reduced from the DOS self-fold, as illustrated schematically. When the band is less than half-filled, the AES intensity should go to zero in this highly correlated system (i.e. $U >> W$), consistent with the initial state rule prescription. .

Now for the many atom system, an additional complication arises, because now the band will not be empty in either the initial or final state. This introduces

additional screening effects. To illustrate this consider the band $\varphi_1\varphi_2...\varphi_i\varphi_j...\varphi_m\varphi_{m+1}...\varphi_n$, with the orbitals 1 through m occupied and m+1 through n unoccupied. The initial and final states can then be written as follows:

hole picture (> half filled)	electron picture (< half filled)	
Ψ_{IS}: $<1skl\varphi_{m+1}^{\cdot}...\varphi_n']$	$<\varphi_1'\varphi_2'...\varphi_i'\varphi_j^{\cdot}...\varphi_m']$	(18)
Ψ_{FS}: $[\varphi_i\varphi_i\varphi_{m+1}...\varphi_n>$	$[1skl\varphi_1\varphi_2...\varphi_m>$,	

where φ_i is an orbital in the final state without a core hole and φ_i' is an orbital in the initial state with a core hole. The Auger matrix element $<\Psi_{IS}[r_{12}^{-1}]\Psi_{FS}>$ then reduces to the two-particle matrix elements within the "orthogonalized final state rule" approximation:

$$<1skl]r_{12}^{-1}[\tilde{\varphi}_i\tilde{\varphi}_j> \qquad <\tilde{\varphi}_i'\tilde{\varphi}_j^{\cdot}]r_{12}^{-1}[1skl> \qquad (19)$$

where

$$\tilde{\varphi}_i = \varphi_i - \Sigma_{unocc} S_{in}\varphi_n^{\cdot} \qquad \tilde{\varphi}_i' = \varphi_i^{\cdot} - \Sigma_{occ} S_{in}\varphi_n. \qquad (20)$$

Here the sums continue over all of the unoccupied or occupied orbitals respectively on the left and right side, and the S_{in} are the overlap integrals $<\varphi_i][\varphi_n^{\cdot}>$, which in perturbation theory are proportional to $1/(E_i-E_n)$.

Within the tight binding approximation, each band orbital can be expressed as a linear sum over the atomic orbitals, $\varphi_n = \Sigma_m c_m(n)f_m$. Furthermore, the Auger profile, $A(E_{nm})$, can be given

$$A(E_{nm}) = \Sigma_{L,S,J}\, I(L,S,J,)\, A[E_{nm}, U_{L,S,J}, c_1(n), c_1(m)] \qquad (21)$$

using the notation of eq. 6 for the Cini expression, where we are summing over all

multiplets, and the coefficients $c_I(k)$ determine the electron density on atom 1 (the one with the core hole) in the orbital n or m. The coefficients I are the intensity for each multiplet determined from the atomic Auger matrix elements and the appropriate coupling coefficients. The hole-hole repulsions depend on the particular multiplet. Above, eq. 20 accounts for the new effect, core hole screening, which introduces non-orthogonality between the initial and final state orbitals and causes dynamic screening effects.

Now consider the case on the left which is more appropriate for the low hole density limit (the nearly filled band) case. As the band fills, the number of terms in the sum over the unoccupied orbitals in eq. 20 decreases so that $\varphi\!\!\!-_i \approx \varphi_i$. Furthermore, well below the Fermi level, the S_{in} coefficients are very small, so that $\varphi\!\!\!-_i \approx \varphi_i$ in any event. This is the origin of the final state rule which indicates that the line shape reflects the DOS appropriate to the final state. When $\varphi\!\!\!-_i \neq \varphi_i$, we have the orthogonalized final state rule, which introduces singularity effects, also referred to as MND effects in Sec. II.B. On the other hand, for the low electron density limit (the nearly empty band), the sum in eq. 20 approaches zero only for the nearly empty band. As the band fills, the projection onto the final state orbitals converts $\varphi\!\!\!-_i'$ to φ_i, so that the final state DOS is still more appropriate, although that this is so is not as clear. Therefore, in both cases, the final state DOS is more appropriate.

Both the initial state electron-electron correlation effects and the non-orthogonality screening effects near the Fermi level tend to make U negative. Indeed, others have attributed the negative U's to these non-orthogonality effects.[Hill,Jenn I] suggest that the effective negative U's exhibited by the transition metals for less than half-filled bands as shown in Table 2 primarily arise from electron-electron coupling in the initial state, although non-orthoganality effects could also be playing a significant role.[RamISFS]

Negative U effects have also appeared in other systems. The $\pi\pi$ Auger contribution for the benzene molecule shows an upward distortion.[RamISFS] It is believed this arises because the total π band (bonding plus antibonding) is half filled in benzene and hence a negative U is appropriate within the initial state rule. Ramaker also has shown that the $\pi\pi$ contribution arising from the reconstructed clean diamond surface within Pandey's π-bonded chain model can be explained by a negative U, which strongly reduces the $\pi\pi$ contribution vs. the $\sigma\pi$ coming from the surface.[Ramdia] Finally, some very interesting correlation effects have been observed in core EELS spectra for Ti and V metals which suggest similar effects.[Erickson]

We can summarize these intuitive discussions as follows:

a) The final state (i.e. ground state for CVV processes) DOS is the most appropriate one in nearly all cases.

b) It is best to use the uncorrelated DOS, or the correlated DOS but without the satellite contributions. Agreement on which of these is best has not yet been obtained.

c) For nearly filled bands, the Auger profile apparently reflects the multiplets from hole-hole coupling in the final state that gives the usual positive U's. For significantly less than half-filled bands, the Auger profile reflects the multiplets of the electrons in the initial state, that gives negative U's in the usual sense.

d) The initial state determines the total intensity in all cases. For less than half filled bands, electron-electron coupling is critical to determining this intensity.

It seems clear that much more rigorous work is required to sort out these complicated correlation and screening effects for initially unfilled bands. We anticipate much more work in this critical area in the near future.

b. Degenerate Bands

The problem of degenerate bands also needs to be considered. Cini has applied the BLA theory along with the full multiplet and intermediate spin-orbit coupling theory, without further simplifying assumptions, to the C KVV line shape of graphite.[cinigrap] The theoretical line shape he obtained was amazingly similar to that obtained empirically by Houston et al., who ignored the multiplet decomposition and applied the Cini expression directly to the full ss (1S), sp(1S + 3S), and pp(1S + 1D + 3P) contributions.[Housgrap] It seems clear that if the correlation effects are not too dramatic, the same 2s + 1L multiplets arising from different bands decouple, and the bands can be treated independently (e.g. the ss(1S) and pp(1S) multiplets decouple). Furthermore for small U's, the different 2s + 1L multiplets arising from the same band apparently can be averaged together to give an effective ss,sp, and pp contribution (e.g. the 1S and 1D multiplets from the pp contribution can be summed before applying the Cini expression). It is not clear from Cini's work whether the large non-spherical effects present in graphite were taken into account.

Although the theoretical line shapes obtained by Cini and Houston et al. were nearly the same, the resultant U's were very different. Houston et al. found U's of 0.6, 1.5, and 2.2 ev for the pp, rp, and rr components (in a slightly different procedure Ramaker et al.[Ramhydc] obtained the values in Table 3 namely 0, 1, and 2 eV), while Cini found values of 5.5, 11, and 11 eV. What can account for these dramatically different U's but with the same line shape? One possible explanation may involve the normalization and/or selection of the individual components of q*q used in eq. 6. Examination of eq. 6 reveals that different normalizations of these components results in different values of DU, for the same distortion. Therefore, Cini's multiplet expansion may give different U values because he included different 2s + 1L multiplet components, whereas

Houston et al utilized just the 3 (rr, rp, and pp) components . The DU's reported in Table 3 are interpreted as Uegg-Uegg', i.e. appropriate for group or cluster orbitals as discussed above, and the values obtained by Houston et al are reasonable in this context. I am not certain what the U's reported by Cini represent? Furthermore, it is not clear from Cini's paper whether he included the two-center hole-hole repulsions, U12, and these obviously have a signficant effect on DU. The original Cini expression ignored all U12's within the Hubbard model (eq. 6). In any event, more theoretical work needs to be done here to fundamentally understand the U parameters obtained for highly covalent systems.

c. Molecules

The application of the Cini expression to the empirical DOS for molecules is another approximation requiring further justification. This is problematic since the empirical DOS contain the vibrational broadening which has nothing to do with the correlation problem. However, vibrational broadening is also present in the empirical DOS for solids: it just is not as evident since banding effects dominate. Extended covalent solids contain banding effects which also do not dictate the correlation. To illustrate this, let us compare the DOS for benzene with that for graphite. The local sp^2 bonding around each C atom is essentially the same and this is reflected in the similar gross features in the DOS as shown in Fig. 6. The small differences arise because vibrational effects dominate in benzene while banding effects (i.e. second, third etc nearest neighbor interactions) dominate for graphite. However, the principal correlation effects are determined by the local bonding. Thus neither the extended banding effects in graphite nor vibrational effects in benzene (both broaden the major DOS features) determine the correlation distortion. It has been shown that the Cini expression mimics the effects of a configuration interaction for molecules. Thus, we intuitively expect that the Cini expression has comparable validity for

molecules and covalent solids. This is true provided the separation, ΔE, between the molecular levels is small compared with the vibrational broadening, ΔV. This does appear to be true for the molecules such as benzene, hexane, and larger molecules, but may not be appropriate for ethylene, etc. involving three or less carbon atoms. In these smaller molecules, multiplets are also more important, so that this approach is certainly not completely satisfactory for these small molecules.

We know that the Cini expression will continue to be used on a wide variety of systems; even in the event of some progress in developing a theory for unfilled and degenerate bands. But much further work is needed to learn of its limitations and validity for a wider variety of materials.

F. Expanding the Applications

Most Auger line shape interpretations to date have been on homogeneous solids, molecules, or at least on well characterized surfaces. And most interpretation schemes in the past require a one-electron DOS, which is then utilized to generate a self-fold for insertion into the Cini expression. The DOS are normally obtained empirically as described above. But the future will demand a study of more complex practical systems. Recent examples of Auger line shape interpretations on more complex systems include studies of explosives[345,346] semiconductors such as TCNQ[347], conducting polymers such as Fe-doped polyacetylene and polypyrroles,[348] electrode surfaces,[349,350] metal clusters,[351,352] petroleum shales,[353] sputtered stainless steel-carbon composite layers,[354] C implanted metals for hardening purposes,[355] surface segregation,[356,357] grain boundary segregation,[358,359] and on vanadium oxide bronzes (e.g. $Na_{0.33}V_2O_5$)[360]. Reviews on the impact of AES on technology,[361,362] electroplating,[363] and ceramics and glasses,[364] have been published recently. As the technology moves to more complex "engineered"

inhomogeneous materials such as multi-elemental alloys, composites, matrices, high temperature superconductors, and interfaces, AES is going to be increasingly useful because of its ability to sample a site or element specific local DOS. Thus, the future of AES is bright, but the theory must advance to be able to handle these increasingly complex systems. Much work remains to be done.

ACKNOWLEDGEMENTS

This work has been funded in part by the Office Of Naval Research. The author gratefully acknowledges help with the references from Mr. Fred Hutson, and thanks Dr. Noel Turner for a careful reading of the manuscript.

1. American Society for Testing and Materials standard practice for elemental identification by Auger electron spectroscopy (E827-88), SIA, Surf. Interface Anal. 14, 419, 1988.

2. Mizokawa, Y., Miyasato, T., Nakamura, S., Geib, K.M. and Wilmsen, C.W., Comparison of the C KLL first derivative Auger spectra from XPS and XES using diamond, graphite, SiC and diamond-like carbon films, Surf. Sci. 182, 431, 1987; The C KLL first derivative XPS spectra as a fingerprint of the carbon state and the characterization of diamondlike carbon films, J. Vac. Sci. Technol. A5, 2809, 1987.

3. Hass, T.W., Grant, J.T. and Dooley III, G.J., Chemical effects in Auger electron spectroscopy, Appl. Phys. 43, 1853, 1972.

4. Bader S.D., Richter L., and Brodsky M.B., Silicon $L_{23}VV$ Auger line shapes and oxygen chemisorption study of Pd_4Si, Solid State Commun., 37, 729, 1981.

5. Thomas, T.D., Extra-atomic relaxation energies and the Auger parameter, J. Elect. Spectrosc. Related Phenom. 20, 111, 1980.

6. Wagner, C.D., Zatko, D.A., Raymond, R.H., Use of the oxygen KLL Auger lines in identification of surface chemical states by electron spectroscopy for chemical analysis, Anal. Chem. 52, 1445, 1980.

7. Wagner, C.D., Pasolj, D.E., Hillery, H.F., Kinisky, T.G., Zix, H.A., Jansen, W.T. and Taylor, J.A., Auger and photoelectron line energy relationships in aluminum-oxygen and silicon-oxygen compounds, J. Vac. Sci. Technol. 21, 933, 1982.

8. Wagner, C.D. and Taylor, J.A., Screening energy involving electrons of remote atoms in photoelectric and Auger transitions, J. Vac. Sci. Technol. A1, 430, 1983: Contributions to screening in the solid state by electron

systems of remote atoms: effects on photoelectron and Auger transitions. J. Vac. Sci. Technol. 28, 211. 1982.

9. Moretti, G. and Porta, P., Auger parameter and chemical state plots for copper- and zinc- containing compounds: charge distribution and screening effects, J. Phys: Condens. Matter. 1989, Suppl. B, 193, 1989.

10. Moretti, G., Cimino, A., Minelli, G. and DeAngelis, B.A., Ionic character of the Mg-O bond in oxide solid solutions studied by the Auger parameter, J. Electron Spectrosc. Related Phenom. 40, 85, 1986.

11. Thomas, T.D. Weightman, P. Valence electronic structure of Au-Zn and Zu-Mg alloys derived from a new way of analyzing Auger-parameter shifts Phys. Rev. B33, 5406, 1986.

12. Lynn, L.C. and Opila, R.L., Chemical shifts in the MNN Auger spectra of Cd, In, Sn, Sb, and Te, SIA, Surf. Interface Anal. 15, 180, 1990.

13. I.F. Ferguson, Auger Microprobe Analysis, Adam Hilger, United Kingdom. 1989.

14. Cubiotti, G., Mondio, G. and Wandelt, K., editors, Auger Spectroscopy and Electronic Structure, Springer-Verlag, Berlin, 1988.

15. Briant, C.L. and Messmer, R.P., Auger Electron Spectroscopy, Treatise on Materials Science and Technology, 30, Academic Press, Inc. San Diego. 1988.

16. Ramaker, D.E., Bonding information from Auger spectroscopy, Applic. Surf. Sci. 21, 1, 1985.

17. Ramaker, D.E., Chemical effects in the carbon KVV Auger line shapes, J. Vac. Sci. Technol. A7, 1614, 1989.

18. Jennison D.R., Understanding core-valence-valence Auger line shapes, J. Vac. Sci. Technol. 20, 548. 1982: Auger line shape analysis of molecules and solids, J. Vac. Sci. Technol. 17, 172, 1980.

19. Turner, N.H., Surface Analysis: x-ray photoelectron spectroscopy and Auger electron spectroscopy. Anal. Chem. Revs. 1988. 377R, 1988; 1990, 113R, 1990; Turner, N.H. and Colton, R.J., Surface Analysis, x-ray, photoelectron, Auger, and secondary ion mass spectroscopy, Anal. Chem. Rev. 1982. 293R, 1982.

20. Seah, M.D. Auger Electron Spectroscopy. National Physical Laboratory, report DMA(A) 40, Feb., 1982.

21. Levenson, L.L., Fundamentals of Auger electron spectroscopy, Scan. Elect. Micros. 1983/IV, 1643, 1983.

22. Holloway, P.H., Fundamentals and applications of Auger electron spectroscopy. Adv. Elect. Elect. Phys. 54, 241, 1980.

23. Madden, H.H., Chemical information from Auger electron spectroscopy. J. Vac. Sci. Technol. 18, 677, 1981.

24. Fuggle, J.C., High resolution Auger spectroscopy of solids and surfaces, in Electron Spectroscopy: Theory, Techniques, and Applications, Vol. 4, ed. by C.R. Brundle and Baker, A.D., (Academic, NY, 1981), p.86.

25. Kleiman, G.G., X-ray excited Auger studies of metals and alloys. Applic. Surf. Aci. 11/12, 730, 1982..

26. Ingrey, S.I.J., Applications of Auger spectroscopy, Canadian J. Spect. 28, 73, 1983.

27. Martensson, N., Hedegard, P. and Johanson, B., Auger energy shifts for metallic elements, Phys. Scripta 29, 154, 1987.

28. Grant, J.T., Surface analysis with Auger electron spectroscopy. Applic. Surf. Anal. 13, 35, 1982.

29. Lundquist, S., Schrieffer, R. The relationship between spectroscopy and bonding. Phys. Scr. 34, 84, 1986.

30. Houston, J.E. Rye. R.R., Local electronic structure information in Auger electron spectroscopy: solid surfaces, p. 65 in Ref. Augbook.

31. Terryn, H., Vereecken, J. and Laudet, A., A new approach to the use of Auger line shape effect as a routine technique for characterization of chemical bonding. Appl. Surf. Sci. 24, 283, 1985.

32. Mroczkowski, S.J., The effect of electron transmission function on calculated Auger sensitivity factors, J. Vac. Sci. Technol. A7, 1529. 1989.

33. Argile, C. and Rhead, G.E., Adsorbed layer and thin film growth modes monitored by Auger electron spectroscopy, Surf. Sci. Rep. 10. 277. 1989.

34. Batchelor, D.R., Bishop, H.E. and Venables, J.A., Auger electron spectroscopy from elemental standards, II. Peak height and area. SIA. Surf. Interface Anal. 14. 700, 1989.

35. Ramaker D.E., Murday J.S. and Turner N.H., Extracting Auger line shapes from experimental data. J. Electron. Spectrosc. Related. Phenom. 17. 45, 1979.

36. Sickafus. E.N., A secondary emission analog for improved Auger spectroscopy with retarding potential analyzers. Rev. Sci Instr. 42. 933. 1971; Linearized secondary-electron cascades from the surfaces of metals I. Clean surfaces of homogeneous specimens. Phys. Rev. B116. 1436, 1977.

37. Matthew. J.A.D., Prutton, M., El Gomati, M.M. and Peacock, D.D., SIA. Surf. Inter. Anal. 11, 173. 1988.

38. Peacock. D.C., Fitting the inelastic tail below experimentally observed Auger peaks. Surf. Sci. 152/153, 895, 1985; Peacock D.C., Duraud. J.P., The shape of the background in AES: nonlinear features in Log N(E) v. Log E, SIA. Surf. Int. Anal. 8, 1. 1986.

39. Weiss, A., Mayer, R., Jibaly, M., Lei, C., Mehl, C. and Lynn, K.G., Auger electron emission resulting from the annihilation of core electrons with low energy positrons, Phys. Rev. 61, 2245, 1988.

40. Haak, H.W., Sawatzky, G.A. and Thomas, T.D., Auger photoelectron coincidence measurements in Copper, Phys. Rev. Lett. 41, 1825, 1978.

41. Bartynski, R.A.,Jenson, E., Garrison K. and Hulbert, S.L., Surface electronic structure of GaAS(111) studied by Auger-photoelectron coincidence spectroscopy, to be published.

42. Hulbert, S.L., Kao, C.C., Veinert, M., Bartynski, R.A., Yang, S., Jensen, E. and Zehner, D.M., A comparison of the surface electronic structure of Ta(100) and TaC(111) by Auger photoelectron coincidence spectroscopy, to be published.

43. Mularie, W.M. and Peria W.T., Deconvolution techniques in Auger electron spectroscopy, Surf. Sci. 26, 125, 1970.

44. Madden H.H. and Houston J.E., KVV Auger spectrum of oxidized lithium. J. Vac. Sci. Technol. 14, 412, 1977; Correction of distortions in spectral line profiles: applications to electron spectroscopies. J. Appl. Phys. 47, 3071, 1976.

45. Burrell, M.C. and Armstrong, N.R., A sequential method for removing the inelastic loss contribution from Auger electron spectroscopic data. Applic. Surf. Sci. 53, 1983.

46. Contini, V., Presilla, C. and Sacchetti, F., On the restoration of Auger line shapes. Surf. Sci. 210, 520, 1989.

47. Nesbesny, K.W. and Armstrong, N.R., Deconvolution of Auger electron spectra for line shape analysis and quantitation using a fast fourier transform algorithm, J. Elect. Spectrosc. Related Phenom. 37, 355, 1986.

48. Rosenberg. N., Tholomier, M. and Vicario, E., Background removal in Auger electron spectroscopy: a new experimental approach, J. Electron Spectrosc. Related Phenom. 46, 331, 1988.

49. Chornik. B.. Bishop. H.E., LeMoel, A. and LeGressus, C., Deconvolution in Auger electron spectroscopy, Scann. Elect. Microsc. 1, 77, 1986.

50. Maxchoff. B.L.. Nebesny, K.W., Zavadil, K.R., Fordemwalt, J.W., Armstrong. N.R., Quantitation of surface electron spectroscopies: problems in correct description of intrinsic line shape and extrinsic energy loss processes. Spect. Acta, B43, 535, 1987.

51. Tofterup. A.L.. Inelastic background subtraction formulas and energy spectra in XPS and AES, Surf. Sci. 227, 157, 1990.

52. Chattarji. D.. The Theory of Auger Transitions, Academic Press, NY. 1976, p. 192.

53. Rye. R.R.. Madey. T.E., Houston, J.E. and Holloway, P.H., Chemical-state effects in Auger electron spectroscopy. J. Chem. Phys. 69, 1504, 1978; Rye. R.R., Houston. J.E.. Jennison, D.R., Madey, T.E. and Holloway. P.H.. Chemical information from Auger spectroscopy. Ind. Eng. Chem. Prod. Res. Dev. 18. 2. 1979; Rye. R.R., Jennison. D.R., and Houston. J.E., Auger spectra of alkanes. J. Chem. Phys. 73, 4867, 1980; Molecular Auger spectroscopy. Accts. Chem Res. 17, 41, 1984; Houston J.E. and Rye. R.R., Auger electron spectra of cycloalkanes C_3-C_6, J. Chem Phys. 24. 71, 1981.

54. Liegener, C.M. Understanding hybridization effects in carbon Auger spectra. Phys. Rev. B41, 7185, 1990.

55. Lander, J.J.. Auger peaks in the energy spectra of secondary electrons from various materials. Phys. Rev. 91, 1382, 1953.

56. Hutson, F.L. and Ramaker, D.E., Identification of resonant excitation and shakeoff contributions to the C KVV Auger line shapes of several gas phase hydrocarbons. J. Chem Phys. 87. 6824, 1987.

57. Mattson R.A. and Ehlert, R.C., Carbon characteristic x-rays from gaseous compounds, J. Chem. Phys. 48. 5465, 1968.

58. Von Barth, U. Grossman, G., Dynamical calculations of x-ray absorption and emission spectra, Phys. Scripta, 21, 580, 1980: Static and dynamical effects of core holes in KLV Auger, SXE, and SXA of simple metals, Physica Scripta 28. 107, 1983; Dynamical effects in x-ray spectra and the final state rule, Phys. Rev. B25, 5150, 1982.

59. Mills, B.E. and Shirley, D.A., X-ray photoemission spectra of the 2s valence orbitals in cylic alkanes in relation to valence bands of amorphous group 4 and 5 elements, J. Am. Chem. Soc. 99, 5885, 1977.

60. Murday, J.S., Dunlap, B.I., Hutson, F.L., and Oelhafen, P., Carbon KVV Auger line shapes of graphite and stage-one cesium and lithium intercalated graphite, Phys. Rev. B24, 4764, 1981

61. Jorgensen, W.L. and Salem, L., The Organic Chemists Book of Orbitals. Academic Press, New York, 1973.

62. Jennison, D.R., Kelber, J.A. and Rye, R.R., Localized Auger final states in covalent systems, Phys. Rev. 25. 1384, 1982.

63 Binkley, J.S., Frisch, M., Raghavachari, K., Defrees, D., Schlegel, H.B., Whiteside, R., Fluder, E., Seeger, R. and Pople, J.A., Gaussian 82, Release H computer code, Carnegie-Mellon University, 1982.

64. Matthew, J.A.D., Comparison of Vibrational broadening in Auger and photoelectron spectroscopy, Phys. Rev. B29, 3031, 1984.

65. Dunlap, B.I., Mills, P.A, and Ramaker, D.E., Semi-empirical X_α calculation of the KVV Auger line shape of O_2, J. Chem. Phys. 75, 300, 1981.

66. Cini, M. and Andrea, A.D., Resonant broadening of quasi-atomic Auger spectra by elementary excitations, J. Phys. C 41, 4469, 1983.

67. Gunnarsson, O. and Schonhammer, K., Dynamical theory of Auger processes, Phys. Rev. B22, 3710, 1980; Interference effects in Auger electron spectroscopy, Phys. Rev. B23, 4350, 1980; One-step description of XPS and Auger processes, Phys. Scripta T1, 115, 1982.

68. Wen-Kai Shumg, K. and Langreth, D.C., Dynamical KLL Auger process in simple metals and their plasmon gain satellites, Phys. Rev. B28, 4976, 1983.

69. Fuggle, J.C., Lasser, R., Gunnarsson, O. and Schonhammer, K., Plasmon gains as a monitor of incomplete relaxation, interference effects and the transition from sudden to adiabatic limits in electron spectroscopies, Phys. Rev. Lett. 44, 1090, 1980.

70. Cini, M. Theory of the Auger effect in solids: plasmon effects in electron spectroscopies of valence states, Phys. Rev. B17, 2486, 1978.

71. Cini, M., Maracci, F. and Platania, R., On the silicon CVV spectra of tetramethylsilane and other molecules in the gas phase, p180 in Augconf.

72. Aksela, H. and Aksela, S., Recent developments in Auger spectroscopy of free atoms. J. Phys Colloque C9, Supple 12, 48, 565, 1987.

73. Aksela, S., Pekkala, T., Aksela, H., Wallenius, M. and Harkoma, M., Free-iron group atoms Fe, Co, and Ni studied by the $L_{23}M_{45}M_{45}$ Auger process. Phys. Rev. A35, 1426, 1987; Aksela, H., Aksela, S., Pekkala, T. and Wallenius, M., Electronic structure of free nickel atoms studied by the $L_{23}MM$ Auger decay, Phys. Rev. A35, 1522, 1987.

74. Aksela, H., Aksela, S., Pulkkinen, H. and Yagishita, A., Shake processes in the Auger decay of resonantly excited $3d^9 4s^2 4s^2 np$ states of Kr, Phys. Rev., A40, 6275, 1989.

75. Aksela, H., Aksela, S., Pulinen, H., Kivimaki, A. and Sairanen, O.P., Shake processes in Auger decay of resonantly excited states of rare gases, Phys. Scr. 41, 425, 1990.

76. Dayan, M. and Pepper, S.V., Study of the Auger line shape of polyethylene and diamond, Surf. Sci. 138, 549, 1984; Pepper, S.V., Electron spectroscopy of the diamond surface, Appl. Phys. Lett. 38, 344, 1981.

77. Siegbahn, K., ESCA Applied to Free Molecules, North Holland Publ. Co. New York, 1969, p. 103.

78. Cini, M., Density of states of two interacting holes in a solid; Solid State Commun. 20, 605, 1976; Two hole resonances in the XVV Auger spectra of solids, Solid. State Commun. 20, 681, 1977; Comment on quantitative Auger spectra in narrow band metals, Phys. Rev. B17, 2788. 1978.

79. Sawatzky GA. Quasiatomic Auger spectra in narrow band metals, Phys. Rev. Lett. 39. 504, 1977; Sawatzky, G.A. and Lenselink. A., Auger line shape in narrow-band metals, Phys. Rev. B21, 1790. 1980.

80. Hutson, F.L. and Ramaker, D.E., Identification of satellites due to resonant excitation and shakeoff in the C KVV Auger line shape of polyethylene, Phys. Rev. B35, 9799, 1987.

81. Houston, J.E., Rogers, J.W., Rye, R.R., Hutson, F.L., and Ramaker, D.E., Relationship between the Auger line shape and the electronic properties of graphite, Phys. Rev. B34, 1215, 1986.

82 Ramaker, D.E. and Hutson. F.L., Direct experimental evidence for antiferromagnetic spin ordering on the (111) - (2 x 1) surface of diamond, Solid State Commun. 63, 335, 1987.

83. Ramaker, D.E., A Final State Rule for Auger Line shapes. Phys. Rev. B25. 7341, 1982.

84. Jennison, D.R., Madden, H.H. and Zehner D.M., Initial state screening effects in metal Auger spectra: boron carbide, Phys. Rev. B21, 430, 1980.

85. Almbladh, C.O., Morales, A.L. and Grossmann, G., Theory of Auger core-valence-valence processes in simple metals. I. Total yields and core-level lifetimes widths, Phys. Rev. B39, 3489, 1989.

86. McGuire, E.J., K-shell Auger transition rates and fluorescence yields for elements Be-Ar, Phys. Rev. 185 1, 1969: K-shell Auger transition rates and fluorescence yields for elements Ar-Xe, Phys. Rev. A2, 273, 1970; L-shell Auger and Koster-Kronig electron spectra, Phys. Rev. A3, 1801, 1971.

87. Walters, D.L. and Bhalla, C.P., Non-relativistic Auger rates, x-ray rates, and fluorescence yields for the K-shell, Phys. Rev. A3, 1919, 1971: Non-relativistic K-shell Auger rates and matrix elements for $4 \leq Z \leq 54$, At. Data 3, 301, 1971: Nonrelativistic Auger rates, x-ray rates and fluorescence yields for the 2p shell, Phys. Rev. A4, 2164, 1971.

88. Chen, M.H., Laiman, E., Crasemann, B., Aoyagi, M. and Mark, H., Relativistic L-shell Auger and Coster-Kronig rates and fluorescence yields. Phys. Rev. A19, 2253, 1979.

89. Chen, M.H. and Crasemann, B., K-LL Auger transition probabilities for elements with low and intermediate atomic numbers, Phys. Rev. A8, 7. 1973: Relativistic radiationless transition probabilities for atomic K- and L-shells, Atomic Data and Nuclear Data Tables 24, 13, 1979; Chen, M.H., Crasemann and B., Mark, H., Relativistic K-shell Auger rates, level widths, and fluorescence yields. Phys. Rev. A21, 436, 1980; Widths and fluorescence yields of atomic L-shell vacancy states, Phys. Rev. A24, 177, 1981.

90. Bambynek, W., Crasemann, B., Fink, R.W., Freund, H.U., Mark, H., Swift, C.D., Price, R.E. and Rao, P.V., X-ray fluorescence yields, Auger, and Coster-Kronig transition probabilities, Rev. Mod. Phys. 44, 716, 1972.

91. Colle, R., Simonucci, S., The continuum orbital problem in the calculation of Auger decay rates: application to neon, Nuovo Cim. Soc. Ital. Fis., D11, 1587, 1989.

92. McGuire, E.J., Research Report SC-RR-69-139, Sandia Laboratories, 1969.

93. Ramaker, D.E., Hutson, F.L., Turner, N.H. and Mei, W.N., Charge transfer, polarization, and relaxation effects on the Auger line shapes of Si, Phys. Rev. B33, 2574, 1986.

94. Ramaker, D.E., Auger Spectroscopy as a Probe of Valence Bonds and Bands, in Chemistry and Physics of Solid Surfaces IV, Vanselow R and Howe R, eds., Springer, Berlin, 1982, p. 19-49.

95. Chen, M.H. and Crasemann, B., X-ray and Auger transition probabilities to the 2p level of multiply ionized sulfur and chlorine, Phys. Rev. A16, 1495, 1977.

96. Chen, M.H., Crasemann, B. and Mark, H., Relativistic KLL Auger spectra in the intermediate coupling scheme with configuration interaction, Phys. Rev. A21, 442, 1980.

97. Chen, M.H., Effects of relativity and correlation on LMM Auger spectra, Phys. Rev. A31, 177, 1985.

98. McGuire, E.J., Configuration interaction effects on the L and M Auger spectra of Cu and Zn, Phys. Rev. A16, 2365, 1977.

99. Vayrynen, J., Differences in $L_{23}MM$ Auger electron spectra of atomic and metallic manganese, J. Elect. Spectrosc. Related Phenom. 22, 27, 1981.

100. Cubiotti, G., Comments on the relationship between Auger line shapes and local electronic structure, in Ref. Augconf, p. 51.

101. Ramaker, D.E., Final state correlation effects in Auger line shapes: application to silicon dioxide, Phys. Rev. B21, 4608, 1980.

102. Dunlap, B.I., Hutson, F.L., and Ramaker, D.E., Auger line shapes of solid surfaces - atomic, band-like, or something else?, J. Vac. Sci. Technol. 18, 556, 1981.

103. Vayrynen, I.J., Leiro, J.A. and Heinonen, M.H., Auger electron spectra of Ca metal and CaO, J. Electron Spectrosc. Related Phenom. 51, 555, 1990.

104. Ramaker, D.E., White, C.T. and Murday, J.S., On Auger induced decomposition/ desorption of covalent and ionic systems, Physics Letters 89A, 211, 1982; Auger Induced desorption of covalent and ionic systems, J. Vac. Soc. Technol. 18, 748, 1981.

105. Knotek, M.L. and Feibelman, P.J., Ion desorption by core-hole Auger decay, Phys. Rev. Lett. 40, 964, 1978.

106. Vos, M., van der Marel, D. and Sawatzky, G.A., Auger line shapes in alloys, Phys. Rev. B29, 3073, 1984.

107. Aksela, S., Aksela, H., Vuontisjarvi, M., Vayrynen, J. and Lahteenkorva, E., Solid state effect in the $M_{45}N_{45}N_{45}$ Auger electron spectrum of cadmium, J. Electron Spectrosc. Relat. Phenom. 11, 137, 1977.

108. Weightman, P., Wright, H., Waddington, S.D., van der Marel, D., Sawatzky, G.A., Diakun, G.P. and Norman, D., Local lattice expansion around Pd impurities in Cu and its influence on the Pd density of states: an extended x-ray-absorption fine-structure and Auger study, Phys. Rev. B36, 9098, 1987.

109. Balzarotti, A., De Crecenzi, M., Messi, R., Motta, N. and Patella, F., Correlation effects on the L_3VV Auger line shape of $Cd_{1-x}Mn_xTe$. Phys. Rev. B36, 7428, 1987.

110. Painter, P.S., Ellis, D.E. and Lubinksy, A.R., Ab-initio calculations of the electronic structure and optical properties of diamond using the discrete variational method. Phys. Rev. B4, 3610, 1971.

111. Madden, H.H., Auger line shape analysis. Surf. Sci. 126, 80, 1983.

112. Hanke, G. and Mueller, K., Low energy Auger transitions of boron in several boron compounds, J. Vac. Sci. Technol. A2, 964, 1984.

113. Rye, R.R. and Houston, J.E., Auger spectra of tetrahedral halides and hydrides. J. Chem. Phys. 78, 4321, 1983.

114. Hutson, F.L., Ramaker, D.E., Dunlap, B.I., Ganjei, J.D. and Murday, J.S., Interpretation of the N KVV Auger line shape from alkali metals nitrates. J. Chem. Phys. 76, 2181, 1982.

115. Houston, J.E., Moore, G., Lagally, M.G., Transition density of states for Si(100) from $L_1L_{23}V$ and $L_{23}VV$ Auger spectra. Solid State Commun. 21, 879, 1977.

116. Barrie, A and Street, F.J., An Auger and x-ray photoelectron spectroscopic study of sodium metal and sodium oxide. J. Elect. Spectrosc. Related Phenom. 7, 1, 1975.

116. Lasser, R., and Fuggle, J.C., Screening effects in the KLV Auger spectra of Na, Mg, Al, and Si. Phys. Rev. B22, 2637, 1980.

118. Weightman, P., Davies, P., and Inglesfield, J.E., Determination of the region of the local density of states of magnesium that is probed by core-core-valence Auger transitions, Phys. Rev. B34, 6834, 1986,

119. Kortboyer, S.W., Grioni, M., Speier, W., Zeller, R., Watson, L.M., Gibson, M.T., Schafers, F., and Fuggle, J.C., Core hole effects on electronic structure: Al in AlNi, J. Phys.:Condens. Matter 1, 5981, 1989.

120. Davies, M., Weightman, P., and Jennison, D.R., Hybridisation effects on the Mg $KL_{23}V$ Auger spectra of MgNi, MgCu, MgZn, MgPd, and MgAg Alloys, Phys. Rev. B29, 5318, 1984.

121. Davies, M. and Weightman, P., Hybridization and screening effects in the Mg KL_1V Auger spectra of Mg-Ni, Mg-Cu, Mg-Zn, Mg-Pd, Mg-Ag, and Mg-Al alloys, Phys. Rev. B30, 4183, 1984.

122. Hannah, P.H., Weightman, P., and Andrews, P.T., The screening of core holes in Al-Mg alloys studied by a comparison of KL_1V and $KL_{23}V$ Auger spectra, Phys. Rev. B31, 6238, 1985.

123. Davis, G.D. and Lagally, M.G., Measurement of valence band Auger spectra for GaAs(11) from Ga and As CCV transitions, J. Vac. Sci. Technol. 15, 1311, 1978.

124. Childs, K.D. and Lagally, M.G., Species-specific densities of states of Ga and As in the chemisorption of oxygen on GaAs(110), Phys. Rev. B30, 5742 (1984).

125. Childs, K.D. and Lagally, M.G., Species-specific densities of states of Ga and As in the chemisorption of CO and C on GaAs(11), J. Vac. Sci. Technol. A3, 1024, 1985.

126. Brockman, R.H. and Russel, G.J., Transition density of states for cleaved and excited-oxygen exposed surfaces of Ge(111) derived from the $M_{23}M_{45}V$ Auger transition, Applic. Surf. Sci. 22/23, 173, 1985.

127. Davies, G.D., Viljoen, P.E., and Lagally, M.G., Comparison of site-specific valence band densities of states determined from Auger spectra and XPS-determined valence band spectra in GeS(001) and GeSe(001), J. Electron Spectrosc. Related Phenom. 21, 135, 1980.

128. Treglia, G., Desionqueres. M.C., Ducastelle, F. and Spanjard. D., Correlation effects on Auger spectra in unfilled d bands metals. J. Phys. C14, 4347 (1981).

129. Andrews, P.T., Collins. T., and Weightman. P., The influence of the number of unoccupied 3d states on the $L_3M_{45}M_{45}$ Auger spectrum of Ni. J. Phys. C, 14. L957, 1981.

130. Andrew, P.T., Collins, T. and Weightman. P., The application of the Cini model to the $L_3M_{45}M_{45}$ Auger spectra of copper alloys. J. Phys. C: Solid State Phys. 19, 435, 1986.

131. Drchal, V. and Kudrnovsky, J., Theory of the Auger spectra of narrow band metals with impurities. Phys. Stat. Sol. 108. 683. 1981: Theory of Auger spectra of disordered alloys, Phys. Stat. Sol. 114. 627. 1982: The theory of the impurity Auger spectrum; the generalized Wolff-Clogston model. Czech. J. Phys. B32, 108, 1982.

132. Yasuda. H. Nakayama. H. and Fujita, H., Electronic structures localized at the boron atom in amorphous iron-boron and iron-boron-phosphorous alloys. Jpn. J. Appl. Phys. 28, 2234, 1989.

133. Bevolo. A.J. and Drehman. A.J., Auger and electron energy loss study of the electronic structure of U-M(M=Fe.Co.Ni) metallic glasses. J. Vac. Sci. Technol. A4. 1589. 1986.

134. Knapp. B.J., Hansen, J.C., Wagner, M.K., Clendening. W.D. and Tobin. J.G., Occupied electronic structure of gold and silver on germanium(111). Phys. Rev. B40. 2814. 1989.

135. Bevolo, A.J. Electronic structure of a uranium platinum compound (UPt_3) and a uranium beryllium compound (UBe_{13}): an Auger and electron energy loss study. J. Less-Common Met. 153. 101. 1989.

136. Weightman, P., Wright, H., Waddington, S.D., vanderMarel D., Sawatzky, G.A., Diakun, G.P. and Norman, D., Local lattice expansion around Pd impurities in Cu and its influence on the Pd density of states: an extended x-ray absorption fine structure and Auger study, Phys. Rev. B36, 9098, 1987.

137. Vos, M., Sawatzky, G.A., Davies, M., Weightman, P. and Andrews, P.T., Impurity Auger spectra: a probe of the local impurity density of states and the impurity electron-electron interactions, Solid State Commun. 52, 159, 1984; Comment on "Theory for the anomalous $M_{45}VV$ Auger spectrum for dilute palladium in silver", Phys. Rev., Lett. 54, 1334, 1985.

138. Hannah, P.H. and Weightman, P., The density of states of Ag impurities in Cd determined by Auger and photoelectron spectroscopy, J. Phys. F: Met. Phys. 16, 1015, 1986.

139. van der Marel, D., Westra, C., Sawatzky, G.A. and Hillebrecht, F.U., Electronic structure of Mn impurities in noble metals, Phys. Rev. B31, 1936, 1985.

140. Cubiotti, G., Mondio, G., Sacchetti, F., and Wandelt, K., A study of the XVV Auger line shape of Fe-Ni alloys, Nuovo Cimento 7, 513, 1986; Cubiotti, G. and Sacchetti, F., XVV Auger and APS spectra of Fe-Ni alloys, Applic. Surf. Sci. 22/23, 168, 1985.

141. Almbladh, C.O. and Morales, A.L., Theory of Auger core-valence-valence processes in simple metals: II. dynamical and surface effects on Auger line shapes, Phys. Rev. B39, 3503, 1989.

142. Vidal, R., Passeggi, M.C.G., Goldberg, E.C. and Ferron, J., Extended Huckel cluster calculations of the $L_{23}VV$ Auger transition in Silcon, Surf. Sci. 201, 97, 1988.

143. Jennison, D.R., Auger electron spectroscopy as a local probe of atomic charge: Si $L_{23}VV$, Phys. Rev. Lett. 40, 807, 1978; Energy band theory of

Auger line shapes: silicon $L_{23}VV$ and lithium KVV, Phys. Rev. B18, 6865, 1978.

144. Davies, M., Jennison, D.R. and Weightman, P., Band structure and screening effects on the KVV and $L_{23}VV$ Auger spectra of metallic Mg, Phys. Rev. 29, 5313, 1984.

145. Contini, V., Presilla, D. and Sacchetti, F., CVV Auger line shapes in aluminum, Solid State Commun. 70, 851, 1989.

146. Feibelman, P.J., McGuire, E.J., and Pandey, K.C., Theory of valence band Auger line shapes. Phys Rev. B15, 2202, 1977; Feibelman, P.J. and McGuire, E.J., Valence band Auger line shapes for Si surfaces: simplified theory and corrected numerical results, Phys. Rev. B17, 690, 1978.

147. Kunjunny, T. and Ferry, D.K., The (100) silicon-silicon dioxide interface. I. theoretical energy structure, Phys. Rev. B24, 4593, 1981.

148. Gadzuk, J.W., Valence-band Auger-electron spectrum for aluminium, Phys. Rev. B9, 1978, 1974.

149 Fitchek, J. and Bose, S.M., Life-time and surface effects on the $L_{23}VV$ Auger spectra of aluminum, Phys. Lett. 54A, 460, 1975.

(?)(?)

150. Woicik, J.C., Pate, B.B. and Pianetta, P., Silicon (111) 2x1 surface states: K-edge transitions and surface-selective $L_{23}VV$ Auger line shape, Phys. Rev. B39, 8593, 1989.

151. Contini, V., Presillo, C. and Sacchete, F., Surface effects in Si Auger spectra. Phys. Rev. Lett. 64, 1844, 1990; Durbin, S.M. and Gog, T., Durbin and Gog reply, Phys. Rev. Lett. 64, 1845, 1990.

152. Schulman, J.N. and Dow, J.D., Many-body contributions to the Auger line shapes of free-electron metals, Phys. Rev. Lett. 47, 371, 1981.

153. Davis, L.R. and Dow, J.D., Rule of corresponding Auger spectra, Solid State Commun. 50, 7, 1984.

154. Sasse, A.G.B.M., Wormeester, H., Van der Hoef, M.A., and van Silfout, A., Transition density of states (TDOS) of the Si(100) 2x1 surface derived from the $L_{23}VV$ Auger line shape compared with cluster calculations, Surf. Sci. 218, 553, 1989; The influence of the 2x1 reconstruction of the Si(100) surface on the Si $L_{23}VV$ Auger line shape. Solid State Commun. 71, 65, 1989.

155. Nelson, A.J., Burnham, N.A., Schwartzlander, A.B., Asher, S.E. and Kazmerski, L.L., Auger analysis of Si-H bonding and H concentration in hydrogenated amorphous Si. J. Vac. Sci. Technol. A4, 1570, 1986.

156. Rye, R.R. and Houston, J.E., Auger spectra of methyl cyanide and related compounds. J. Chem. Phys. 75, 2085, 1981.

157. Aksela, S., Kellolumpu, M. and Harkoma, M., Study of $L_{23}M_{45}M_{45}$ Auger spectra of Zn and Cu in molecular $ZnCl_2$ and $CuCl_3$ vapours. J. Elect. Spectrosc. Related Phenom. 32, 177, 1983.

158. Liegener, C.M., Calculations on the Auger spectrum of F_2. Phys. Rev. A28, 256, 1983; Improved calculations on the outer valence Auger spectrum of F_2. J. Chem. Phys. 79, 2924, 1983.

159. Gutsev, G. L., A comparison of results of calculations by various methods on the KVV Auger spectra of the CO molecule, Mole. Phys. 57, 161, 1986.

160. Ohrendorf, E., Koeppel, H., Cederbaum, L.jS., Trantelli, F. and Sgamellotti, A., On the Auger spectrum of ethylene, J. Elect. Spectrosc. Related Phenom. 651, 211, 1990.

161. Stucky, G.D., Rye, R.R., Jennison, D.R. and Kelber, J.A., Auger line shape studies of the bonding in transition metal carbonyls and nitrosyls. J. Amer. Chem. Soc. 104, 595, 1982; Jennison, D.R., Stucky, G.D., Rye, R.R. and

Kelber, J.A., Analysis of transition metal carbonyl Auger line shapes. Phys. Rev. Lett. 46, 911, 1981.

162. Ortiz, J.V., Qualitative propagator theory of AX_4 Auger spectra. J. Chem. Phys. 81, 5873, 1984.

163. Gutsev, G., Electronic structure and N KVV Auger spectrum of ammonium radical, Teor. Eksp. Khim. 21, 10, 1985.

164. Korshak, V.V., Kudryavtsev, Y.P., Khvostov, V.V., Guseva, M.B. and Babaev, V.B., Study of carbyne electronic structure by the Auger spectroscopy. Dokl. Akad. Nauk SSSR. 280, 402, 1985; Electronic structure of carbynes studied by Auger and electron energy loss spectroscopy. Carbon, 25, 735, 1987.

165. Suoninen, E.J., Thomas, T.D., Anderson, S.E., Runyan, M.T. and Ungier, L., An XPS-AES study of gaseous xanthates and related sulfur-containing compounds. J. Electron. Spectrosc. Related Phenom. 35, 259, 985.

166. Wannber, B., Svensson, S., Keane, M.P., Karlsson, L. and Baltzer, P., Isotope effects in the Auger electron spectra of HBr and DBr. Chem. Phys. 133, 281, 1989.

167. Liegener, C.M., Calculation of the Auger spectra of clusters modelling solid hydrogen fluoride, Phys. Stat. Sol. B156, 441, 1989.

168. Carroll, T.X., Ji, D., and Thomas, T.D., Carbon and Oxygen KLL and Sulfur LMM Auger spectra of OCS. J. Electron. Spectrosc. Related Phenom. 51, 471, 1990.

169. Fournier, P.G., Eland, J.H.D., Millie, P., Svensson, S., Price, S.D., Fournier, J., Comtet, G., Wannbert, B., Karlsson, L., Experimental and theoretical studies of the doubly charged dioxonitrogen (NO_2^{2+}) ion. J. Chem. Phys. 89, 3553, 1988.

170. Rye. R.R., Jennison, D.R. and Houston, J.E., The calculation of molecular and cluster Auger spectra. Chem Phys. Lett. 69, 435, 1980.

171. Higashi. M., Hiroike. E. and Nakajima, J., Calculations of the Auger transition rates in molecules. I. Effects of the nonspherical potential application to CH_4, Chem. Phys. 68, 377, 1982.

172. Ortenburger. I.B. and Bagus. P.S., Theoretical analysis of the Auger spectra of CH_4, Phys. Rev. A11, 1501, 1975.

173. Hillier, I.H. and Kendrick, J., Configuration interaction calculations of the Auger spectrum of methane. hydrogen fluoride. water. and carbon monoxide. Mol Phys. 31, 849, 1976; Kvalheim, O.M., Final state correlation effects on the Auger transition rates of methane, Chem. Phys. Lett. 86. 159. 1982.

174. Agren. H., On the interpretation of molecular valence Auger spectra. J. Chem. Phys. 75. 1267. 1981; Agren, H. and Siegbahn, H., Semi-internal correlation in the Auger electron spectrum of H_2O, Chem. Phys. Lett. 69. 424. 1980.

175. Jennison,D.R., Kelber. J.A. and Rye R.R., Configuration interactions effects in molecular Auger decay rates, Chem. Phys. Lett. 77. 604. 1981: Jennison. D.R., Initial-state relaxation effects in molecular Auger spectra. Phys. Rev. A23, 1215, 1981.

176. Kvalheim, O.M. and Faegri, K., Correlation effects in the Auger spectra of hydrogen fluoride and neon, Chem. Phys. Lett. 67, 127. 1979; Final-state correlation effects on the Auger transition rates of methane. Chem. Phys. Lett. 86. 159. 1982.

177. Liegener, C.M., Calculations on the Auger spectrum of ethylene and acetylene. Chem Phys. 92. 97. 1985.

178. Tarantelli. F., Sgamellotti. A., Cederbaum. L.S. and Schirmer. J., Theoretical investigations of many dicationic states and the Auger spectrum. J. Chem., Phys. 86. 2201. 1987.

179. Larkins, F.P., Semi-empirical Auger electron energies. I. General method and K-LL line energies. J. Phys. B9, 47. 1976.

180 Larkins. F.P., Interpretation of the Auger electron spectra of nitrous oxide. J. Chem Phys. 86. 3239. 1987.

181. Carlson. T.A., The nature of secondary electrons created as the result of electron shakeoff and vacancy cascades. Radiat. Res. 64. 53. 1975: Carlson TA, Nestor Jr. CW, Tucker TC, and Malik FB., Calculation of electron shakeoff for elements from Z=2 to 92 with use of self consistent field wavefunctions, Phys. Rev. 169, 27, 1968.

182. Ramaker. D.E. and Murday. J.S., Factors contributing to the Si $L_{23}VV$, Si $L_1L_{23}V$ and O KVV Auger line shapes in SiO_2. J. Vac. Sci. Technol. 16. 510. 1979.

183. Kamath. P.V., Prabhaharan, K., Rao. C.N.R., An investigation of molecules adsorbed on transition metals by Auger electron spectroscopy. Indian J. Phys. 60B. 84, 1986.

184. Chesters. M.A., Hopkins. B.L., Taylor, P.A., and Winton. R.I., Decomposition of ethylene on W(100) studied by Auger spectroscopy. Surf. Sci. 83, 181. 1979.

185. Chesters, M.A. and Linder, D.R., Study of the adsorption of acetylene on Cu(100) using Auger electron spectroscopy, Stud. Surf. Sci. Catal. 48. 249. 1988.

186. Katayama.Y., Kobayashi, K.L.I. and Shiraki. Y., Interatomic Auger transition spectroscopy as a probe for the study of O_2 and CO adsorption on Al. Surf. Sci. 86. 549, 1979.

187. Chesters, M.A. and Lennon, D., Adsorption of carbon tetrachloride on Ni(111), Stud. Surf. Sci. Catal. 48, 263, 1989.

188. Hwang, S.Y., Kong, A.C.F. and Schmidt, L.D., Surface chemistry of carbon-nitrogen bonds on Rh(111). II. Nitromethane and nitroethane, J. Phys. Chem. 93, 8334, 1989.

189. Netzer, F.P. and Matthew, J.A.D., Auger spectra of CO, C_2H_4, C_2N_2, and C_6H_6 adsorbed on Pt(111), J. Electron Spectrosc. Relat. Phenom. 16, 359, 1979.

190. Johnson, P.D., Farrell, H.H. and Smith, N.V., Carbon KVV Auger spectroscopy using a plane-grating monochromator at the National Synchrotron Light Source, Vacuum 33, 775, 1983.

191. Laramore, G.E., Model calculations for the C(KVV) and O(KVV) Auger transitions for CO on Ni(100), J. Vac. Sci. Technol. A3, 1618, 1985.

192. Koel, B.E., White, J.M. and Loubriel, G.M., C(KVV) Auger line shape of chemisorbed CO, J. Chem. Phys. 77, 2665, 1982.

193. Baker, M.D., Channing N.D.S. and Chesters, M.A., Auger spectra of CO chemisorbed on Pt(111) and Cu(111), Surf. Sci. 111, 452, 1981.

194. Netzer, F.P., Auger line shape analysis for characterization of molecular surface reaction products, Applic. Surf. Sci. 7, 189, 1981.

195. Cini, M. and D'Andrea, A., Auger CVV spectra of chemisorbates, beyond the approximation of static screening, Nouvo Cim. Soc. Ital. Fis. D6, 25, 1985.

196. Schonhammer, K. and Gunnarsson, O., Many body effects in deep level spectroscopy from adsorbates, Surf. Sci. 89, 575, 1979.

197. Koel, B.E., Neiman, D.L., Auger line shape determination of the hybridization of ethylene adsorbed on Ni(100), Chem. Phys. Lett. 130, 164, 1986.

198. Hutson, F.L., Ramaker, D.E., Koel, B.E. and Gebhard, S.C., Interpretation of the carbon Auger line shapes for the adsorption and decomposition of ethylene on Ni(100), Surf. Sci., to be published.

199. Bischof, P., Hashmall, J.A., Heilbronner, E., and Hornung, V., Photoelectron spectroscopic determination of the correlation energy in conjugate double bonds, Helv. Chim. Acta 52, 1745, 1969.

200. Hutson, F.L., Ramaker, D.E., Koel, B.E., Spectroscopic evidence for carbon-carbon bonding in "carbidic" layers on metals, Surf. Sci., to be published.

201. Caputi, L.S., Chiarello, G. and Pagagno, L., Carbonaceous layers on Ni(110) and (100) studied by AES and EELS. Surf. Sci. 259, 1985.

202. Ramaker, D.E., Evidence for vertical C_2 on Ni as a precursor for graphite nucleation, to be published.

203. Darling, G.R., Pendry, J.B. and Joyner, R.W., A theoretical study of the structure and reactivity of carbon and graphite layers on nickel surfaces. Surf. Sci. 221, 69, 1989.

204 Rye, R.R., Greenlief, C.M., Goodman, D.W., Hardegree, E.L. and White, J.M., Auger spectra of C_2-hydrocarbons on Ni(100), Surf. Sci. 203, 101, 1988.

205. Chesters, M.A., Linder, D.R., Study of the adsorption of acetylene on copper (100) using Auger electron spectroscopy, Stud. Surf. Sci. Catal. 1988, 249, 1989.

206. Bhattacharya, A.K. and Chesters, M.A., The adsorption and decomposition of methanol on Fe(111) studied by Auger electron spectroscopy, J. Catal. 109, 314, 1988.

207. Sasse, A.G.B.M., Wormeester, H., Van der Hoef, M.A., Keim, E.G. and Van Silfhout, A., Use of a partial local density of states calculation to

characterize the Auger electron Si $L_{23}VV$ transitions of thin oxide layers. J. Vac., Sci. Technol. A7, 1623, 1989.

208. Chao, S.S., Tyler, J.E., Takagi, Y., Pai, P.G., Lucovsky, G., Lin, S.Y., Wong, C.K., Mantini, M.J., J. Vac. Sci. Technol., A4, 1574, 1986.

209. Igbal, A., Bates, C.W.,, Jr., Allen, J.W., Electron spectroscopy study of the Si-O bonding and the polarization screening near the Si-SiO_2 interface. Appl. Phys. Lett. 47, 1064, 1985.

210. Sasse, A.G.B.M., Wormeester, H., van der Hoef, M.A., van Silfhout, A., Calculated and measured Auger line shapes in clean Si(100) 2x1, silicon oxide and silicon oxynitride. J. Phys.: Condens. Matter. 1, 10175, 1989.

211. Keim, E.B., Si-O bond formation on the Si(100) 2x1 surface at the early stage of oxidation as observed by AES, Surf. Sci. 148, L641, 1984.

212. Xu, Z., Dai, D. and Zou, H., Line shape analysis for Si $L_{23}VV$ Auger spectra of cleaved Si(111) surfaces with adsorbed oxygen. Wuli Xuebao 34, 32, 1985.

213. Vidal, R., Passeggi, M.C.G., The first stages of oxidation of amorphous Si: a study of the Si $L_{23}VV$ Auger line shape. J. Phys.: Condens. Matter, 1, 5783, 1989.

214. Liegener, C.M., Ab initio Green's function calculations on the Auger spectra of polyethylene, Phys. Rev., to be published.

215. Morgen, P., Seawar, K.L. and Barbee, T.W., Jr., Auger electron spectroscopy and sputter/Auger analyses of thin films of silicon carbide (SiC_x). J. Vac. Sci. Technol. A3, 2108, 1985.

216. Khvostov, V.V., Guseva, M.B., Babaev, V.G., Rylova, O.Y., Auger spectroscopy studies of the electronic structure of amorphous carbon films. Surf. Sci. 169, L253, 1986: Guseva, M.B., Babaev, V.G., Khvostov, V.V., Rylova, O.Y., Ivanovskii, G.F., Sleptsov, V.V. and Elinson, V.M.,

Electronic structure of amorphous hydrogenated carbon films, Poverkhnost, 11, 101, 1987.

217. Mizolawa, U., Miyasato, T., Nakamura, S., Geib, K.M. and Wilmsen, C.W., The C KLL first-derivative x-ray photoelectron spectroscopy spectra as a fingerprint of the carbon state and the characterization of diamondlike carbon films. J. Vac. Sci. Technol. A5, 2809, 1987.

218. Rye, R.R., Correlation in the Auger Spectrum of Polyethylene, Phys. Rev. B 39, 103 9, 1989.

219. Kelber, J.A., Rye, R.R., Nelson, G.C. and Houston, J.E., Auger spectroscopy of polyethylene and polyethylene oxide. Surf.Sci. 116, 148, 1982.

220. Lurie, P.G. and Wilson, J.M., The diamond surface. I) The structure of the clean surface and the interaction with gases and metals. Surf. Sci. 65, 453, 1977.

221. Ritsko, J.J., Electron energy loss spectroscopy of pristine and radiation damaged polyethylene, J. Chem. Phys. 70, 5343, 1979.

222. Seki, K., Hashimoto, S., Sato, N., Harada, Y., Ishii, K., Inokuchi, H., and Kanbe, J., Vacuum ultraviolet photoelectron spectroscopy of hexatriacolane (n-$C_{36}H_{74}$) polycrystals: a model compound of polyethylene. J. Chem. Phys. 66, 3644, 1977.

223. Turner, N.H., Ramaker, D.E. and Hutson, F.L., Is the Cini-Sawatzky model valid for one-dimensional systems?, to be published.

224. Rubloff, G.W., Microscopic properties and behavior of silicide interfaces. Surf. Sci. 132, 268, 1983.

225. Neckel, A., Rastl, P., Eibler, R., Weinberger, P., and Schwarz, K., Results of self-consistent band-structure calculations for scandium nitride, scandium monoxide, titanium carbide, titanium nitride, titanium monoxide, vanadium

monocarbide, vanadium mononitride, and vanadium monoxide, J. Phys. C 9, 579, 1976.

226. Papaconstantopoulos, D.A. and Economou, E.N., Slater Koster parametrization for Si and the ideal vacancy calculation, Phys. Rev. B22, 2903, 1980.

227. Sarma, D.D., Speier, W., Zeller, R., vanLeuken, E., de Groot, R.A. and Fuggle, J.C., The electronic structure of NiAl and NiSi, J. Phys., Condens. Matter 1, 9131, 1989.

228. Sancrotti, M., Abbati, I., Calliari, L., Marchetti, F., Bisi, O., Iandelli, A., Olcese, G.L., Palenzona, A., Many-body effects at the Si L23VV Auger Line shape: the case of Ca silicides, Rapid Commun. 37, 4805, 1988; Calliari, L., Marchetti, F., Sancrotti, M., Bisi, O., Iandelli, A., Olcese, G.L. and Palenzona, A., Silicon valence states in calcium silicides: A Si L23VV Auger line shape analysis, Phys. Rev. B41, 7569, 1990.

229. Bevolo, A.J., and Shanks, H.R., Valence band study of Mg_2Si by Auger spectroscopy, J. Vac. Sci. Technol. A1, 574, 1983.

230. Sancrotti, M., Rizzi, A., Marchetti, F., Chemical bond at the Si(111)/Yb interface via Auger line shape spectroscopy analysis, Phys. Rev. 37, 3120, 1988.

231. Sancrotti, M., Abbati, I., Rizzi, A., Calliari, L., Marchetti, F., and Bisi, O., Ca silicides as prototypical systems for modelling the electron states at the Si(111)/Yb interface: a Si $L_{23}VV$ Auger line shape investigation, Surf. Sci. 189/190, 300, 1987.

232. Wallart, X., Nys, J.P., Dalmai, G., Lefebvre, I., and Lannoo, M., Combined experimental and theoretical study of the Si $L_{23}VV$ Auger line shape during the Ti-Si interface formation, Europhysics Letters 10, 587, 1989.

233. del Pennino, U., Sassaroli, P., Valeri, S., Bertoni, C.M., Bisi, O., and Calandra, C., Effects of chemical environment in the line shape of silicon $L_{23}VV$ Auger spectra of nickel silicides. J. Phys. C: Solid State Phys. 16. 6309, 1983.

234. Morgen, P., and Jorgensen, B., The Si($L_{23}VV$) and Pt(N_7OO) line shapes at Pt/Si interfaces and in PtSi, Surf. Sci. 208, 306, 1989.

235. Calliari, L., Marchetti, F., Sancrotti, M., Metastability of the Si(111)/Cu interface: a spatially resolved Auger line shape spectroscopy investigation. Phys. Rev. B34, 521, 1986.

236. Rossi, G. and Lindau, I., Compound formation and bonding configuration at the Si-Cu interface. Phys. Rev. B28. 3597. 1983.

237. Dement'ev, A.P. and Lyubimova, T.A., The chemical bond and the structure of the LVV Auger spectrum of Si in Cu_3Si. Poverkhnost, 7. 47, 1985.

238. Munoz, M.C., Sacedon, J.L., Soria, F., and Martines, V., Chemisorption of Si on Al(111) surfaces: a local chemical bond analysis from Auger transition density of states. Surf. Sci. 172. 442. 1986.

239. Wittmer, M., Oelhafen, P., and Tu, K.N., Electronic structure of iridium silicides. Phys. Rev. B33, 5391, 1986.

240. Zajac, G., Zak, J., and Bader, S.D., Line shape analyses of XVV Auger spectra of p(1x1) $V_3Si(100)$: evidence for autoionization emission. Phys. Rev. B22, 6649, 1983.

241. Calliari, L., Sancrotti, M., and Braicovich, L., Agglomeration at Si/Au interfaces: a study with spatially resolved Auger line shape spectroscopy. Phys. Rev. B30, 4885, 1984.

242. Shulga, J.M. and Gutsev, G.L., On the intensity ratio $I(KL_{23}L_{23})/I(KL_1L_1)$ of the Auger carbon lines in a series of metal

carbides, J. Electron. Spectrosc. Relat. Phenom. 34, 39, 1984; ibid, Gutsev, G., Shul'ga, Y.M. and Borod'ko, Y.G., Poverkhnost 4, 104, 1985.

243. Shulga, Y.M., Gutsev, G.L. and Rubtsov, V.I., A Comparison of the C KVV Auger spectra of NbC and $NbN_{0.7}C_{0.3}$, Phys. Stat. Sol. 129, 683, 1985; Gutsev, G.L., Shulga, Y.M. and Borodko, Y.G., The discrete variational Xa method interpretation of the C KVV and Ti $L_{23}M_{23}V$ Auger spectra of TiC., Phys. Stat. Sol. 121, 595, 1984.

244. Pehrsson, P.E. and Ramaker, D.E., Chemical and localization effects in the Auger line shapes of transition metal compounds, J. Vac. Sci. Technol. A3. 1315, 1985; ibid, to be published.

245. Madden, H.H., Nelson, G.C. and Wallace, W.O., Auger electron spectra from boron carbide. Phys. Rev. B31, 3667, 1985.

246. Shul'ga, Y.M., Rubtsov, V.I., Kolyagin, V.A., Chuzhko, R.K. and Khodan, A.N., Study of the electronic structure of V_4C_3 by high energy resolution Auger spectroscopy, Fiz. Met. Metalloved. 66, 858, 1988; Rubtsov, V.I., Shul'ga, Y.M. and Borodko, Y.G., Line shape analysis of vanadium carbide valence band Auger spectra, Poverkhnost 8, 93, 1988.

247. Hoermandinger, G., Weinberger, P. and Redinger, J., Calculation of CVV Auger spectra for nonstoichiometric VC, Phys. Rev. B40, 7989, 1989; Theoretical calculations of CCV Auger spectra: applications to the LMV transitions of Ti in nonstoichiometric TiC, TiN, and TiO. Phys. Rev. B38, 1040, 1988..

248. Gruzalski, G.R., Zehner, D.M. and Ownby, G.W., Electron spectroscopic studies of tantalum carbide. . Surf. Sci. Lett. 157, L395, 1985; Gruzalski, G.R. and Zehner, D.M., Defect states in substoichiometric tantalum carbide. Phys. Rev. B34, 3841, 1986; Charge-distribution changes

accompanying the formation and changes in the composition of HfC_x and TaC_x, Phys. Rev. B42, 2768, 1990.

249. Fiermans, L., Hoogewij, R. and Vennik, J., Electron spectra of transition metal oxide surfaces, Surf. Sci. 47, 1, 1975.

250. Shul'ga, Y.M., Rubtsov, V.I., Gutsev, G.L. and Borod'ko, Y.G., On the change of the N KVV Auger line in the series ZrN, NbN, and Mo_2N, Poverkhnost 7, 86, 1987; Electronic structure and LMV Auger spectra of TiN and VN, Metallofizika 9, 96, 1987; On the N KVV Auger line shape sensitivity to the nitrogen content of the Fe-N system, Poverkhnost 9, 57, 1988.

251. Vanden Berghe, R. and Vlaiminck, R., On the N KLL spectra of some nitrides, SIA, Surf. Inter. Anal. 10, 316, 1987.

252. Moon, D.W., Bieliler, R.J. and Winograd, N., Coverage dependent structural changes during chlorine adsorption on Ag(11), J. Chem. Phys. 85, 1097, 1986.

253. Nishigaki, Auger electron spectroscopy of TiO_2:inter- and intra-atomic transitions connected with the valence band, Surf. Sci. 125, 762, 1983.

254. Rao, C.N.R. and Sarma, D.D., Interatomic Auger transitions in transition metal oxides, Phys. Rev. B25, 2927, 1982.

255. Thurgate, S.M. and Raikar, G.N., Auger line shape analysis of Zn_3P_2, Appl. Surf. Sci. 26, 51, 1986; Raikar, G.N., Klauber, C. and Thurgate, S.M., Auger and XPS study of band structure of Zinc Phosphite, Surf. Sci. 177, L1035, 1986.

256. Shul'ga, Y.M., Gutsev, G.L., Rubtov, V.I. and Borod'ko, Y.B., N KVV Auger spectra of nitrided iron and electronic structure of γ-Fe_4N, Metallofizika, 8, 22, 1986.

257. Vaughan D.J. and Tossell, J.A., Interpretation of the Auger electron spectra of sulfide minerals, Phys. Chem. Miner. 13, 347, 1986.

258. Nebesny. K.W. and Armstrong, N.R., Reactions of clean lithium surfaces with SO_2: molecular Auger line shape analysis and reaction kinetics. Langmiur 1, 469, 1985: Nebesny, K.W., Zavadil, K., Burrow, B. and Armstrong. N.R., Reactions of clean Li surfaces with SO_2, O_2, and H_2O: Auger line shape analysis and x-ray photoelectron spectroscopic analysis of the initial product layers. Surf. Sci. 162, 292, 1985.

259. Robert. R.H. and Ramsey. J.A., An AES study of the initial oxidation of Ni(110) and the influence of Al in clean NiAl, J. Electron Spectrosc. Related Phenom. 52. 185. 1990.

260. Kyeongjae. C and Oh. S.J., $M_{45}N_{45}X$ Auger line shapes of La compounds from one-step model calculations, Phys. Rev. B39, 9576, 1989.

261. Fujimori. A., Suga. S., Negishi. H., and Inoue, M., XPS and AES study of the electronic structure of intercalation compounds metal-titanium sulfide (M_xTiS_2) (M= Mn. Fe. Co. and Ni), Phys. Rev. B38, 3676, 1988.

262. McBreen. P.H. and Polak. M., Low-energy Auger and autoionization emissions of clean and oxygen-exposed Fe-Ti intermetallic and Fe_2Ti_4O. Surf. Sci. 163. L666. 1985.

263. Sancrotti. M., Ciccacci. F., Fanfoni, M., Nataletti, P. and Chiaradia. P., Cu and Ag interface formation on GaP(110) via Auger line shape spectroscopy. Surf. Sci. 211, 651. 1988.

264. Veal. B.W. and Paulikas. A.P., Final state screening and chemical shifts in photoelectron spectroscopy. Phys. Rev. B31, 5399, 1985: Phys. Rev. Lett. 51. 1995. 1983.

265. Ramaker, D.E.,Turner, N.H., and Hutson, F.L., Understanding core-level decay processes in the high-temperature superconductors. Phys. Rev. B38, 11368, 1988.

266. vanderLaan, G., Westra, C., Haas, C. and Sawatzky, G.A., Satellite structure in photoelectron and Auger spectra of copper dihalides. Phys. Rev. B23, 4369, 1981.

267. Zaanen,J., Westra, C., and Sawatzky, G.A., Determination of the electronic structure of transition metal compounds: 2p x-ray photoemission spectroscopy of nickel dihalides. Phys. Rev. B33, 8060, 1986.

268. deBoer, D.K.G., Haas, C., and Sawatzky, G.A., Exciton satellites in photoelectron spectra. Phys. Rev. B29, 4401, 1984.

269. Ramaker, D.E., Utilization of a Hubbard U model to understand the valence band photoelectron data for the high temperature superconductors. Phys. Rev. B38, 11816, 1988.

270. Gadzuk, J.W. and Sunjic, M., Excitation energy dependence of core-level x-ray photoemission spectra line shapes in metals. Phys. Rev. B12, 524, 1975.

271. Chen, C.T., DiDio, R.A., Ford, W.K. and Plummer, E.W., Dynamics of adsorbate core-hole decay. Phys. Rev. B32, 8434, 1985.

272. Bar-Deroma, R., Felsteiner, J., Brener,R. and Ashkenazi, J., Auger spectra, band structure, Coulomb parameters, and ionic changes in lanthanum strontium barium copper oxide ($La_{1.85}(SrBa)_{0.15}CuO_4$). Physica C 1989, 162, 1989.

273. Fuggle, J.C., Weijs, P.J.W., Schoori, R., Sawatzky, G.A., Fink, J., Nucker, N., Durham, P.J. and Temmerman, W.M., Valence bands and electron correlation in the high T_c superconductors. Phys. Rev. B37, 123, 1988.

274. Balzarotti, A., DeCrescenzi, M., Giovannella, C., Messi, R., Motta, N., Patella, F. and Sgarlata, A., Electronic correlations in $YBa_2Cu_3O_{7-d}$ from

Auger spectroscopy, Phys. Rev. B36, 8285, 1987; Valence charge fluctuations in $YBa_2Cu_3O_{7-d}$ from core-level spectroscopies, Phys. Rev. B38, 6461, 1988.

275. van der Marel D., van Elp, J., Sawatzky, G.A., Heitmann, D., x-ray photoemission, bremsstrahlung isochromat, Auger electron, and optical spectroscopy studies of Y-Ba-Cu-O thin films, Phys. Rev. B37, 5136, 1988.

276. Ramaker, D.E., Turner, N.H., Murday, J.S., Toth, L.E., Osofsky, M., and Hutson, F.L., Observed trends in the x-ray photoelectron and Auger spectra of high-temperature superconductors, Phys. Rev. B36, 5672, 1987.

277. Ramaker, D.E., Turner, N.H., Hutson, F.L., Understanding core-level decay processes in the high-temperature superconductors, Phys. Rev. B38, 11368, 1988.

278. Hillebrecht, F.U., Fraxedas, J., Ley, L., Trodahl, H.J., Zaanen, J., Braun, W., Mast, M., Petersen, H., Schaible, M., Bourne, L.C., Pinsukanjana, P. and Zettl, A., Experimental electronic structure of $Bi_2CaSr_2Cu_2O_{8+\delta}$, Phys. Rev. B39, 236, 1989.

279. Shen, Z.X., Lindberg, P.A.P., Lindau, I., Spicer, W.E., Eom, C.B. and Geballe, T.H., Electronic structure of Bi-Ca-Sr-Cu-O superconductors studied by photoelectron spectroscopy, Phys. Rev. B38, 7152, 1988.

280. Kohiki, S., Hirochi, K., Adachi, H., Setsune, K. and Wasa, K., Superconductivity and Cu valence of Bi-Sr-Ca-Cu-O thin films, Phys. Rev. B38, 9201, 1988.

281. Khvostov, V.V., Babaev, V.G. and Shibaev, P.V., Auger spectroscopy studies of the 3d band of copper oxides, Solid State Commun. 72, 875, 1989.

282. Meyer, H.M., Hill, D.M., Weaver, J.H., Nelson, D.L., Gallo, C., Occupied electronic states of single-crystal $Bi_2Ca_{1+x}Sr_{2-x}Cu_2O_{8+y}$, Phys. Rev. B38, 7144, 1988; also Weaver, J.H., private communication.

283. Ghijsen, J., Tjeng, L.H., van Elp, J., Eskes, H., Westerink, J., Sawatzky, G.A., Czyzyk, M.T., Electronic structure of Cu_2O and CuO, Phys. Rev. B38, 11322, 1988.

284. Fuggle, J.C., XPS, UPS, and XAES studies of oxygen adsorption on polycrystalline Mg at approximately 100 and 300K, Surf. Sci. 69, 581, 1977.

285. Tjeng, L.H., Meinders, M.B.J., van Elp, J., Ghijsen, J., Sawatzky, G.A., Johnson, R.L., Electronic structure of Ag_2O, Phys. Rev. B41, 3190, 1990.

286. Fuggle, J.C., The status of high energy spectroscopic studies of high Tc superconductors, Intn. J. Mod. Phys. B1, 1185, 1988.

287. Humbert, P. Deville, J.P., Oxygen Auger emission and final state screening in oxides, J. Phys. Coll. C9, suppl 12, 48, 927, 1987; ibid, Oxygen Auger spectra of some transition-metal oxides: relaxation energies and d-band screening, J. Phys. C: Solid State Phys. 20, 4679, 1987.

288. Sawatzky, G.A. and Post, D., X-ray photoelectron and Auger spectroscopy study of some vanadium oxides, Phys. Rev. B20, 1546, 1979.

289. Salmeron, M., Baro, A.M. and Rojo, J.M., Interatomic transitions and relaxation effects in Auger spectra of several gas adsorbates on transition metals, Phys. Rev. B13, 4348, 1976.

290. Ramaker, D.E., Understanding electronegativity effects in core-level electron spectroscopies: application to the high temperature superconductors, J. Elect. Spectrosc. Related Phenom. 51, 341, 1990.

291. Weiss, A., Mehl, D., Koymen, A.R., Lee, K.H. and Lei, C., Elimination of the secondary electron background in Auger electron spectroscopy using low energy positron excitation, J. Vac. Sci. Technol. A8, 2517, 1990.

292. Lei, C., Mehl, D., Koymen, A.R., Gotwald, F., Jibaly, M. and Weiss, A., Apparatus for positron annihilation-induced Auger Electron spectroscopy, Rev. Sci. Instrum. 60, 3656, 1989.

293. Mehl, D., Koymen, A.R., Jensen, K.O., Gotwald, F. Weiss, A., Sensitivity of positron-annihilation-induced Auger-electron spectroscopy to the top surface layer. Phys. Rev. B41, 799, 1990.

294. Jensen K.O. and Weiss, A., Theoretical study of the application of positron induced Auger electron spectroscopy, Phys. Rev. B41, 3928, 1990.

295. Schultz, P.J. and Lynn, K.G., Interaction of positron beams with surfaces, thin films, and interfaces, Rev. Mod. Phys. 60, 701, 1990.

296. Gunnarsson, O. and Schonhammer, K., Additional information in Auger electron photoelectron coincidence spectroscopy, Phys. Rev. Lett. 46, 859, 1981.

297. Doering, J.P., Coplan, M.A., Cooper, J.W. and Moore, J.H., Electron correlation in an Auger process, Phys. Rev. A41, 535, 1990.

298. Sawatzky, G.A., Auger photoelectron coincidence spectroscopy, p. 168 in Ref. Augbook.

299. Chen, C.T., DiDio, R.A., Ford, W.K., Plummer, E.W., and Eberhardt, W., Dynamics of adsorbate core-hole decay, Phys. Rev. B32, 8434, 1985.

300. Larkins, F.P., Eberhardt, W., Lyo, I.W., Murphy, R. and Plummer, E.W., The core hole decay of N_2O following core to bound state excitations. J. Chem. Phys. 88, 2948, 1988.

301. Ungier, L. and Thomas, T.D., Non-dipole excitations of core holes by electron impact; Multiplet splitting in CO and N_2, Chem. Phys. Lett. 96, 247, 1983.

302. Eberhardt, W., Stohr, J., Feldhaus, J., Plummer, E.W., and Sette, F., Correlation between electronic emission and fragmentation into ions following soft-x-ray excitation of the N_2 molecule, Phys. Rev. Lett. 51, 2370, 1983.

303. Eberhardt, W., Plummer, E.W., Chen, C.T. and Ford, W.K., Deexcitation electron spectroscopy: a probe for the localization of valence wavefunctions in free and adsorbed molecules, Aust. J. Phys. 39, 853. 1986.

304. Carlson, T.A., Gerard, P., Krause, M.O., von Wald, L., Taylor, J.W., Grimm, G.A. and Pullen, B.P., Resonant Auger processes for molecules as studied with angle resolved electron spectrometry, J. Elect. Spectrosc. Related Phenom., 47, 227. 1988.

305. Aksela, S., Tan, K.H., Aksela, H. and Bancroft, G.M., Si(LVV) Auger and resonance Auger spectra of SiF_4 molecules with the use of synchrotron radiation, Phys. Rev. A33, 258. 1986.

306. Illing, G., Porwol, T., Hemmerich, I., Domotor, G., Kuhlenbeck, H., Freund, H.J., Liegener, C.M. and Von Niessen, W., Electron spectroscopy of adsorbates via autoionization of core-to-bound excited states: experiment and theory, J. Electron. Spectrosc. Related Phenom. 51, 149. 1990.

307. Eberhardt, W., Dudde, R., Rocco, M.L.M., Koch, E.E. and Bernstorff, S., Dynamic screening effects observed in the deexcitation of core electron excited states in molecules, J. Electron Spectrosc. Related Phenom. 51, 373. 1990.

308. Sarma, D.D., Carbone, D., Sen, P. and Gudat, W., Synchrotron-radiation study of the satellites in Ni $L_3M_{45}M_{45}$ Auger spectra, Phys. Rev. B40, 12542, 1989.

309. Carroll, T.X. and Thomas, T.D., Deexcitation electron spectroscopy of core-excited O_2, J.Chem Phys. 92, 7171. 1990.

310. Lapiano-Smith, D., Lee, K., Ma, C.I., Wu, K. and Hanson, D.M., Auger decay and autoionization of core hole excited states in molecular oxygen, J. Electron Spectrosc Related Phenom. 51, 221, 1990.

311. Chen, J., Lin, C.L., Qiu, S.L., Strongin, M. and den Boer, M.L., Auger and x-ray absorption studies of solid moleculear oxygen, J. Vac. Sci. Technol. A8, 2591, 1990.

312. Larsson, M., Baltzer, P., Svensson, S., Wannberg, B., Martensson, N., Naves de Brito, A., Correia, N., Keane, M.P., Carlsson-Gothe, M. and Karlsson, L., X-ray photoelectron, Auger electron and ion fragment spectra of O_2 and potential curves of O_2^{2+}, J. Phys. B: At. Mol. Opt. Phys. 23, 1175, 1990.

313. Sambe, H. and Ramaker, D.E., An interpretation of the O_2 Auger electron spectrum, Chem. Phys. 104, 331, 1986.

314. Larkins, F.P., Theoretical interpretation of molecular Auger spectra, J. Elect. Spectrosc. Related Phenom. 51, 115, 1990.

315. Landolt, M. Mauri, D., Spin-polarized Auger spectroscopy from magnetically ordered solids, Phys. Rev. Letters, 49, 1783, 1982.

316. Allenspach, R. Landolt, M., Spin polarized Auger spectroscopy from Fe(100), Surf. Sci. 171, L479, 1986.

317. Allenspach, R. and Taborelli M. and Landolt, M., Oxygen on Fe(100): an initial oxidation study by spin polarized Auger spectroscopy, Phys. Rev. 55, 2599, 1985.

318. Taborelli, M., Allenspach, R., Boffa, G. and Landolt, M., Magnetic coupling of surface adlayers: Gd on Fe(100), Phys. Rev. Lett. 56, 2869, 1986.

319. Paul, O., Taborelli, M. and Landolt, M., Magnetic and spectroscopic properties of epitaxial overlayers of Fe on Au(100) studied with spin polarized Auger and secondary electrons, Surf. Sci. 211/212, 724, 1989.

320. Umback, F. and Hussian, Z., Angle dependent changes of Auger line shapes from adsorbed molecules, Phys. Rev. Letters 52, 257, 1984.

321. Umbach. E.. Angular dependence and final state effects in the Auger spectra of adsorbed molecules. Comments Atomic and Mole. Phys. 18, 23, 1986.

322. Steinruck. H.P., Pach. T. and Huber. W., A low coverage study of NO on Ni(111) by angle resolved Auger electron spectroscopy at resonance excitation. Phys. Scripta 41. 177. 1990.

323. Wurth. W.. Weimer. J.J.. Hudeczek. E. and Umback. E.. New information on CO+K coadsorption by analysis of angle resolved Auger line shapes. Surf. Sci. 173, L619, 1986.

324. Wurth, W.. High resolution Auger spectroscopy of adsorbed molecules. Vacuum 40. 3, 1990.

325. Rogers.. J.W.. Jr., Houston. J.E.. and Rye. R.R.. Angular dependence of the Auger line shape of graphite. Microbeam Anal. 21. 115. 1986.

326. Mikhailov. G.M., Lisetshii. E.M., Khristenko. S.V.. Zimont. S.L.. Vetchinkin. S.I., Dadali. Y.V., and Borod'ko. Y.G.. Angular dependence of the fine structure of the Auger spectrum of graphite. Fiz. Tverd. (Leningrad) 29, 2186. 1987 [Soviet Physics Solid State 29. 1260. 1987].

327. Hoflund. G.B., A technique for performing angle resolved Auger electron spectroscopy (ARAES) and angle resolved electron energy loss spectroscopy (ARELS). in Ref. Augconf.

328. Mroz, S. and Mroz, A., Angular dependences in Auger electron emission from the Ni(001) face, Surf. Sci. 224, 235, 1989.

329. Asensio. M.C., Michel, E.G., Alvares, J., Ocal. D.. Miranda. R. and Ferrer. S.. A structural study of the K adsorption site on a Si (001) 2x1 surface: dimers. cores. or both. Surf. Sci. 211/212, 31. 1989.

330. Xu. M.L. and Van Hove. A.. Surface structure determination with forward focusing electrons. Surf. Sci. 207. 215. 1989.

331. Cronacher, H., Heinz, K., Muller, L., Xu, M.L. and Van Hove, M.A., Forward focusing of Auger and Kikuchi electrons for surface structure determinations: Ni(100) and oxidized Mg(0001), Surf. Sci., 209, 387, 1989.

332. Cini, M., Theory of Auger XVV spectra of solids: many body effects in incompletely filled bands, Surf. Sci. 87, 483, 1979.

333. Cini, M. and Verdozzi, C., Correlation effects in photoemission and Auger spectra of Palladium, p. 122 in Ref. Augconf.

334. Cini, M. and Verdozzi, C., Photoemission and Auger CVV spectra of partially filled bands: a cluster approach, Solid State Commun. 57, 657, 1986; Many body effects in the electron spectroscopies of incompletely filled bands, Nuovo Cim. D9, 1 (1987).

335. Liebsch, A. Effect of self-energy corrections on the valence band photoemission of Ni, Phys. Rev. Lett. 43, 1431, 1979; Ni d band self-energy beyond the low density limit, Phys. Rev. B23, 5203, 1981.

336. Bennet, P.A., Fuggle, J.C., Hillebrecht, F.U., Lenselink, A. and Sawatzky, G.A., Electronic structure of Ni and Pd alloys III. Correlation effects in Auger spectra of Ni alloys, Phys. Rev. B27, 2194, 1983.

337. Cubiotti, G., Guilliano, E.S., Ginatempo, B. and Stancanelli, A., Influence of the Coulomb correlation in partially filled d-bands on the electronic spectra of disordered alloys, Nuovo Cim. 2, 853, 1983.

338. Cini, M. and Andrea, A.D., On the theory of the Auger CVV line shape of graphite, p. 139 in Ref. Augconf.

339. Sawatzky, G.A., Experimental probes of electron correlation effects and the influence on the electronic structure, p. 2 in Ref. Augconf.

340. deBoer, D.K.G., Haas, C. and Sawatzky, G.A., Auger spectra of compounds of Sc, Ti, Cr, J. Phys. F: Met. Phys. 14, 2769, 1984.

341. Hedegard, P. and Hillebrecht, F.U., Edge effects in Auger spectroscopy for the early transition metals, Phys. Rev. B34, 3045, 1986.

342. Jennison, D.R., Hillebrecht, F.U. and Fuggle, J.C., Many-body effects in the CVV spectra of Metals, Mg, vs. Ti, J. Vac. Sci. Technol. A2, 1049, 1984.

343. Ramaker, D.E. and Hutson, F.L., Interpretation of Auger line shapes on systems with half-filled valence bands, J. Vac. Sci. Technol. A5, 630, 1987.

344. Erickson, N.E., Powell, C.J. and Ramaker, D.E., New correlation effects observed for inner shell excitations in titanium and vanadium, Phys. Rev. Lett. 58, 507, 1987.

345. Rogers, J.W., Jr., Rye, R.R. and Houston, J.E., The carbon Auger line shape of t-stilbene and 2,4,6,2',4',6'-hexanitrostilbene, Chem. Phys. Lett. 150, 147, 1988.

346. Rogers, J.W., Peebles, H.C., Rye, R.R. and Houston, J.E., A carbon Auger line shape study of nitroaromatic explosives, J. Chem. Phys. 80, 4513, 1984.

347. Martino, G., Mezzasalma, A.M., Mondio, G. and Saitta, G., KVV Auger spectra of tetracyanoquinodimethane semiconducting films, Thin Solid Films 176, 283, 1989.

348. Lesiak, B., Jablonski, A., Zagorska, M. and Jozwik, A., SIA Surf. Interface Anal. 12, 461, 1988.

349. Salaita, G.N., Davidson, L.L., Lu, F., Walton, N., Wellner, E., Stern, D.A., Batina, N., Frank D.G., Lin, C.H., Benton, C.S. and Hubbard, A.T., Electrochemical reactivity of 2,2',5,5'-tetrahydroxybiphenyl and related compounds adsorbed at Pt(111) surfaces: studies by EELS, LEED, Auger spectroscopy and cyclic voltammetry, J. Electroanal. Chem. 245, 253, 1988.

350. Gui, J.Y., Kahn, B.E., Lin, C.H., Lu, F., Salaita, G.N., Stern, D.A., Zapien, D.C. and Hubbard, A.T., Studies of adsorbed unsaturated alcohols at well-defined Pt(111) electrode surfaces by cyclic voltammetry assisted by

vibrational spectroscopy (EELS) and Auger spectroscopy, J. Electroanal. Chem. 262, 169, 1988.

351. DeCrescenzi, M., Diociaiuti, M., Lossi, L., Picozzi, P. and Santucci, S., Size effects on the linewidths of the Auger spectra of Cu clusters, Surf. Sci. 178, 348, 1986.

352. Cini, M., DeCrescenzi, M., Patella, F., Motta, N., Sastry, M., Rochet, F., Pasquali, R. and Balzarotti, A., Palladium clusters on graphite: evidence of resonant hybrid states in the valence and conduction bands, Phys. Rev. 41, 5685, 1990.

353. Kink, J.A. and Subbarao, S.C., The characterization of surface carbon on organic bearing shale by Auger line shape analysis, Applic. Surf. Sci. 21, 268, 1985.

354. Craig, S., Harding, G.L. and Payling, R., Auger line shape analysis of carbon bonding is sputtered metal-carbon thin films. Surf. Sci. 124, 591, 1983.

355. Singer, I.L., Surface analysis, ion implantation and tribological processes affecting steels, Applic. Surf. Sci. 18, 28, 1984.

356. Luckman, G., Studies of surface segregation kinetics by Auger electron spectroscopy, p. 17 in Ref. Augbook.

357. Abashkin, V.G., Dement'ev, A.P., Dzhibuti, T.M., Ivanova, O.P., Auger S LVV spectra for segregation on the surfaces of 3d-metals, Poverkhnost 11, 48, 1989.

358. Grabke, H.J., Contributions of AES in four metallurgical studies, SIA, Surf. Interface Anal. 14, 686, 1989.

359. Briant, C.L., Metallurgical applications of Auger electron spectroscopy, p. 111 in Ref. Augbook.

360. Curelaru. I.M., Din, K.S., Suoninen, E. and Minni, E., Localization vs. delocalization of orbitals in the quasi-one-dimensional conductor $Na_{0.33}V_2O_5$, Solid State Ionics 18/19, 245, 1986.

361. Paterson, P.J.K., Auger electron spectroscopy for materials surface analysis, Materials Forum 10, 144, 1987.

362. Briggs, D.,The impact of surface science on technology, Surf. Sci. 189/190, 801, 1987.

363. Landolt, D. and Mathieu, H.J., The use of surface science methods in electroplating, Proc. Electrochem. Soc. 87, 467,1987.

364. Myhra, S., Smart, R.St. C. and Turner, P.S.,The surfaces of titanate minerals, ceramics, and silicate glasses: surface analytical and electron microscope studies, Scanning Microsc. 2, 715, 1988.

Table 1 Comparison of the atomic Auger intensity ratios for Si CVV and CCV Auger line shapes (From Ref. Ramsi).

Line shape	s/p or sl/pp	Intensity ratio[a]	Intensity ratio[b]
KL_1V	s/p	0.79	0.75 ± 0.1
$KL_{23}V$	s/p	0.23	0.3 ± 0.1
$L_1L_{23}V$	s/p	0.64	0.8 ± 0.4
$L_{23}VV$	ss/pp	0.01	0.025 ± 0.001
	sp/pp	0.10	0.38 ± 0.02
KVV	ss/pp	0.10	0.15 ± 0.02
	sp/pp	0.48	0.46 ± 0.02

[a]Intensity ratios (e.g. A_{ccs}/A_{ccp}) obtained from the fit of eq. 6 to the experimental data.

[b]Intensity ratios (e.g. A_{css}/A_{ccp}) obtained from Fig. 8, similar such plots for the other Auger transitions.Ramsi.Ramrev1 and from Ref. Babenkov.

Table 2 Summary of satellite intensities in percent.[a]

k-vvv	kvv	ke-v	ke-vve	kv-vvv	k-vvv
Methane	51	0	12	20	17
Ethane	52	0	12	21	15
Cyclohexane	54	0	8	19	19
Polyethylene	67	3	11	17-21	0
Ethylene	50	2	13	20	15
Benzene	56	1	6	21	16

[a]From Ref. ramhydc.

Table 3 Summary of ΔU and δ parameters obtained empirically for the theoretical kvv line shape.[a]

Molecule	ΔU (eV)			δ[b] (eV)		
Alkanes	CH-CH	CH-CC	CC-CC	CH-CH	CH-CC	CC-CC
Methane	0			12		
Ethane	1	1	0	12	10	10
Cyclohexane	3	3	1.25	9	9	9
Polyethylene	3	3	1.25	0	0	0
Diamond			2.			0
Alkenes	$\sigma\sigma$	$\sigma\pi$	$\pi\pi$	$\sigma\sigma$	$\sigma\pi$	$\pi\pi$
Ethylene	2	1	0	9	11	11
Benzene	2	1	0	8	6	6
Graphite	2	1	0	0	0	0

[a]From Ref. Ramhyd.

[b]A positive δ indicates a shift to higher two-hole binding energy.

Table 4 Comparison of empirical effective U parameters

d^0	d^0	d^0	d^1	d^2	d^3	d^4	d^5	d^6	d^7	d^8	d^9	d^{10}
U^e_{pp} (eV) as reflected in O KVV line shape of metal oxides.[a]												
SiO_2	MgO	TiO_2			MnO_2		Fe_2O_3	FeO		O/Ni	CuO	ZnO
10.5	11.3	9.6			5.5		4.8	6.4		5.4	10.5	11.6
GeO_2	BaO		Nb_2O_5									Cu_2O
10.5	11.3		6.1									5.7
	Al_2O_3		VO_2	V_2O_3	V_2O_5							Ag_2O
	14.2		3.7	4.3	5.2							7.0
												HgO
												11.7
U^e_{dd} (eV) as reflected in metal $L_{23}VV$ line shape of elemental metals.[b]												
Si	Mg	Al	Sc	Ti	V	Cr	Mn	Fe	Co	Ni	Cu	Zn
			-2.	-1.	0.5	-0.1	0.	1.2	1.2	4.2	8.0	9.7

[a] U's originally tabulated and collected by Fuggle.[fugg] Values empirically obtained as follows: V_xO_y by Sawatzky and Post,[post] Na_2O by Barrie and Street.[Barrie] MgO by Fuggle.[fugg] O/Ni by Salmeron et al.[salmeron] Cu_2O by Ghijsen.[ghijsen] Ag_2O by Tjeng.[tjeng] CuO by Fuggle,[fugg] and the remaining by Humbert and Deville.[deville]

[b] Values obtained by deBoer et al.[deboer]

FIGURE CAPTIONS

Fig. 1. The S $L_{23}VV$ Auger spectrum from Li_2SO_4 powder pressed onto an In substrate. (From Ref. Ramext)

a) The Auger line shape N(E) with the estimated background EB(E) utilizing eq. 1.

b) The resultant background subtracted spectrum, A(E), and the backscattered spectrum, L(E), observed from a 140 eV primary electron beam incident on the sample. The latter data were taken with a CMA in the normal mode and are not corrected for the analyzer transmission distortions.

c) The "true" Auger spectrum, $A_t(E)$, obtained after deconvoluting out the electron-loss contributions and correcting for sample and spectrometer transmission. The solid and dashed lines in both b) and c) indicate two different estimates of the background and the final A(E) spectra obtained with these background estimates. These two spectra give some indication of the uncertainties involved in the line shape extraction.

Fig. 2. The C KVV Auger line shapes taken in the gas phase for various carbon molecules as indicated.[Ryealk] (From Ref. Ramrev2)

Fig. 3. a) Total one electron DOS (solid line) for cyclohexane determined empirically as described in the text. The s (dashed line), p_{CH} (dotted line), and p_{CC} (dot-dashed line) components, determined as described in the text, are also shown. The vertical lines indicate the electron density on any carbon atom for each MO as obtained from a

GAUSSIAN 82 calculation.[Gauss] The energies of each vertical line are placed at those obtained empirically from PES data.[Bischof] Schematic diagrams[salem] of four of the molecular orbitals are also given.

b) XPS and XES data for cyclohexane as utilized to obtain the DOS in a) above.[Mills. Mattson] (From Ref. Ramhydc)

Fig. 4. A schematic representation of the potential energy curves of a two-hole state, one-hole state, and the ground state.[Matthews] The horizontal axis represents some generalized internuclear axis. The spread in energy, Γ_n, due to vibronic motion is indicated. (From ref. Matthews; used with permission)

Fig. 5. Comparison of C_2H_6 C KVV experimental (EXP) and theoretical (THY) spectra as reported by Jennison et al.[Jenn] The bars indicate the positions and relative intensities of the vertical electronic transitions as obtained from theoretical SCF calculations. The smooth curve was produced by summing the Gaussian broadened bars utilizing a constant width to provide optimal agreement with experiment. (From Ref. Jenn; used with permission)

Fig. 6. Comparison of the experimental C KVV Auger line shapes (solid line) obtained from the literature for diamond,[Dayan] graphite[housgrap], benzene,[Seigbahn] cyclohexane.[Ryealk] and polyethylene[Dayan] with the self-fold of the DOS (dotted iine) obtained as described in the text. (From Ref. Ramhydc)

Fig. 7. Summary of the various processes giving rise to the total Auger line shape (From Ref. Ramhydc). Core, VB and CB indicate the core level, valence band (or filled orbitals), and conduction band (or empty orbitals) respectively. Spec. (spectator) and part. (participant) indicate the subsequent fate of the resonantly excited electron during the Auger process. I.s and f.s. indicate initial-state and final-state and refer to the state in which the shakeoff event occurs relative to the Auger decay. N*N and N (N = σ in eq. (6)) refer to the approximate line shape, i.e. either a DOS self-fold, or just the DOS, with the relative size of ΔU in the Cini expression (eq. 6) indicated. The resonant satellites occur only under electron excitation.

Fig. 8. Comparison of the $L_{23}VV$ theoretical and experimental atomic Auger matrix elements, $A_{cll'}$, for atoms in the 2nd and 3rd rows of the periodic table (From Ref. ramrev1). Here, $A_{cll'}$ is the matrix element per filled shell as indicated by eq. 10. and has been normalized for each atom such that A_{cpp} is 100. The theoretical data of Mcguire[Mcguire] (solid line) have been scaled by factors f_{ss} = 1.97, f_{sp} = 1.23, f_{sd} = 1.33, f_{pd} = 1.27, and f_{dd} = 2.06, that from Walters and Bhalla[WNB] (dashed line) by f_{ss} = 1.94, f_{sp} = 1.03, f_{sd} = 1.32, f_{pd} = 1.24, and f_{dd} = 2.05, to correspond to the Ar (Z = 18) ss and sp and the Kr (Z = 36) sd, pd, and dd experimental data. The data from Chen and Crasemann[CNC] (cross-hatched symbols) for Ar, Zn and Kr are unscaled. The crossed symbols for Z = 29 refer to a CI calculation for Cu.[McGuire2]

Fig. 9. Comparison of the bandwidth (Γ_{nd}) with the effective hole-hole repulsion (U^e_{ndnd}) for the metals with electron configuration d^6s^2 to $d^{10}s^2p^2$ (from Ref. Ramrev1). Metals with band-like and atomic-like line shapes are indicated; those between the dashed lines are "transitional".

Fig. 10. Comparison of the CVV Auger line shapes for the "transitional" metals as indicated in Fig. 9 with the fold of the one electron DOS. The vertical bars from Cu and Ag indicate results from an atomic calculation. E_x is the core binding energy, E_a the Auger electron kinetic energy. (From Ref. Ramrev1)

Fig. 11. Illustration of the effective hole-hole repulsions U^e_{xx}, U^e_{bb}, and U^e_{gg} ($U^e = \Delta U$ in eq. 5) and the corresponding interaction parameter, Γ, γ, or V for the NO_3^- anion. GO, BO, and AO refer to group (or cluster), bond and atomic orbitals, respectively.

Fig. 12. Comparison of the Mg and Al KL_1V and $KL_{23}V$ spectra for the metals or alloys indicated. (From Ref. Mgalloys, used with permission). The horizontal shading for Al_8Mg_{92} is an internal photoemission line which overlaps the Al KL_1V spectrum. The diagonal shaded areas in each case represents roughly the s contribution to the KL1V line shape. ΔZ is the difference between the core charge on the local site versus that on its neighbors assuming the equivalent cores model.

Fig. 13. Comparison of the Ni $L_{23}M_{45}M_{45}$ Auger spectra for the alloys indicated (From Ref. Andrews; used with permission). The outline of the spectrum for pure Ni has been superimposed on the alloy spectra to aid comparison.

Fig. 14. The inset in each case show the theoretical Pd DOS calculated within the Clogston-Wolff model with t = 0.6 (appropriate for the unrelaxed lattice assumed in the impurity calculations) and t = 0.2 (giving optimal agreement with the Auger line shape and indicating a lattice expansion). The Auger profile was calculated using the corresponding DOS, and hole-hole repulsion parameter, $U(^1G_4)$. equal to 3.0 eV. The U values for the other multiplets were obtained using calculated Slater integrals. F^n, and the jj intermediate coupling scheme. (From Ref. pdlattic; used with permission)

Fig. 15. Comparison of the experimental Si $L_{23}VV$ Auger line shape for elemental Si with the theoretical line shape obtained utilizing optimal matrix elements (dashed line) and with the matrix elements predicted from Fig. 8 (dotted line) (both sets of matrix elements are given in Table 1). The theoretical fits were obtained with U = 0 in eq. 6.

Fig. 16. Comparison of the experimental (EXP) Li KVV and Al LVV Auger line shapes with theoretical results from various levels of approximation. "BULK" indicates the results obtained from the bulk theoretical DOS calculated within a self-consistent linear muffin-tin-orbital (LMTO) approximation. "FSR" refers to the final state rule result which accounts for the non-orthogonality between the valence

orbitals in the presence and lack of a core hole. "MND" refers to the full dynamical results, which includes the singularity factors near the Fermi level (sometimes also called the "orthogonalized FSR"[Ramfsr]). "SURF" refers to the results obtained from a slab calculation, and thus accounts for surface effects. (From Ref. almbladh; used with permission)

Fig. 17. a) Comparison of the C KVV experimental[Ryealk] and theoretical Auger line shapes for ethylene gas. The various contributions (kvv, kv-vvv, k-vvv, ke-v, ke-evv) were obtained as described in the text. (From Ref. Ramhydc)

b) Comparison of the experimental and theoretical Auger line shapes for ethylene chemisorbed on Ni(100) at 100 K (π-bonded ethylene). The three component (VV, Vπ^*, $\pi^*\pi^*$) line shapes were obtained as described in the text. The relative intensities were obtained by least squares fit to the experimental data. (From Ref. Ramethyl).

Fig. 18. a) Comparison of the experimental C KVV line shape for ethane[Ryealk] with the total theoretical line shape obtained as described in the text.

b) The total theoretical line shape and each of the components as indicated. (From Ref. Ramhydc)

Fig. 19. C KVV x-ray excited Auger line shapes for ethylene chemisorbed on Ni(100) at 100K followed by heating to the indicated annealing temperature as reported by Ramaker et al.[Ramethyl]

Fig. 20. The Auger spectral shifts as a function of temperature obtained from the C_2H_4/Ni(100) Auger spectra of Rye et al.[Ryeethyl] The energy scale along the left vertical axis is essentially the effective U at 20K, and the shift from this energy with increasing temperature, due either to changing U or changing ionization potential (IP). The right vertical axis is proportional to the pressure of D_2 and is appropriate for the D_2 temperature programmed desorption (TPD) data. The TPD data reveal that beginning at 300K, the ethylene begins to dissociate on the Ni surface. (From Ryethyl, used with permission)

Fig. 21.. a) Comparison of the experimental Auger line shape for polyethylene from Kelber[kelber] and Dayan and Pepper[dayan] with the theoretical total line shape determined as described in the text. The components in order of increasing energy are kv-vvv, kvv, ke-vve, and ke-v. (From Ref. Rampoly)

b) The C KVV Auger line shapes for the H terminated[dayan] surface of diamond. The A(E) line shape results after the background subtraction and deconvolution procedures. The H-terminated line shape is more representative of the bulk since C-H bonds are more similar to bulk C-C bonds than the π bonds existing in the clean surface. Also shown is a comparison of the H terminated line shape with the theoretical kvv line shape. The s *s, s *p, and p *p components have maxima at 248, 258, and 268 eV, respectively. (From Ref. Ramdia)

Fig. 22. The Si $L_{23}VV$ Auger line shape for Pd_4Si. The insert shows the calculated Si partial DOS (upper) and its self-fold (lower). The

peaks labeled 'a' through 'e' are assigned in the text. (From Ref. Bader; used with permission).

Fig. 23. Comparison of the experimental (solid line) Si $L_{23}VV$ Auger line shape for the three Ca-silicides indicated, with the self-fold of the theoretical DOS, $N_p(E) + 0.3\ N_s(E)$, (dotted line). The factor of 0.3 in front of the s DOS is to account for the reduced ss and sp components seen in elemental solid Si. Also shown for Ca_2Si is a result where the Cini-Sawatzky expression was used to distort the self-fold with $U_{sp} = U_{ss} = 3$ eV and $U_{pp} = 0$ eV. (From Ref. casi: used with permission)

Fig. 24. Comparison of the C KVV dN(E)/dE Auger line shape for the metal carbides indicated. Note the changing intensity of the shoulder around 270 eV, and the changing nature of the singlet and triplet structure around 260 eV. (From Ref. Gutsev; used with permission)

Fig. 25. The O $KL_{23}L_{23}$ Auger spectrum and O $2p^4$ DOS for Ag_2O. The dotted line shows the experimental O spectrum on a two-hole binding energy scale. The top solid line shows the singlet contribution and the bottom the triplet contribution (reduced by a factor of 3) to the O $2p^4$ DOS as calculated using a $(Ag_4O_5)^{6-}$ cluster with an O atom in the center. A Lorentzian broadening of 2.4 eV has been applied. Also shown are the unbroadened states (solid lines) and the multiplet split atomic states (dashed lines). (From Ref. Tjeng: used with permission)

Fig. 26. a) Comparison of the experimental L_3VV Auger spectra for the CuX_2 materials.[vanderlaan] The data for X = Cl and Br were shifted by -1.5 and -2.5 eV, respectively, to bring them into registry with that for X = F. The data for Cl and Br were Gaussian broadened by 2 eV for clearer comparison with the F data.

b) Comparison of $L_3M_{23}V$ Auger data for the CuX_2.[vanderlaan] The data for X = Cl and Br were shifted by -2.75 and 3 eV for registry with the F data. The Cl and Br data were broadened by 2 eV.

c) Comparison of L_3VV Auger data for Cu_2O, CuO,[vanderlaan] and Bi(2212) [data reported by Weaver,[weaver] Hillebrecht,[hillebrecht] and Kohiki[hohiki]. No shifts or broadening were performed here.

d) Comparison of $L_3M_{23}V$ data for CuCl, Cu and $CuCl_2$.[vanderlaan] The data for $CuCl_2$ is exactly as in b) above, and the Cu and CuCl were broadened by 2 eV and placed in registry with that for $CuCl_2$. (From ref. Ramjes)

Fig. 27. Comparison of electron induced (EAES) and positron annihilation induced (PAES) Cu MVV Auger spectra for Cu(110). The incident beam energies were 3 KEV and 25 eV for the electron and positron beam respectively. (From Ref. Weiss; used with permission)

Fig. 28. Comparison of the total Cu $L_{23}M_{45}M_{45}$ Auger spectrum of elemental Cu with the Auger photoelectron coincident spectra (APECS) data in coincidence with the L_3 ($2p_{3/2}$), L_2($2p_{1/2}$), and L_1(2s) lines; respectively. The AES spectrum is a computer-generated spectrum in which the multiplet structure is composed from Lorentzians with a full-width half maximum of 1.6 eV, and

multiplet structure and intensities given by theoretical matrix elements and then fit to the experimental data. (From Ref. Sawatzky; used with permission).

Fig. 29. Comparison of nonresonant photon (XAES) and electron (EAES) excited Auger data with resonantly excited Auger (DES) data.[Carroll02] The dominant peaks are indicated as interpreted by Sambe and Ramaker.[Sambe] The vertical lines indicate the expected peak positions for transitions to states of O_2^+ as calculated by Carrol and Thomas.[Carroll02]

Fig. 30. The effective spin polarization, P_{eff}, (defined as in the text) and the $M_{23}M_{45}M_{45}$ Auger intensity from Fe(100) after appropriate background subtraction. (From Ref. Spaes: used with permission)

Fig. 31. a) Angle resolved Oxygen KVV Auger spectra for CO co-adsorbed with K on Ru(001) taken at the polar angles, θ, indicated.
b) Quantitative evaluation of the peak intensity for peak 4 (the $4a_1$-$1b_1$ transition) in comparison with model calculations assuming different tilt angles of the CO molecules with respect to the surface.

Fig. 32. LATTICE - An illustration of a ferromagnetic lattice with a low density of minority spins leading to a metallic system.
DOS and PES - The schematic total DOS and occupied DOS.
PES *PES - The self-convolution of the PES.
AES - The expected Auger spectrum which only has contributions from those states with two electrons per atom.

ISR - a schematic illustration of the application of the Initial State Rule prescription described in the text and illustrated in Fig. 33. (Top 5 panels after Ref. Sawatzky).

Fig. 33. Schematic illustration of the final (FS) and initial (IS) state rules applied to a single-band rectangular DOS, N(E), with greater and less than half-filled valence bands, respectively. The DOS self-fold N *N and the Cini distorted self-fold, C(N *N), are also indicated. The cross hatched areas show the occupied portions of N and N *N, and the resultant Auger line shape in C(N *N). (After Ref. Ramisfs).

LIST OF FIGURES

Fig.		Section
1.	Extracting line shapes	IIA1
2.	Rye gas phase data	IIB2
3.	DOS Hexane	IIB2
4.	Matthew width curve	IIB3
5.	Jennison Ethane	IIB3
6.	Exp. vs. theory	IIB4
7.	Satellite notation	IIB4
8.	LVV matrix elements	IIC2
9.	U vs Γ TM's	IIC3a
10.	Intermediate TM's	IIC3a
11.	NO_3: AO,GO,BO	IIC3b
12.	Weightman CCV	IIIA1
13.	Weightman holes	IIIA2
14.	Weightman PdAg exp	IIIA2
15.	Si ss and pp	IIIB
16.	Albladh	IIIB
17.	Ethylene	IIIC
18.	Ethane	IIIC
19.	Koel's chemisorbed ethylene	IIID
20.	Rye's U curve	IIID
21.	Poly and diamond	IIIE
22.	Bader Si	IIIF
23.	Calcium Sicides	IIIF
24.	Carbides- Gutsev	IIIF

25. Sawatzky O KVV IIIF

26. CuX_2 plots IIIG

27. Texas-PAES IVA

28. Coincident-Sawatzky IVB

29. O_2 DES IVB

30. Spin aligned Auger IVC

31. Menzel -angle resolved IVD

32. Sawatzky illustration IVE4

33. Negative U's IVE

TABLES

1. Si matrix elements IIC2

2. Sat. int. IIIC4

3. ΔU and σ IIIC

4. U's O KLL and TM neg. U's IIIF

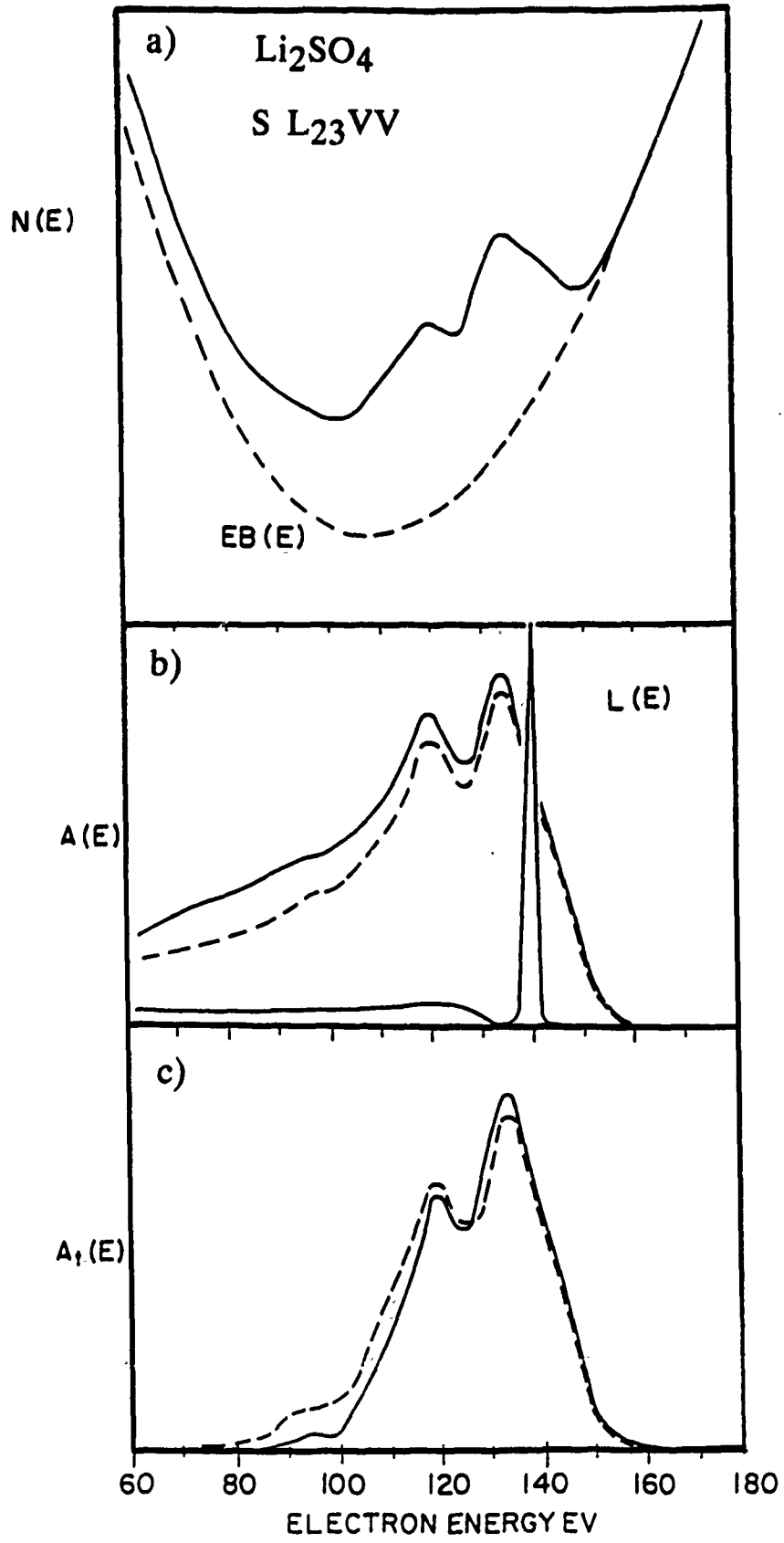
a)
Li_2SO_4
S $L_{23}VV$
N(E)
EB(E)
b)
L(E)
A(E)
c)
A_t(E)
60
80
100
120
140
160
180
ELECTRON ENERGY EV

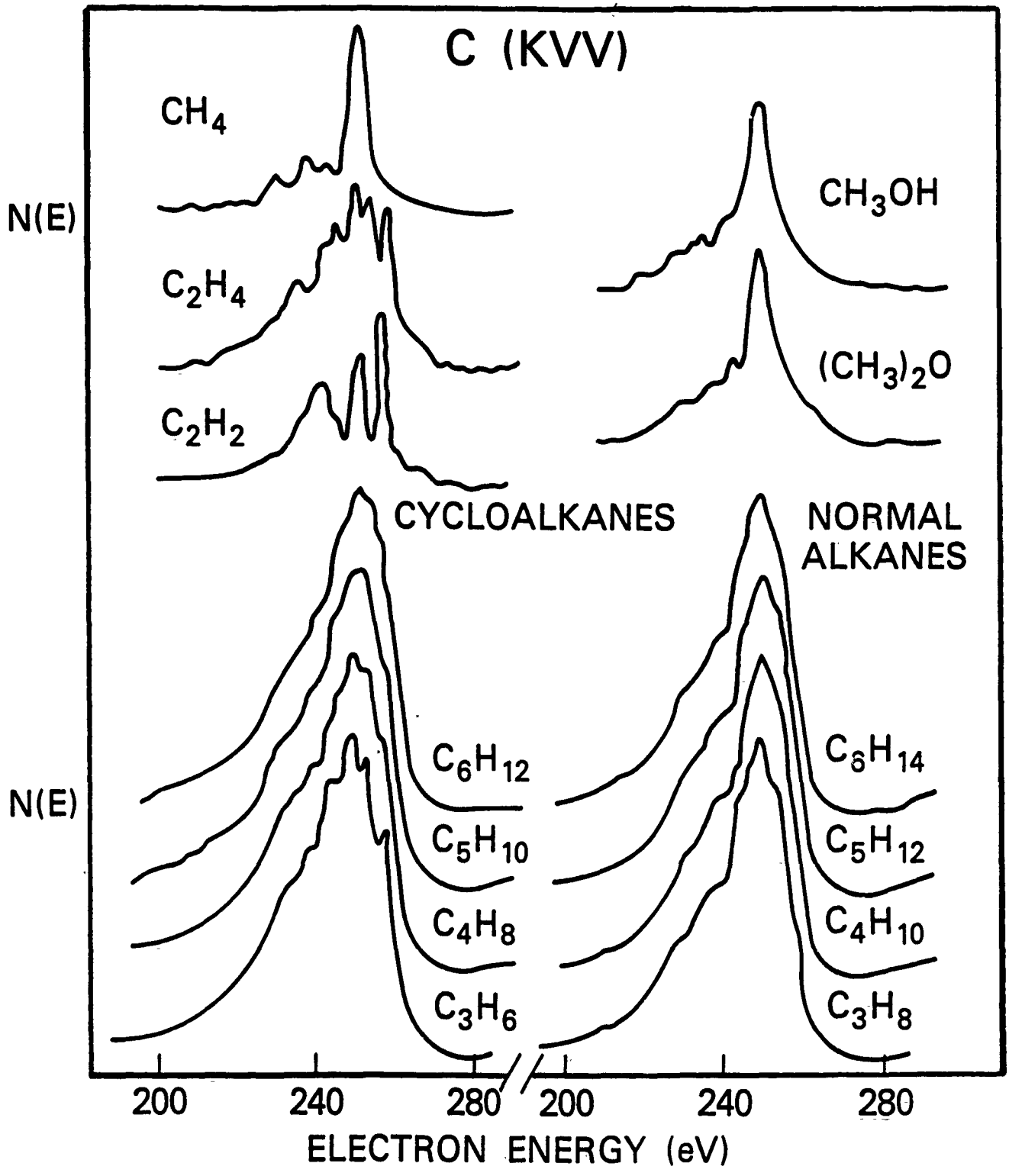
C (KVV)
CH4
C2H4
C2H2
CH3OH
(CH3)2O
N(E)
CYCLOALKANES
NORMAL ALKANES
C6H12
C5H10
C4H8
C3H6
C6H14
C5H12
C4H10
C3H8
N(E)
200
240
280
200
240
280
ELECTRON ENERGY (eV)

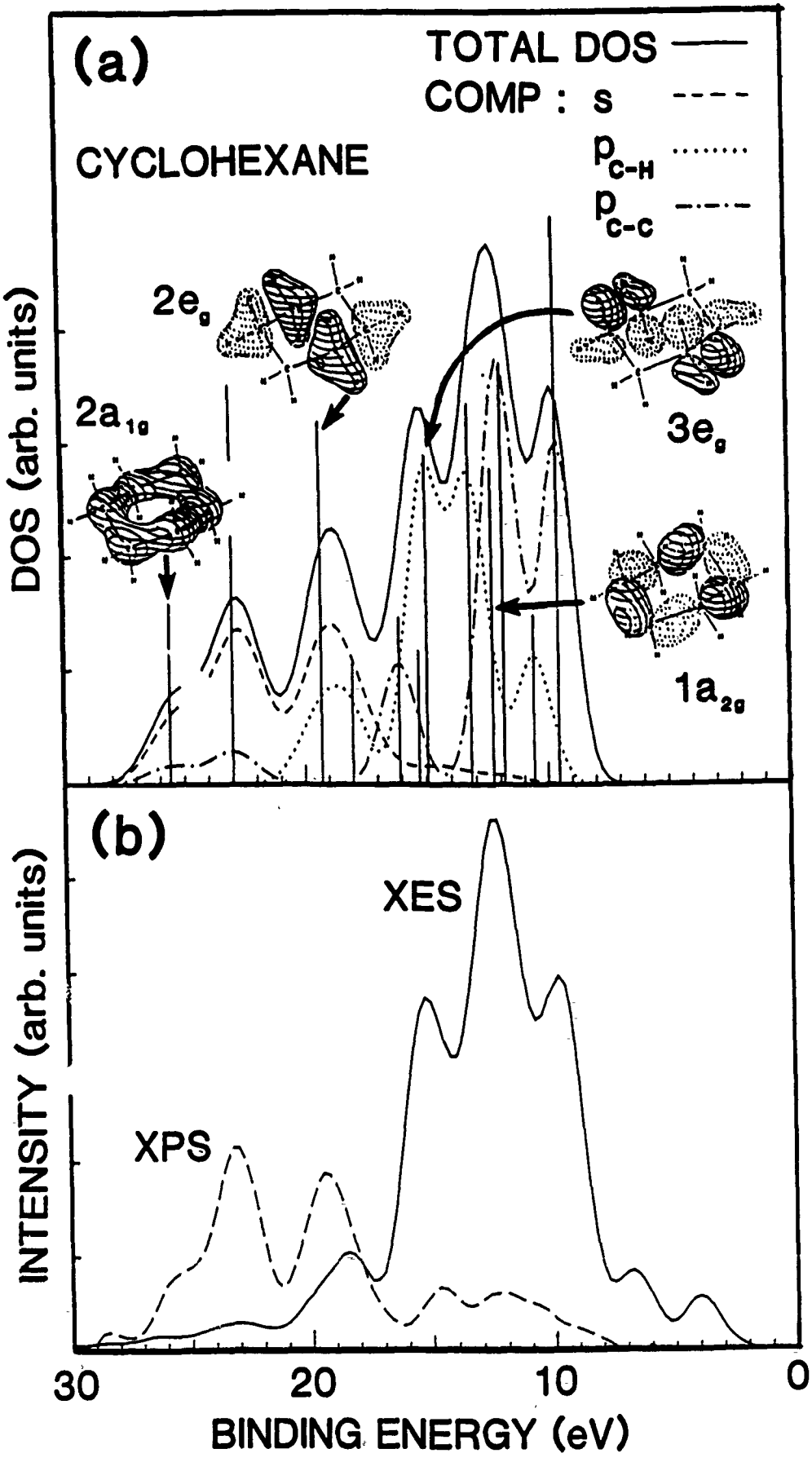
(a)
TOTAL DOS
COMP : s
p_{C-H}
p_{C-C}
CYCLOHEXANE
$2e_g$
$2a_{1g}$
$3e_g$
$1a_{2g}$
DOS (arb. units)
(b)
XES
XPS
INTENSITY (arb. units)
30
20
10
0
BINDING ENERGY (eV)

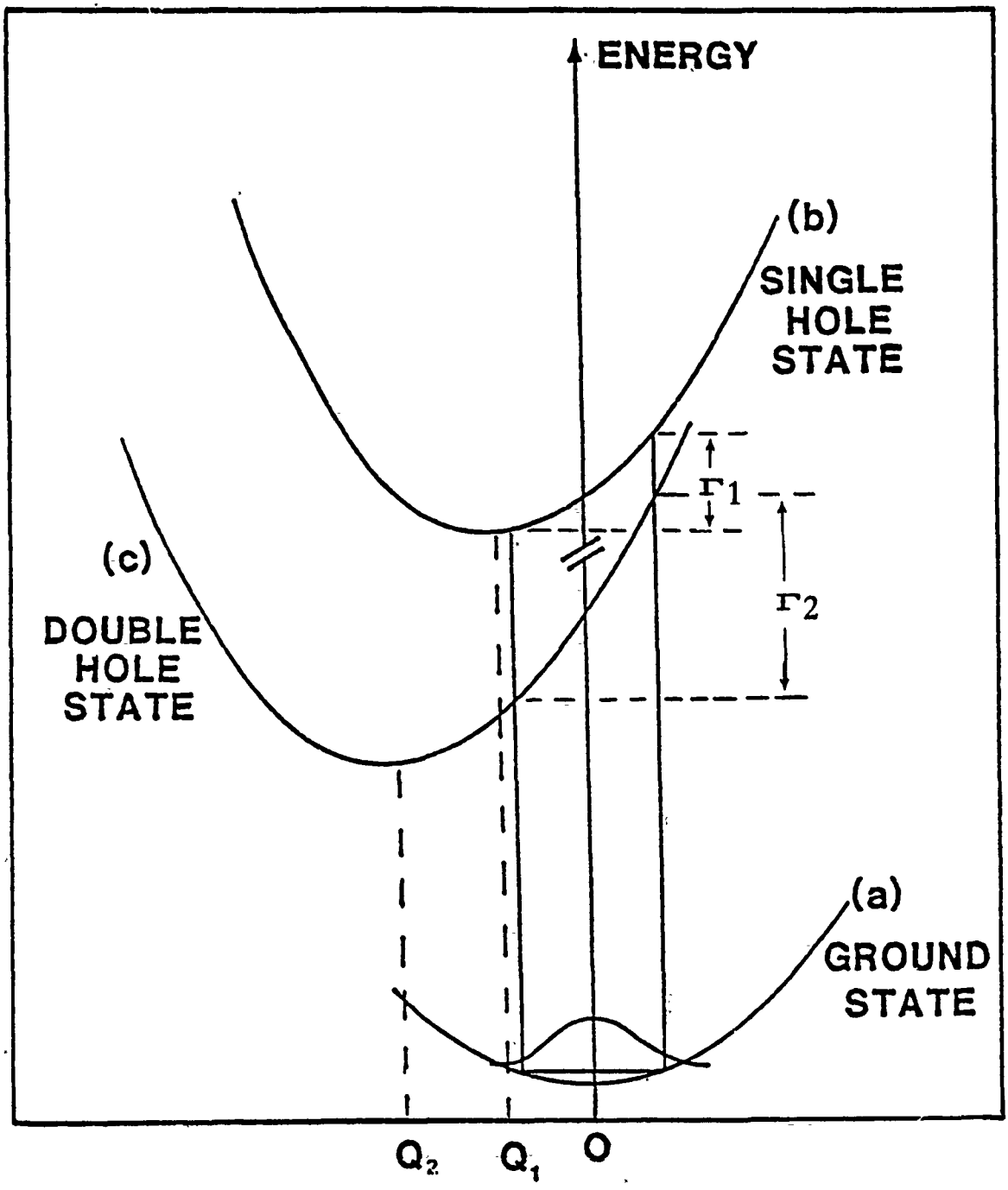
ENERGY
(b)
SINGLE
HOLE
STATE
Γ1
Γ2
(c)
DOUBLE
HOLE
STATE
(a)
GROUND
STATE
Q2
Q1
O
Configuration Coordinate Q

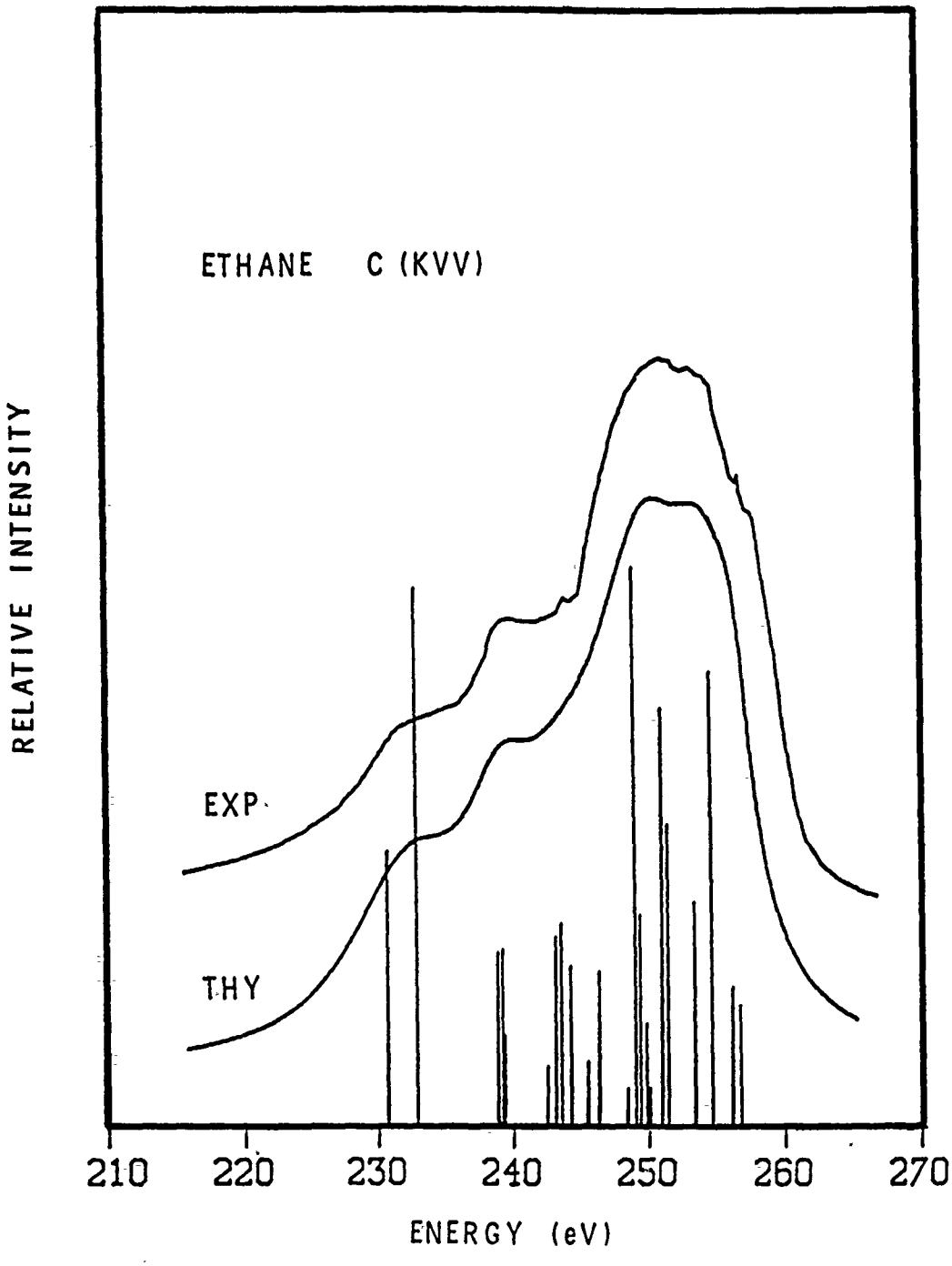
ETHANE C (KVV)
RELATIVE INTENSITY
EXP
THY
210
220
230
240
250
260
270
ENERGY (eV)

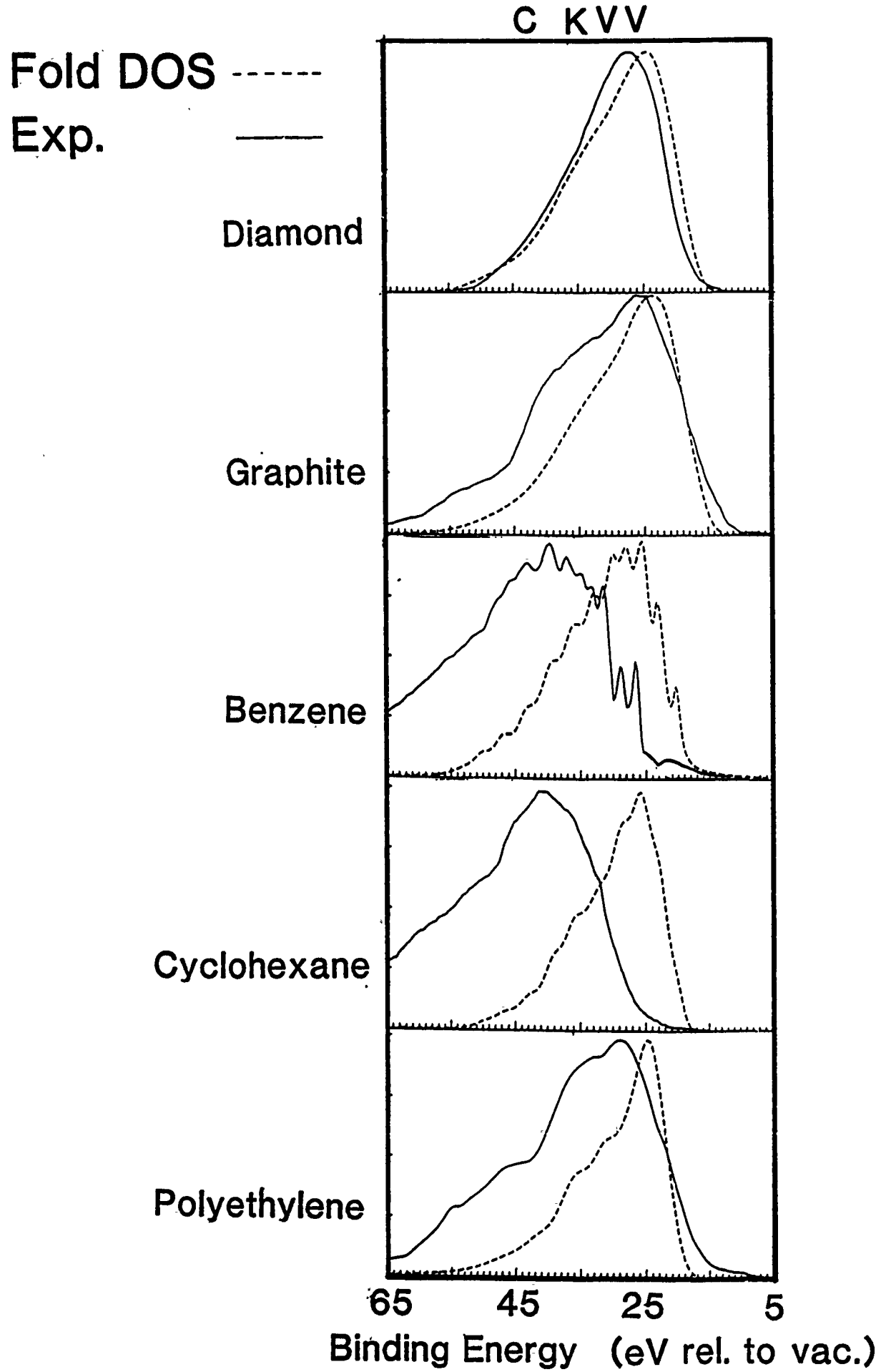
C KVV
Fold DOS ------
Exp. ——
Diamond
Graphite
Benzene
Cyclohexane
Polyethylene
65
45
25
5
Binding Energy (eV rel. to vac.)

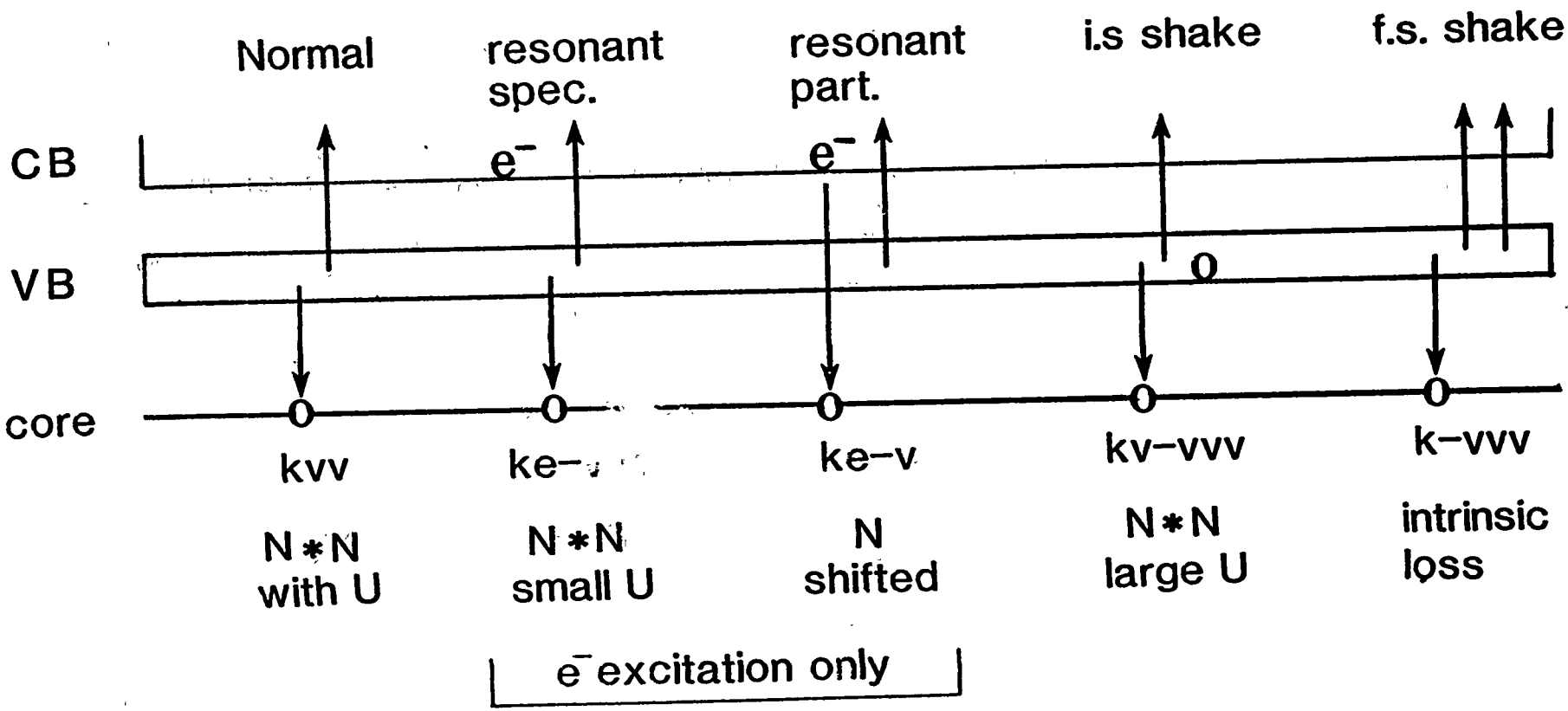
Normal
resonant spec.
resonant part.
i.s shake
f.s. shake
CB
VB
core
e⁻
e⁻
kvv
ke–
ke–v
kv–vvv
k–vvv
N*N with U
N*N small U
N shifted
N*N large U
intrinsic loss
e⁻ excitation only

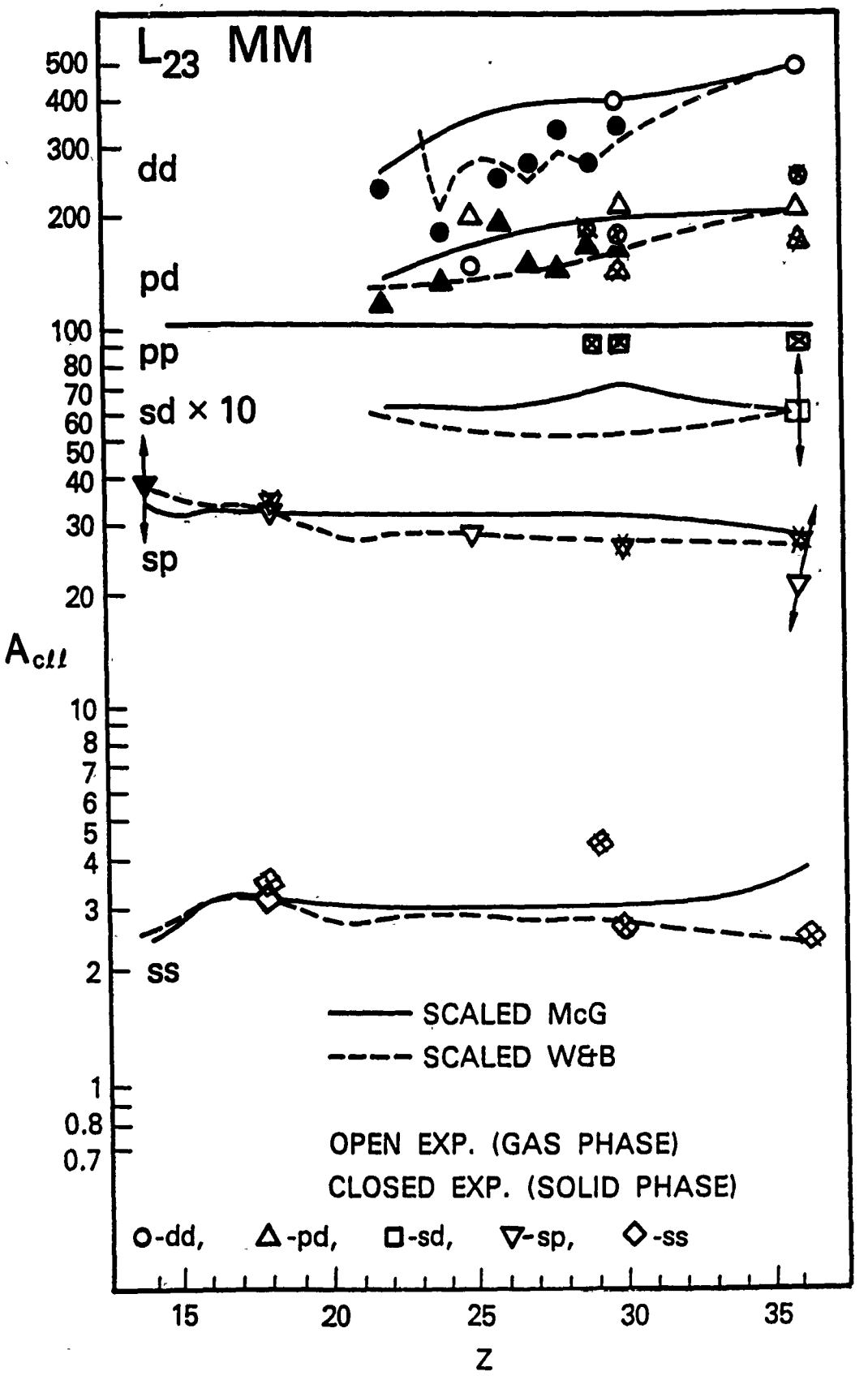
L_{23} MM
500
400
300
200
100
80
70
60
50
40
30
20
10
8
7
6
5
4
3
2
1
0.8
0.7
dd
pd
pp
sd × 10
sp
ss
A_{cll}
SCALED McG
SCALED W&B
OPEN EXP. (GAS PHASE)
CLOSED EXP. (SOLID PHASE)
O-dd, Δ-pd, □-sd, ▽-sp, ◇-ss
15
20
25
30
35
Z

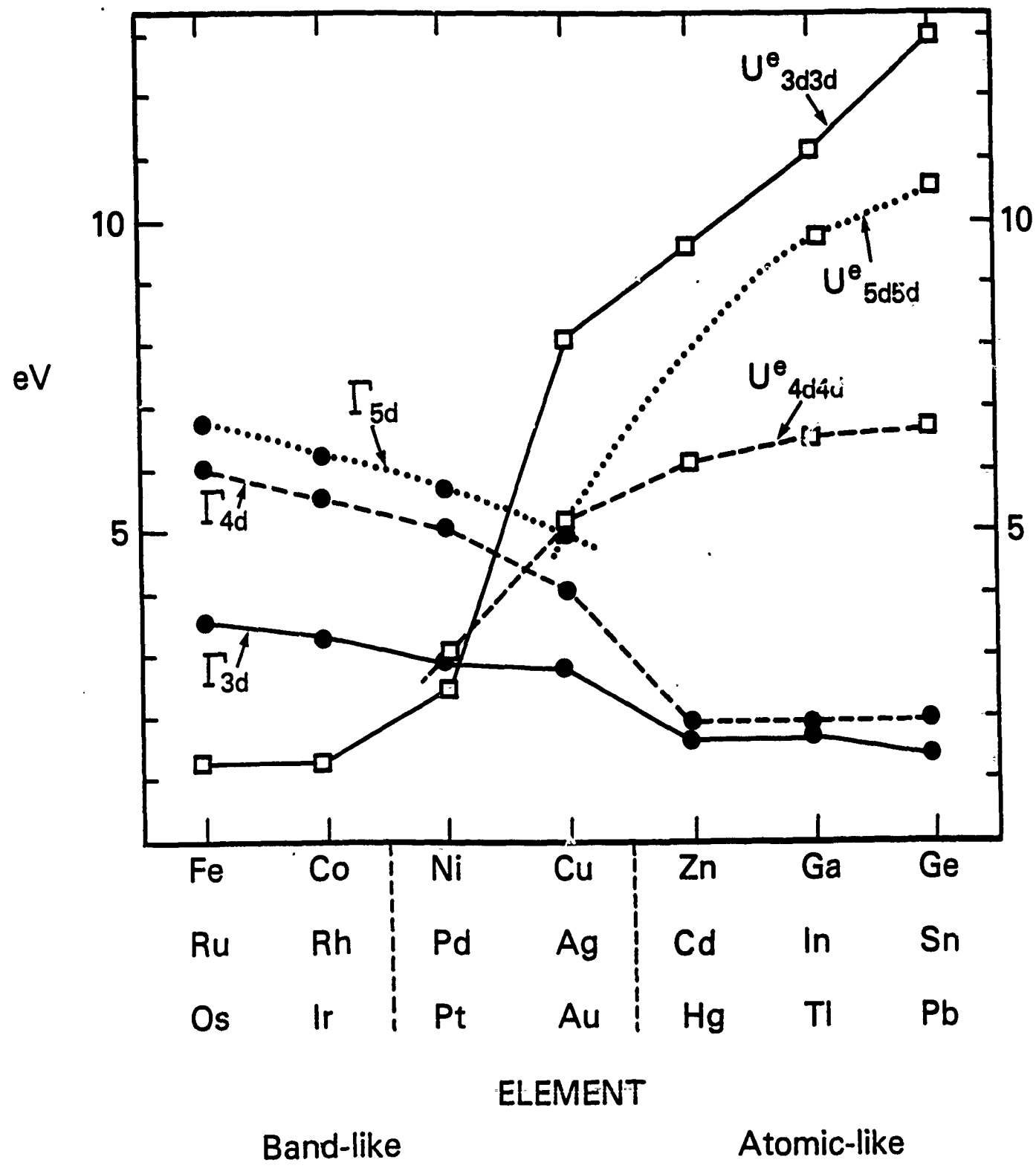
eV
10
5
10
5
U^e_{3d3d}
U^e_{5d5d}
U^e_{4d4d}
Γ_{5d}
Γ_{4d}
Γ_{3d}
Fe Co Ni Cu Zn Ga Ge
Ru Rh Pd Ag Cd In Sn
Os Ir Pt Au Hg Tl Pb
ELEMENT
Band-like
Atomic-like

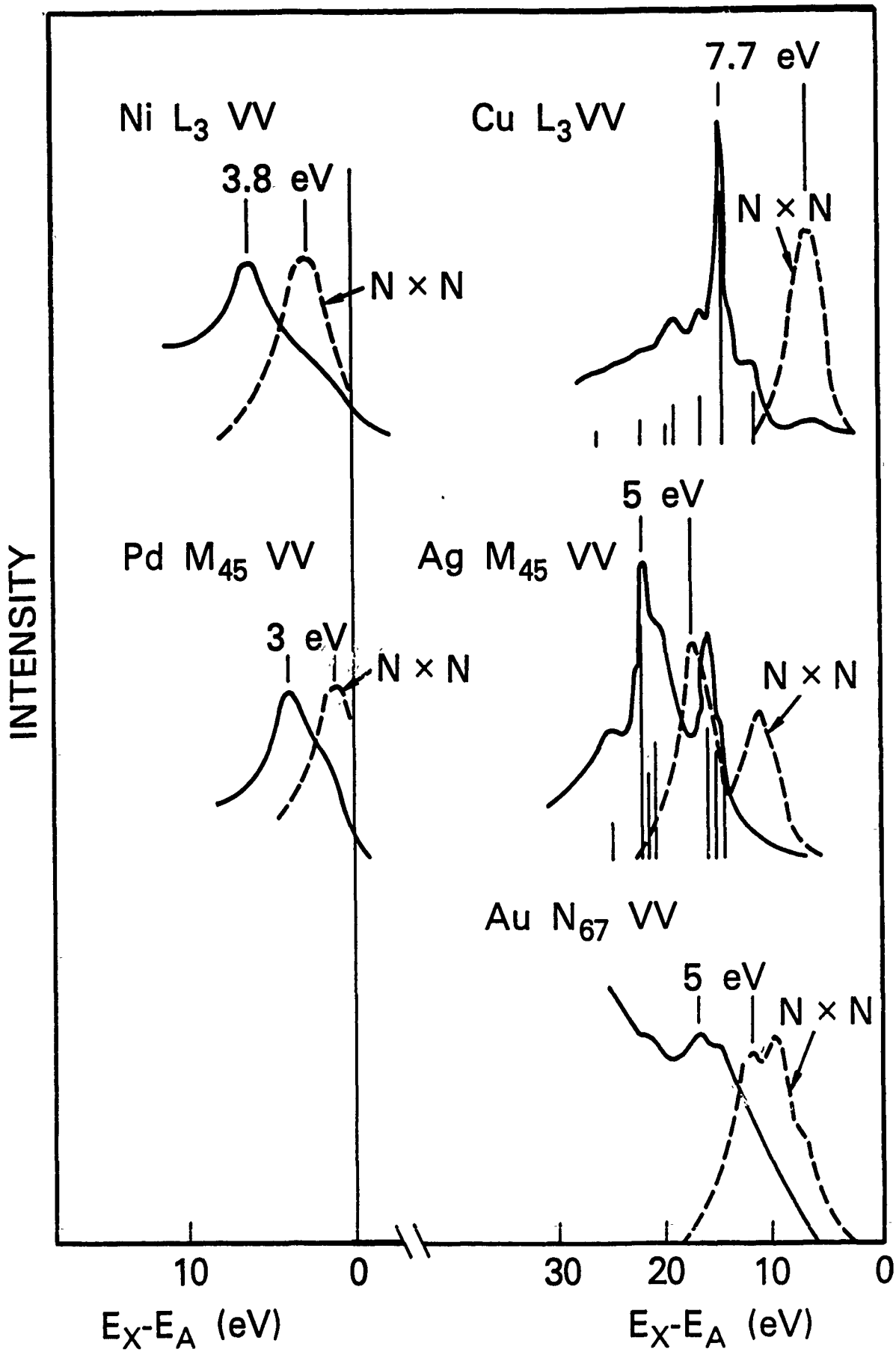
Ni L_3 VV
3.8 eV
N × N
Cu L_3VV
7.7 eV
N × N
Pd M_{45} VV
3 eV
N × N
Ag M_{45} VV
5 eV
N × N
Au N_{67} VV
5 eV
N × N
INTENSITY
10
0
30
20
10
0
E_X-E_A (eV)
E_X-E_A (eV)

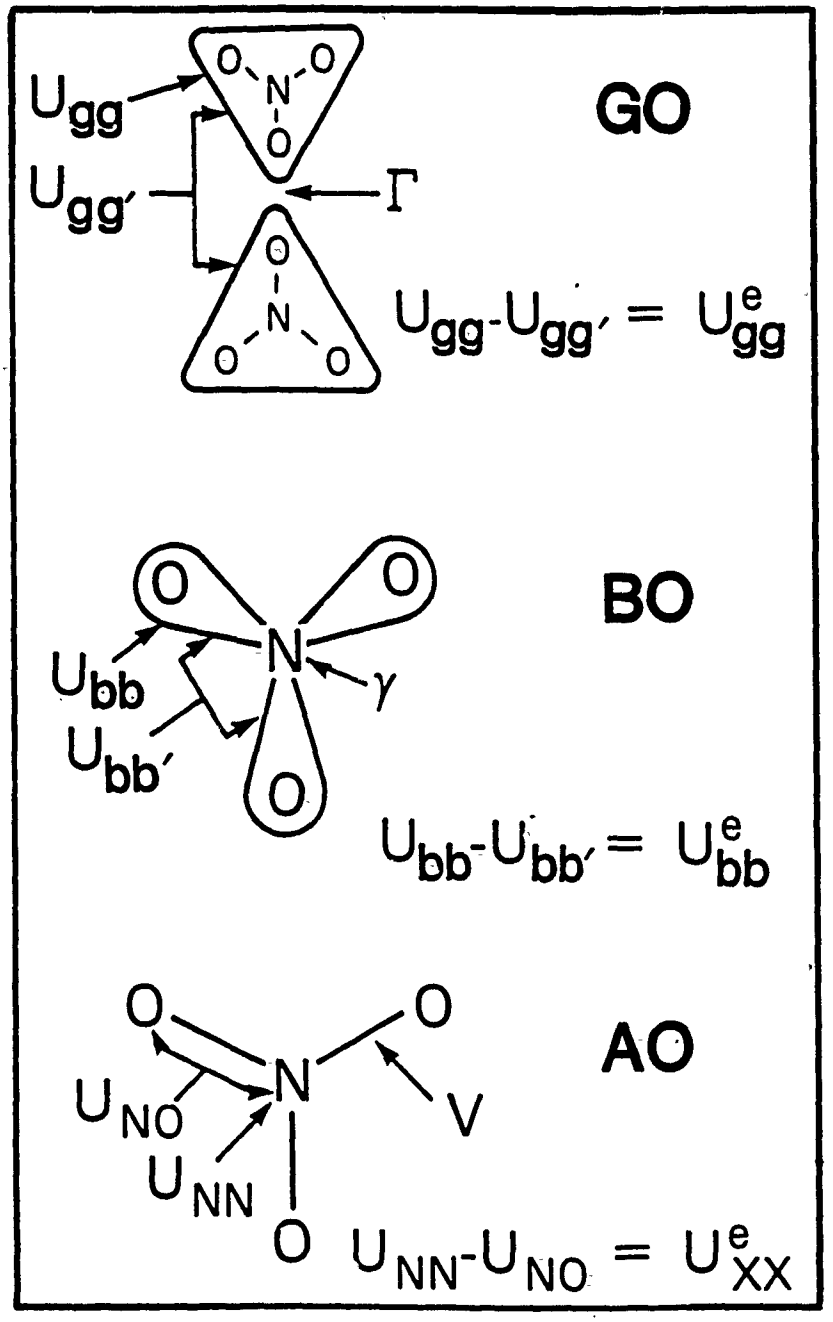
GO
U_{gg}
$U_{gg'}$
Γ
$U_{gg}-U_{gg'} = U^e_{gg}$
BO
U_{bb}
$U_{bb'}$
γ
$U_{bb}-U_{bb'} = U^e_{bb}$
AO
U_{NO}
U_{NN}
V
$U_{NN}-U_{NO} = U^e_{XX}$

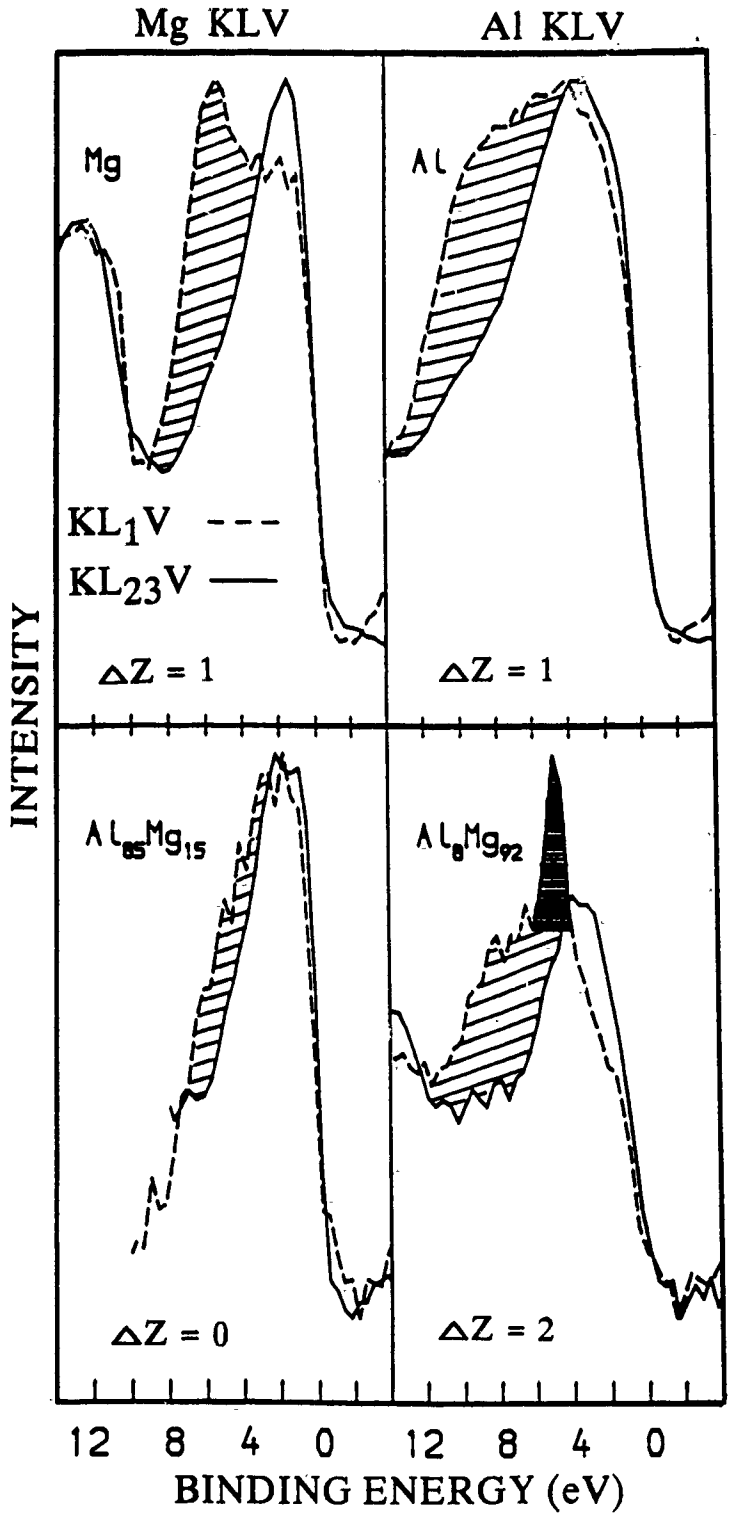
Mg KLV
Al KLV
Mg
Al
KL1V
KL23V
ΔZ = 1
ΔZ = 1
Al85Mg15
Al8Mg92
ΔZ = 0
ΔZ = 2
INTENSITY
12 8 4 0 12 8 4 0
BINDING ENERGY (eV)

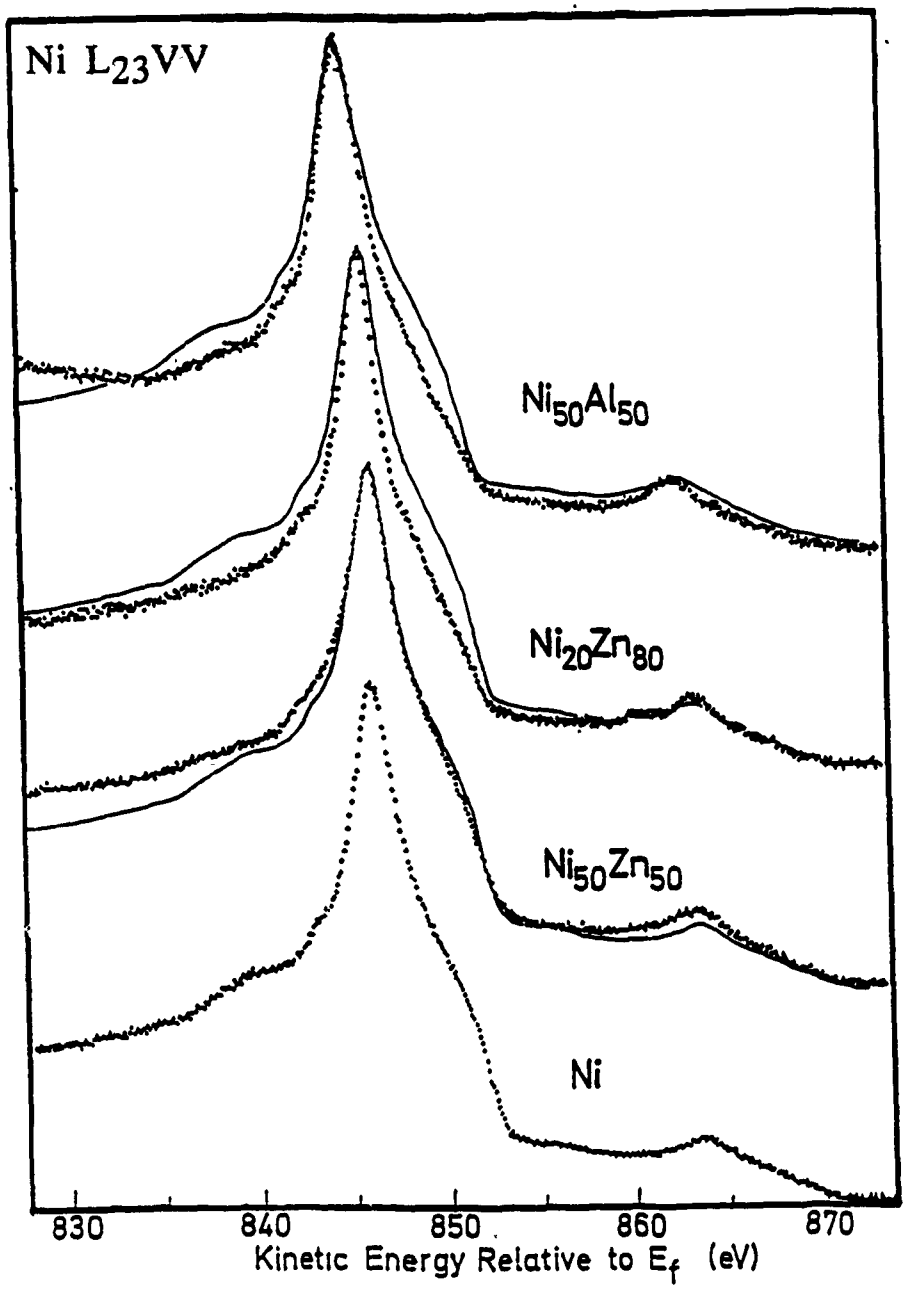
Ni $L_{23}VV$
$Ni_{50}Al_{50}$
$Ni_{20}Zn_{80}$
$Ni_{50}Zn_{50}$
Ni
830
840
850
860
870
Kinetic Energy Relative to E_f (eV)

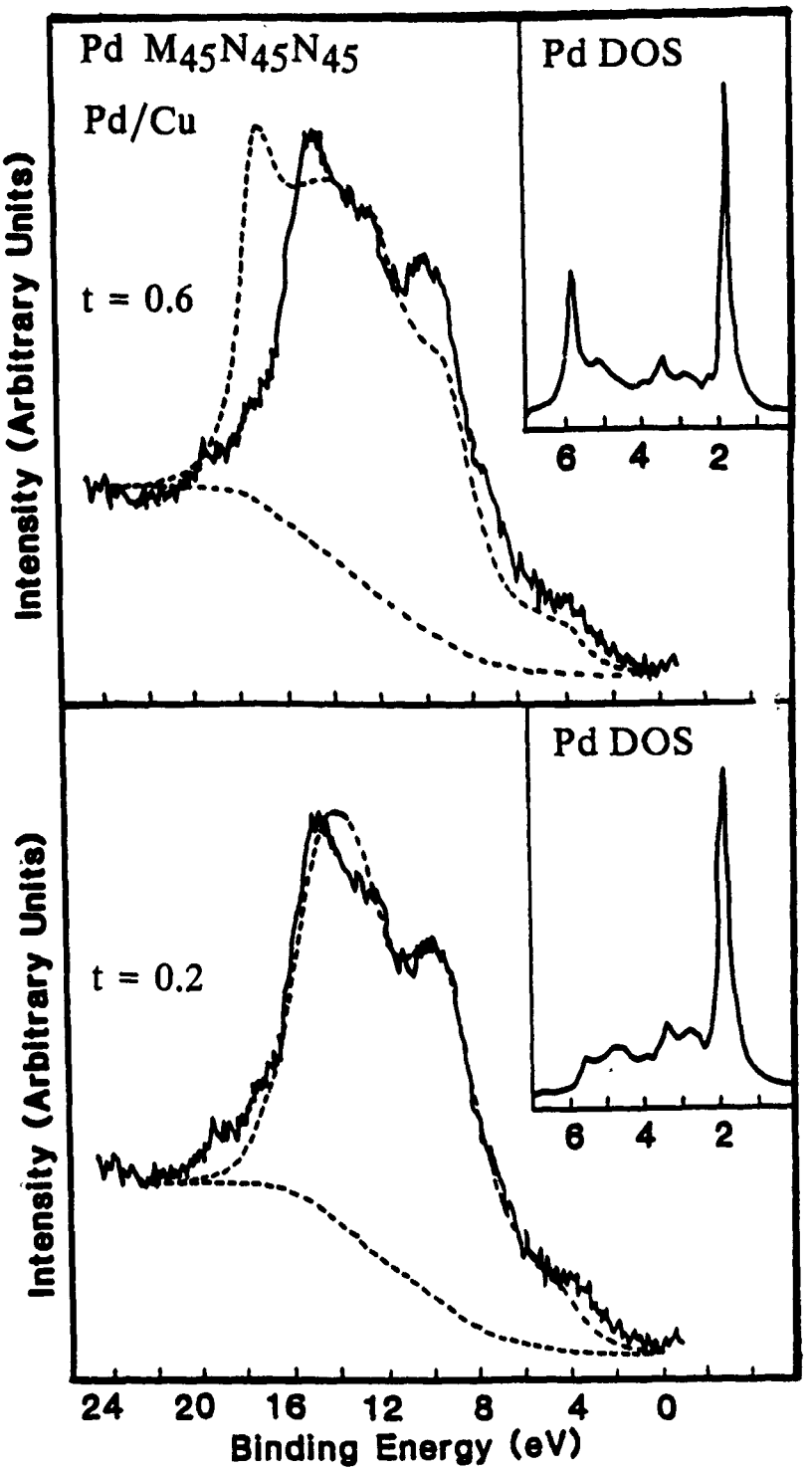
Pd $M_{45}N_{45}N_{45}$
Pd/Cu
t = 0.6
Pd DOS
6 4 2
Intensity (Arbitrary Units)
t = 0.2
Pd DOS
6 4 2
Intensity (Arbitrary Units)
24 20 16 12 8 4 0
Binding Energy (eV)

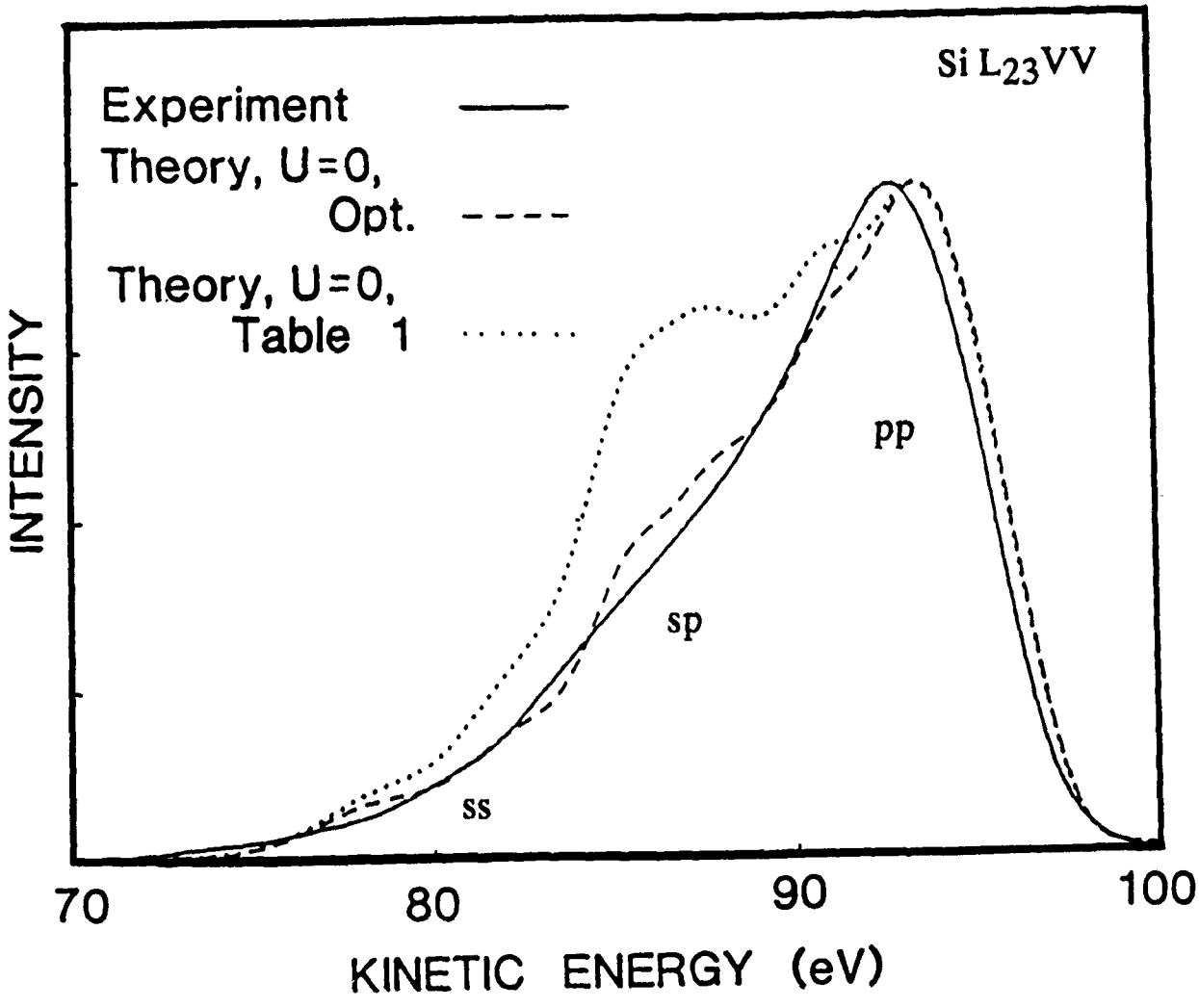
Si $L_{23}VV$
Experiment
Theory, U=0, Opt.
Theory, U=0, Table 1
INTENSITY
pp
sp
ss
70
80
90
100
KINETIC ENERGY (eV)

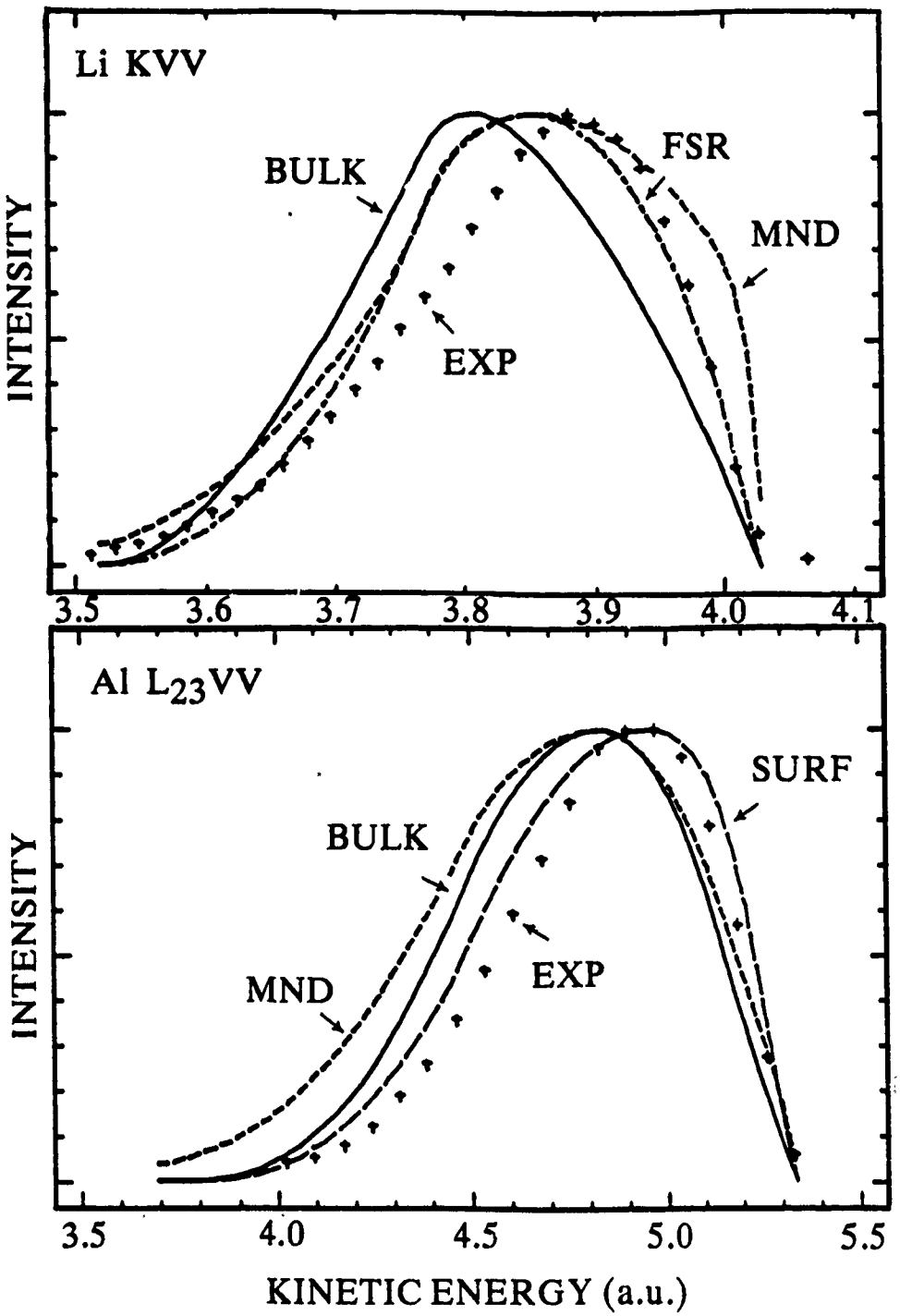
Li KVV
BULK
FSR
MND
EXP
INTENSITY
3.5
3.6
3.7
3.8
3.9
4.0
4.1
Al $L_{23}VV$
SURF
BULK
MND
EXP
INTENSITY
3.5
4.0
4.5
5.0
5.5
KINETIC ENERGY (a.u.)

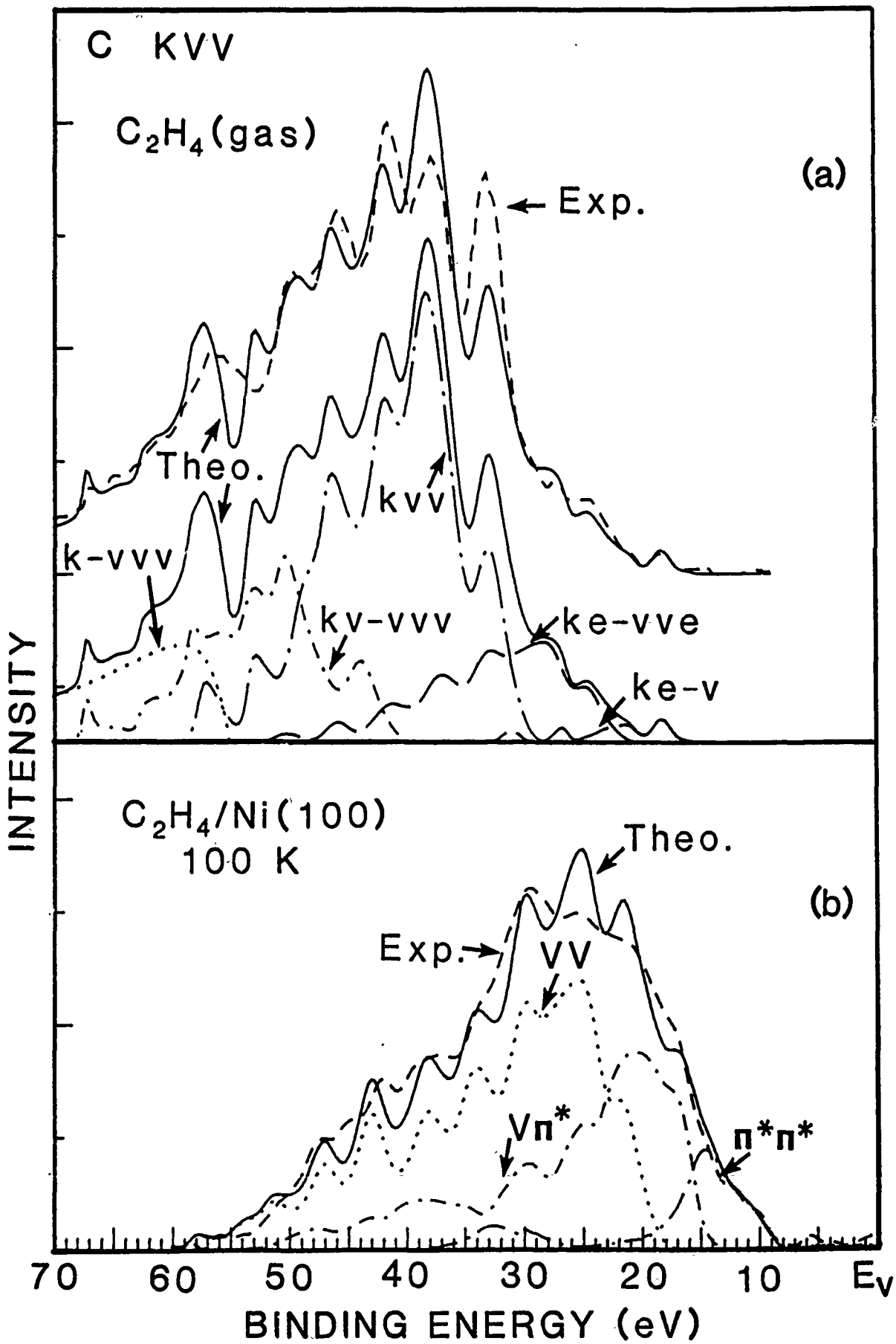
C KVV
C_2H_4(gas)
(a)
Exp.
Theo.
kvv
k-vvv
kv-vvv
ke-vve
ke-v
C_2H_4/Ni(100)
100 K
(b)
Theo.
Exp.
VV
Vπ*
π*π*
INTENSITY
70
60
50
40
30
20
10
E_V
BINDING ENERGY (eV)

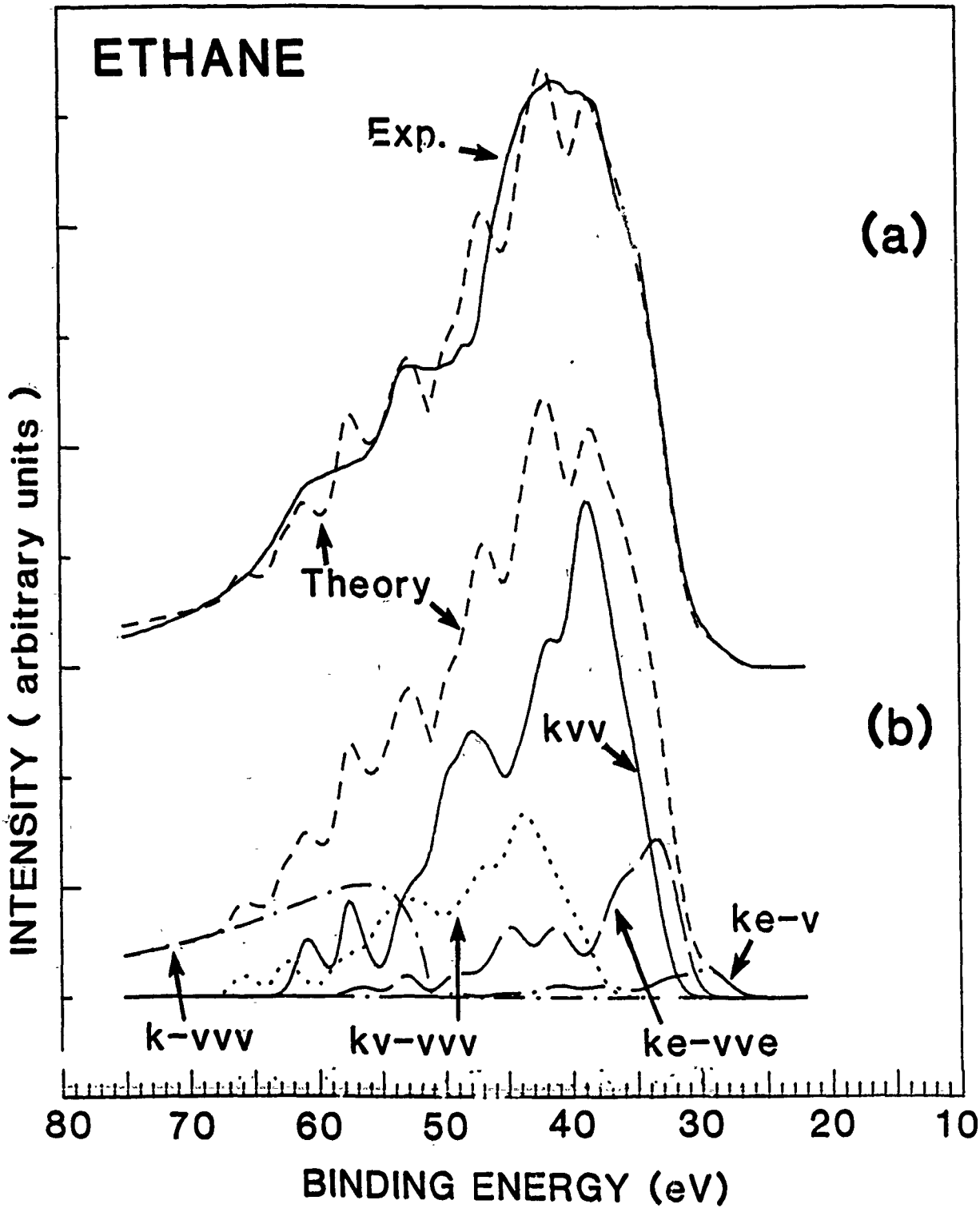
ETHANE
Exp.
Theory
(a)
(b)
kvv
ke-v
k-vvv
kv-vvv
ke-vve
INTENSITY (arbitrary units)
80
70
60
50
40
30
20
10
BINDING ENERGY (eV)

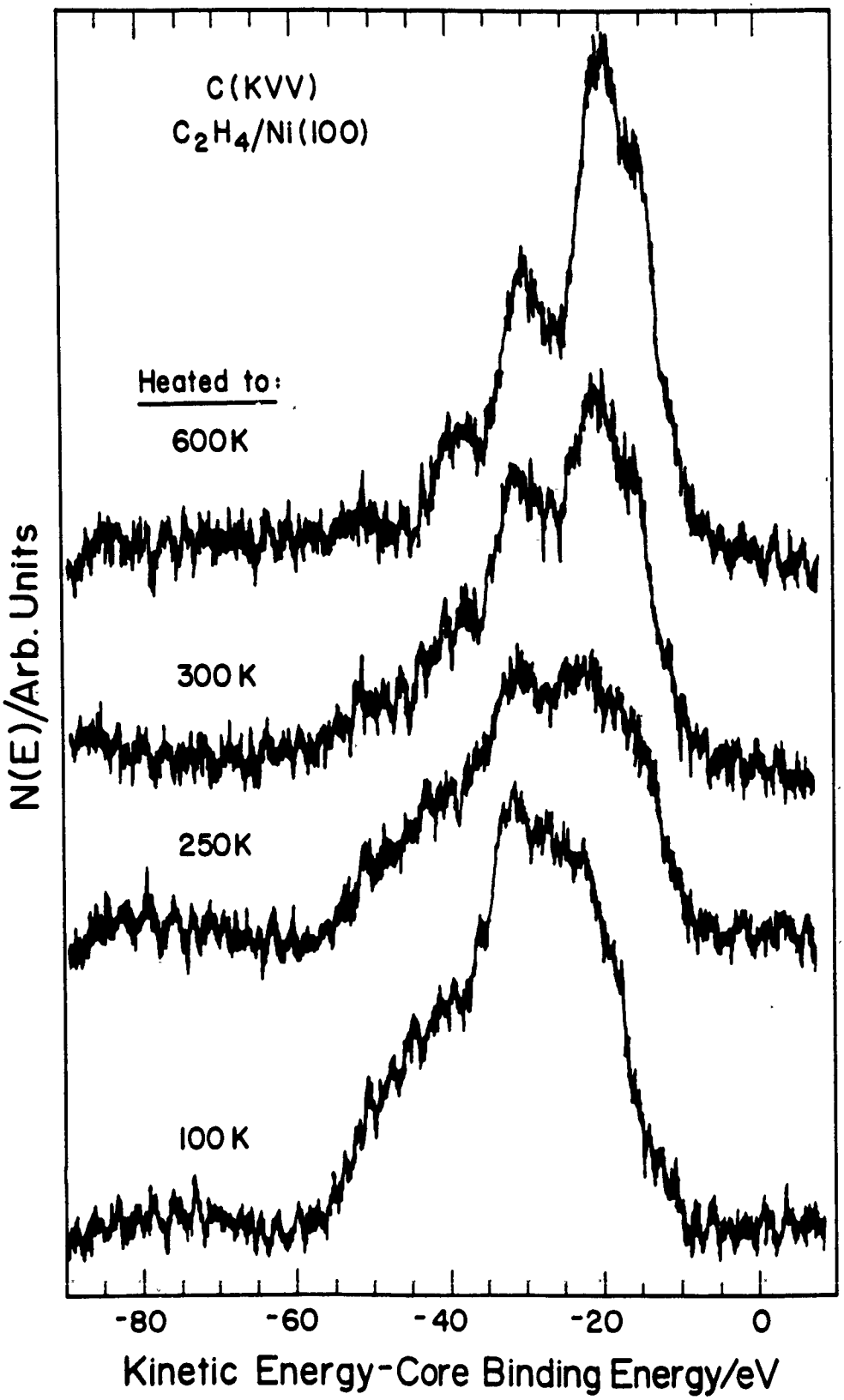
C(KVV)
C_2H_4/Ni(100)
Heated to:
600K
300K
250K
100K
N(E)/Arb. Units
-80
-60
-40
-20
0
Kinetic Energy-Core Binding Energy/eV

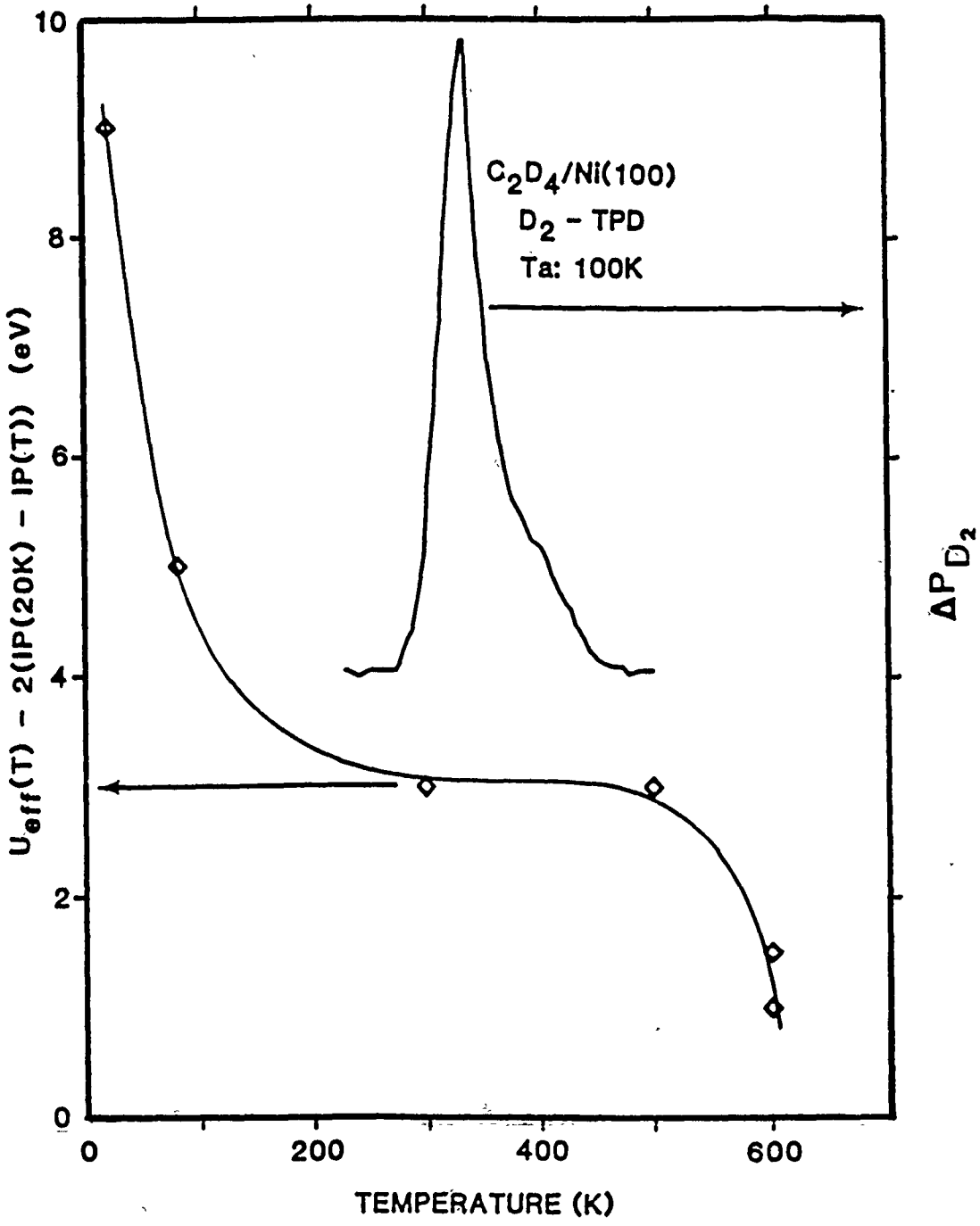
10
8
6
4
2
0
0
200
400
600
TEMPERATURE (K)
$U_{eff}(T) - 2(IP(20K) - IP(T))$ (eV)
ΔP_{D_2}
$C_2D_4/Ni(100)$
D_2 - TPD
Ta: 100K

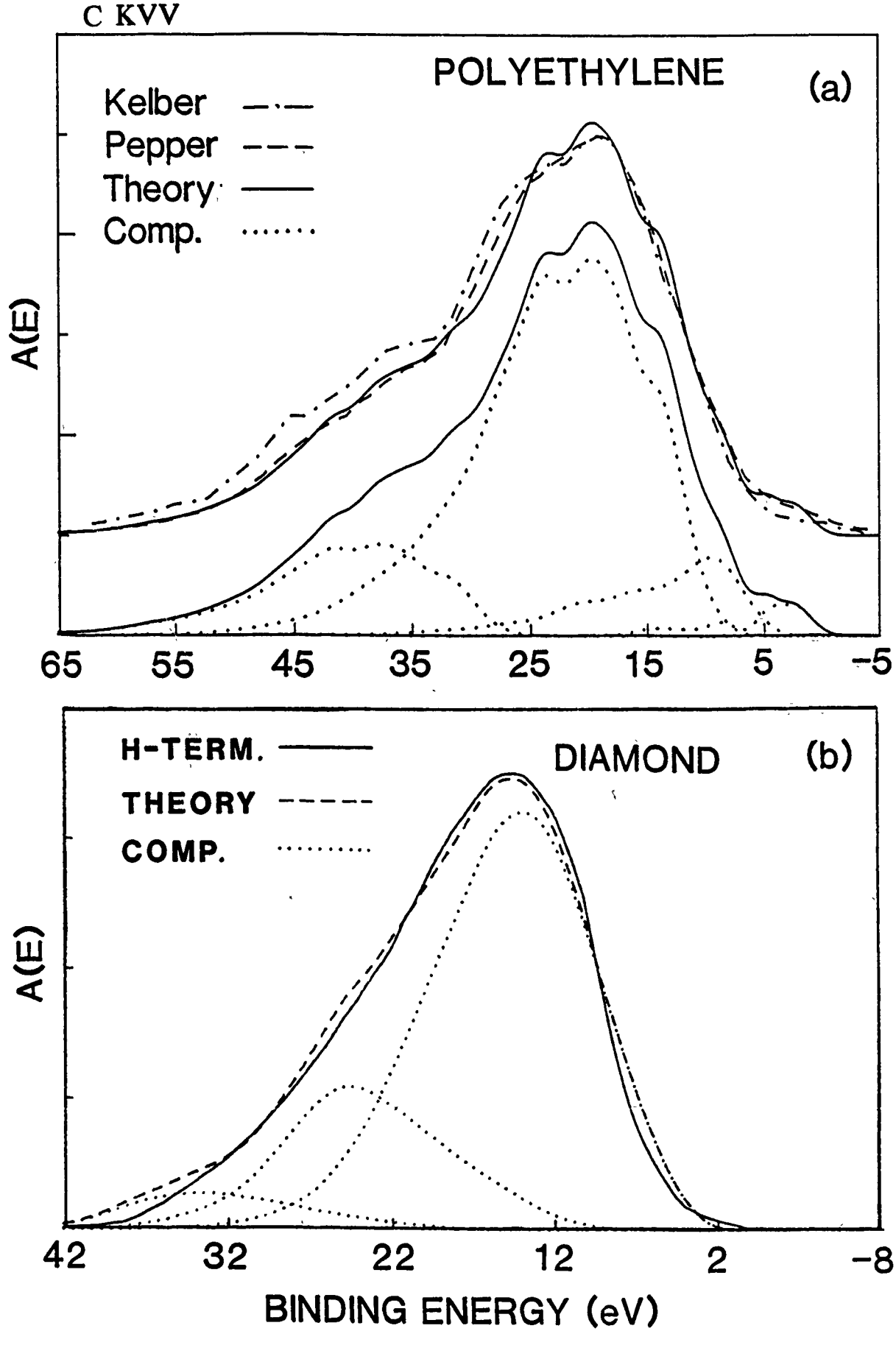
C KVV
POLYETHYLENE
(a)
Kelber
Pepper
Theory
Comp.
A(E)
65
55
45
35
25
15
5
-5
H-TERM.
THEORY
COMP.
DIAMOND
(b)
A(E)
42
32
22
12
2
-8
BINDING ENERGY (eV)

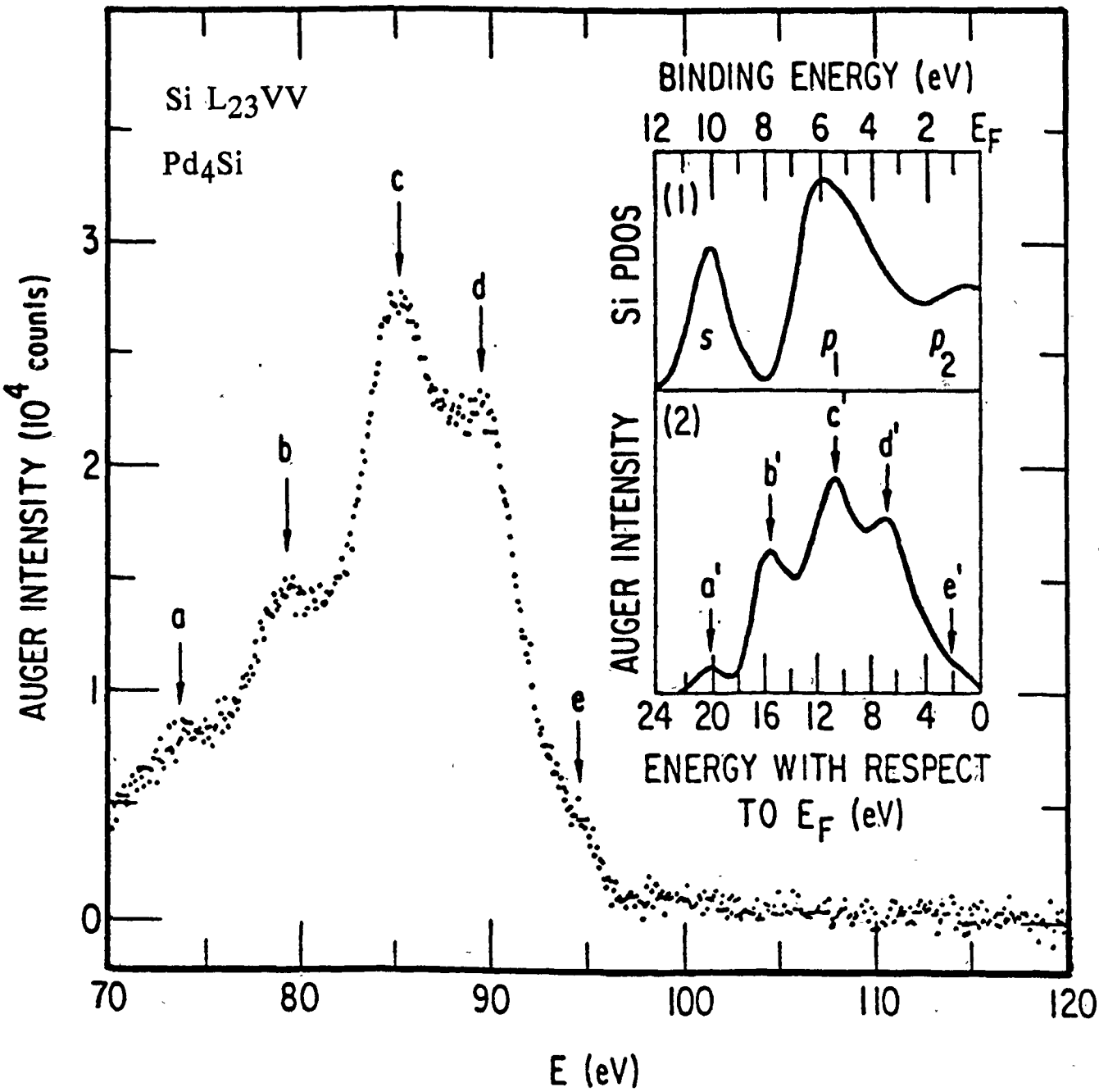
Si $L_{23}VV$
Pd_4Si
AUGER INTENSITY (10^4 counts)
E (eV)
a
b
c
d
e
BINDING ENERGY (eV)
12 10 8 6 4 2 E_F
(1)
Si PDOS
s
p_1
p_2
(2)
AUGER INTENSITY
a'
b'
c'
d'
e'
24 20 16 12 8 4 0
ENERGY WITH RESPECT TO E_F (eV)

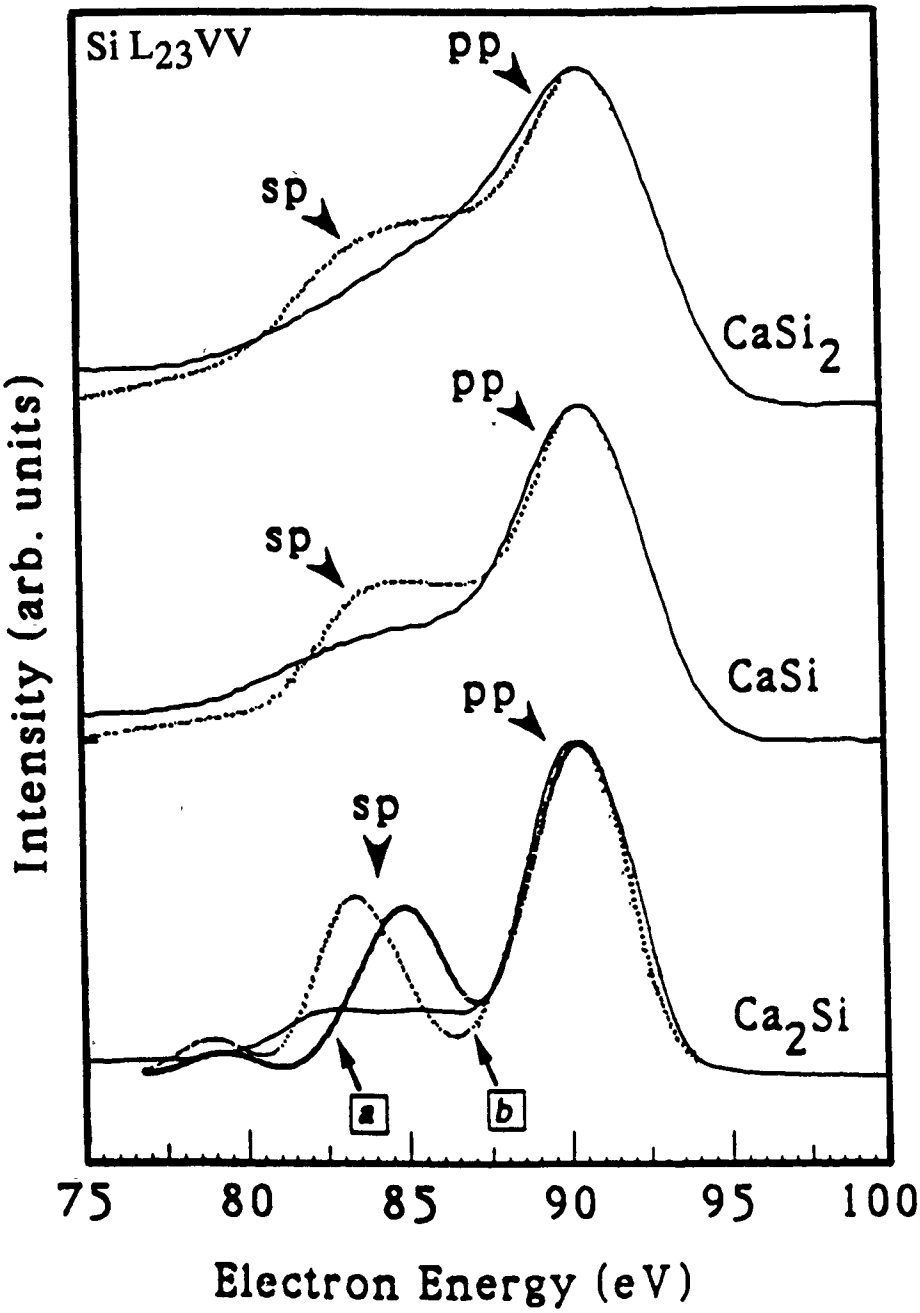
Si $L_{23}VV$
pp
sp
$CaSi_2$
pp
sp
CaSi
pp
sp
Ca_2Si
a
b
Intensity (arb. units)
75
80
85
90
95
100
Electron Energy (eV)

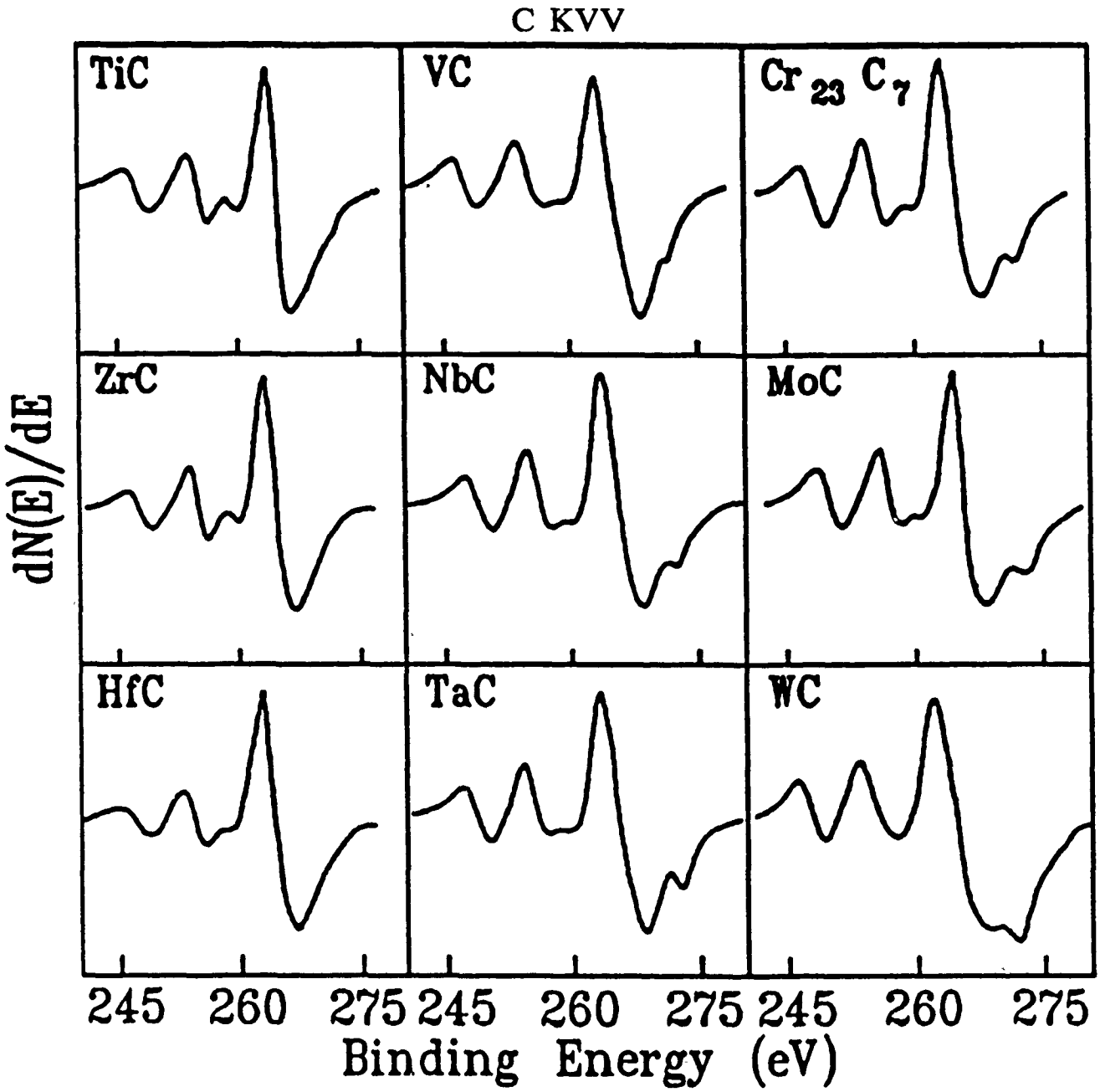
C KVV
TiC
VC
Cr 23 C 7
ZrC
NbC
MoC
HfC
TaC
WC
dN(E)/dE
245 260 275 245 260 275 245 260 275
Binding Energy (eV)

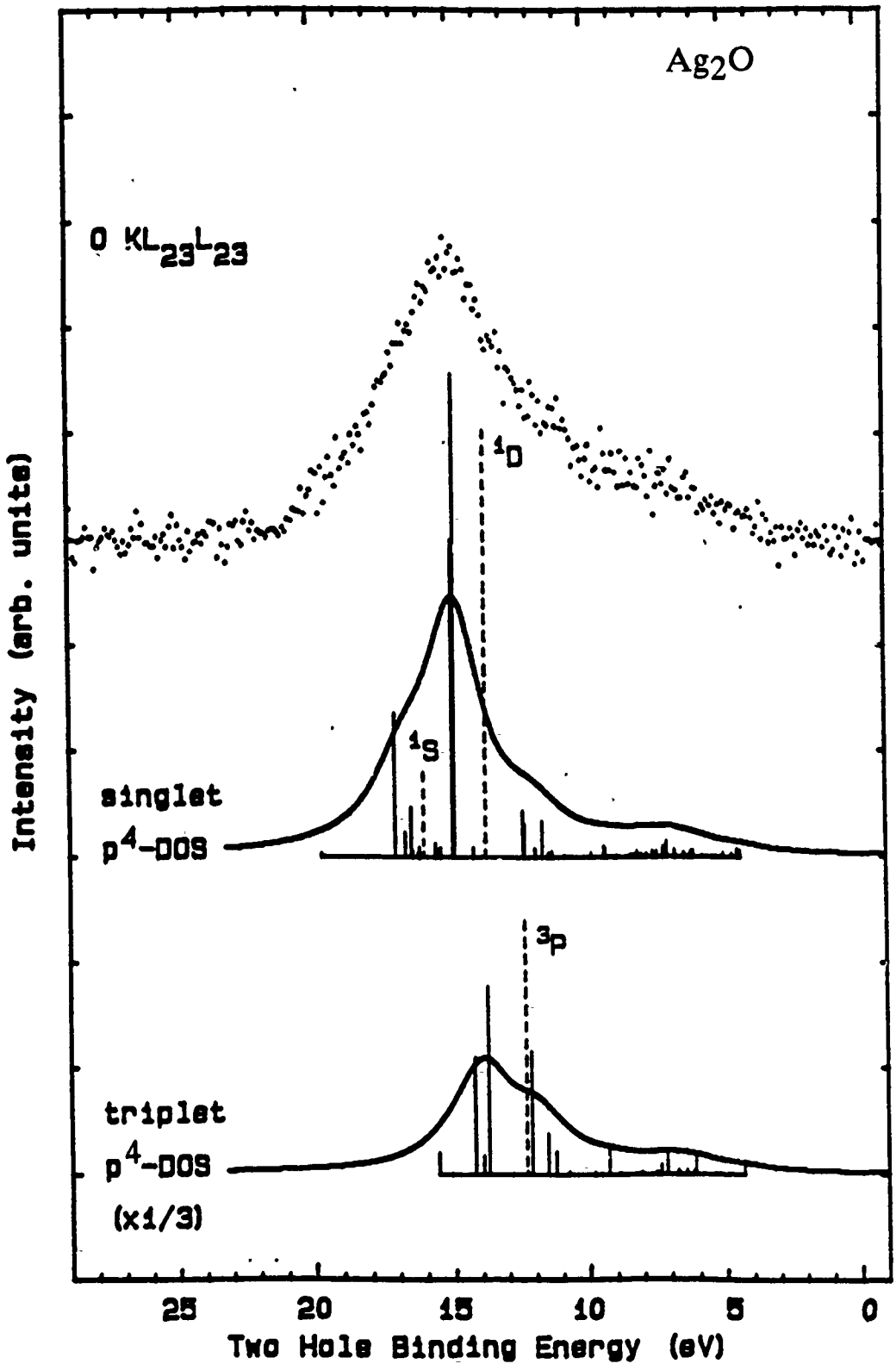
Ag2O
O KL23L23
1D
1S
singlet
p4-DOS
3P
triplet
p4-DOS
(x1/3)
Intensity (arb. units)
25
20
15
10
5
0
Two Hole Binding Energy (eV)

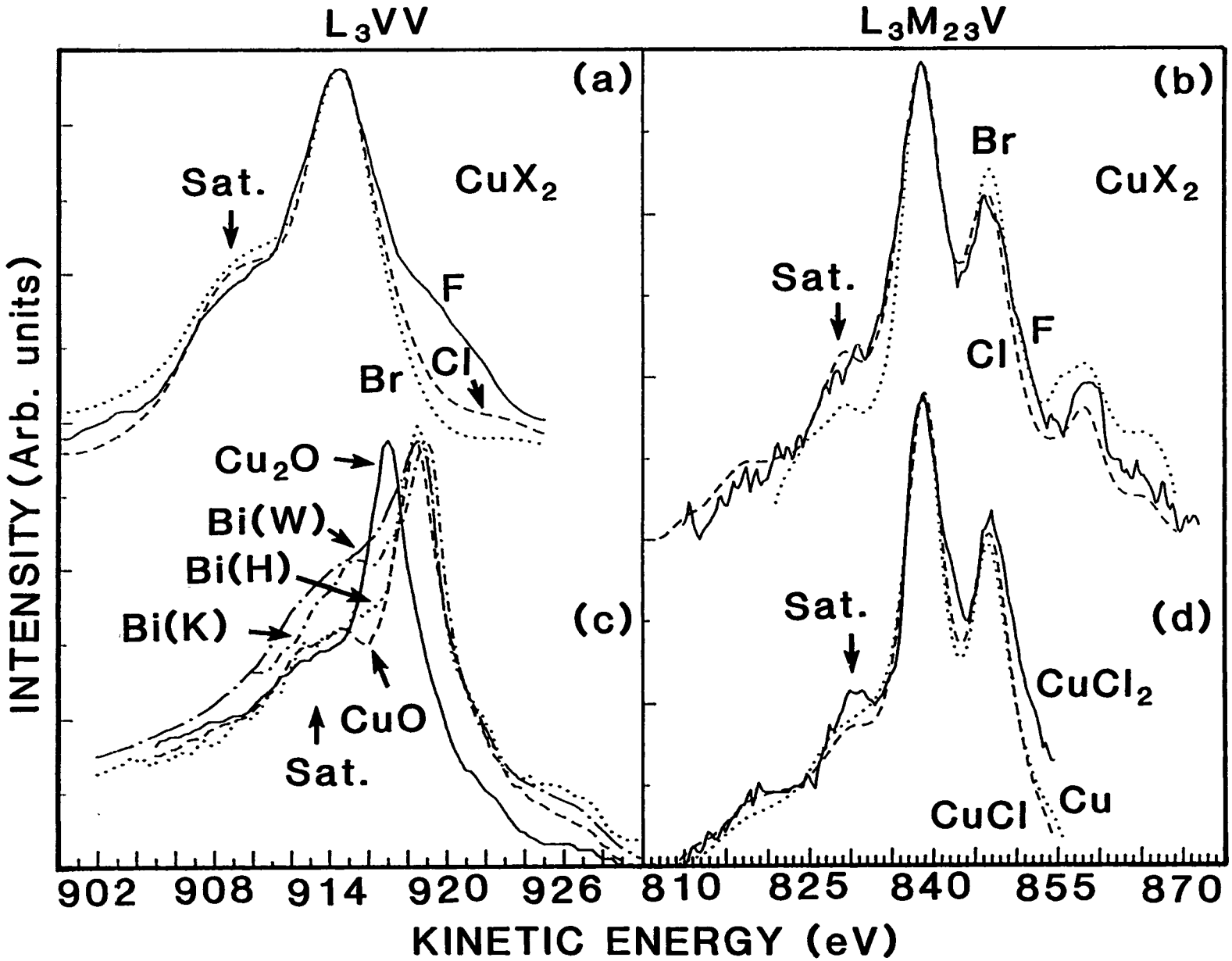
L3VV
L3M23V
(a)
(b)
(c)
(d)
Sat.
CuX2
F
Br
Cl
Cu2O
Bi(W)
Bi(H)
Bi(K)
CuO
Sat.
Br
CuX2
Sat.
Cl
F
Sat.
CuCl2
CuCl
Cu
INTENSITY (Arb. units)
902 908 914 920 926 810 825 840 855 870
KINETIC ENERGY (eV)

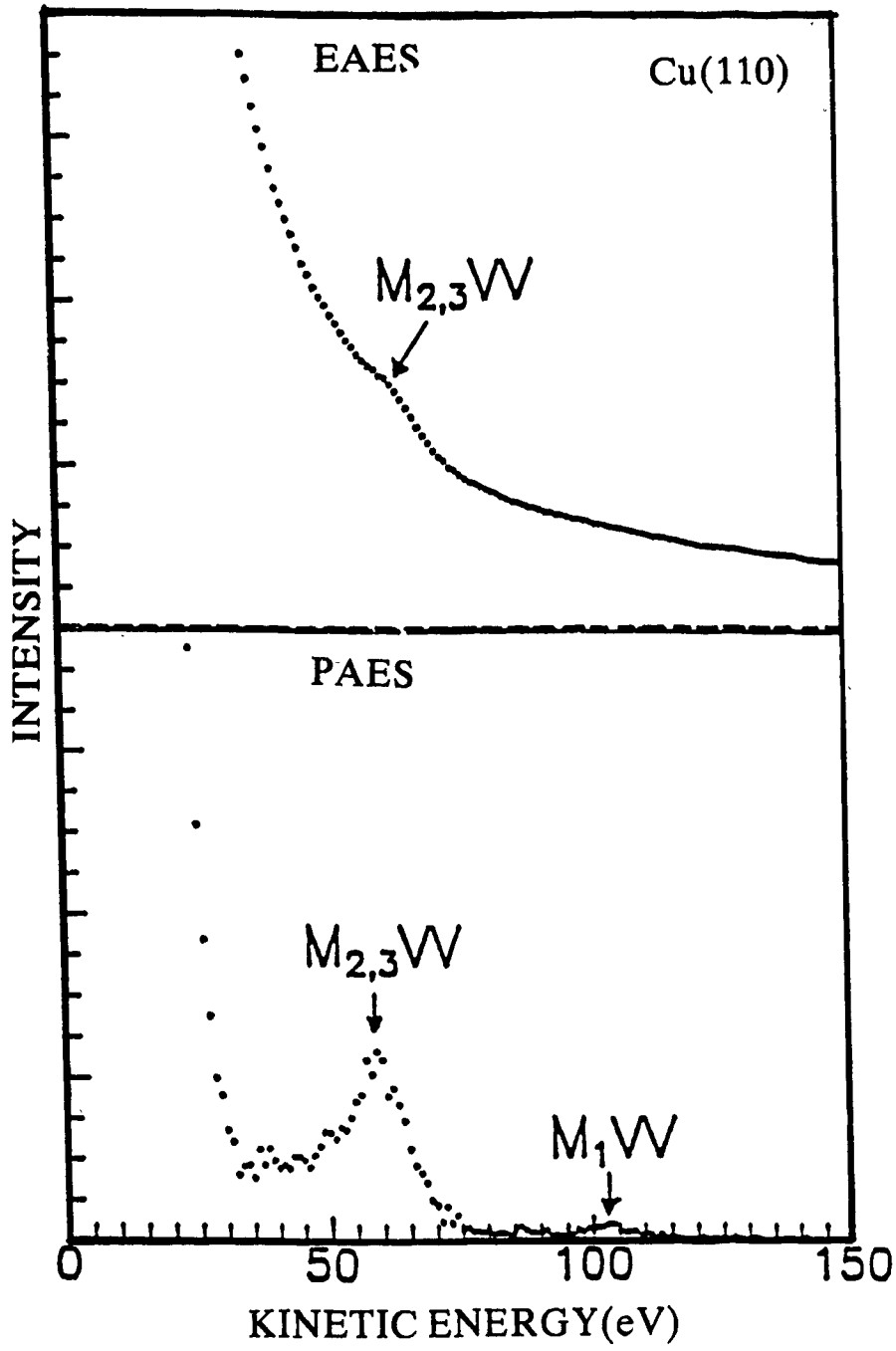
EAES
Cu(110)
M2,3VV
PAES
M2,3VV
M1VV
INTENSITY
0
50
100
150
KINETIC ENERGY(eV)

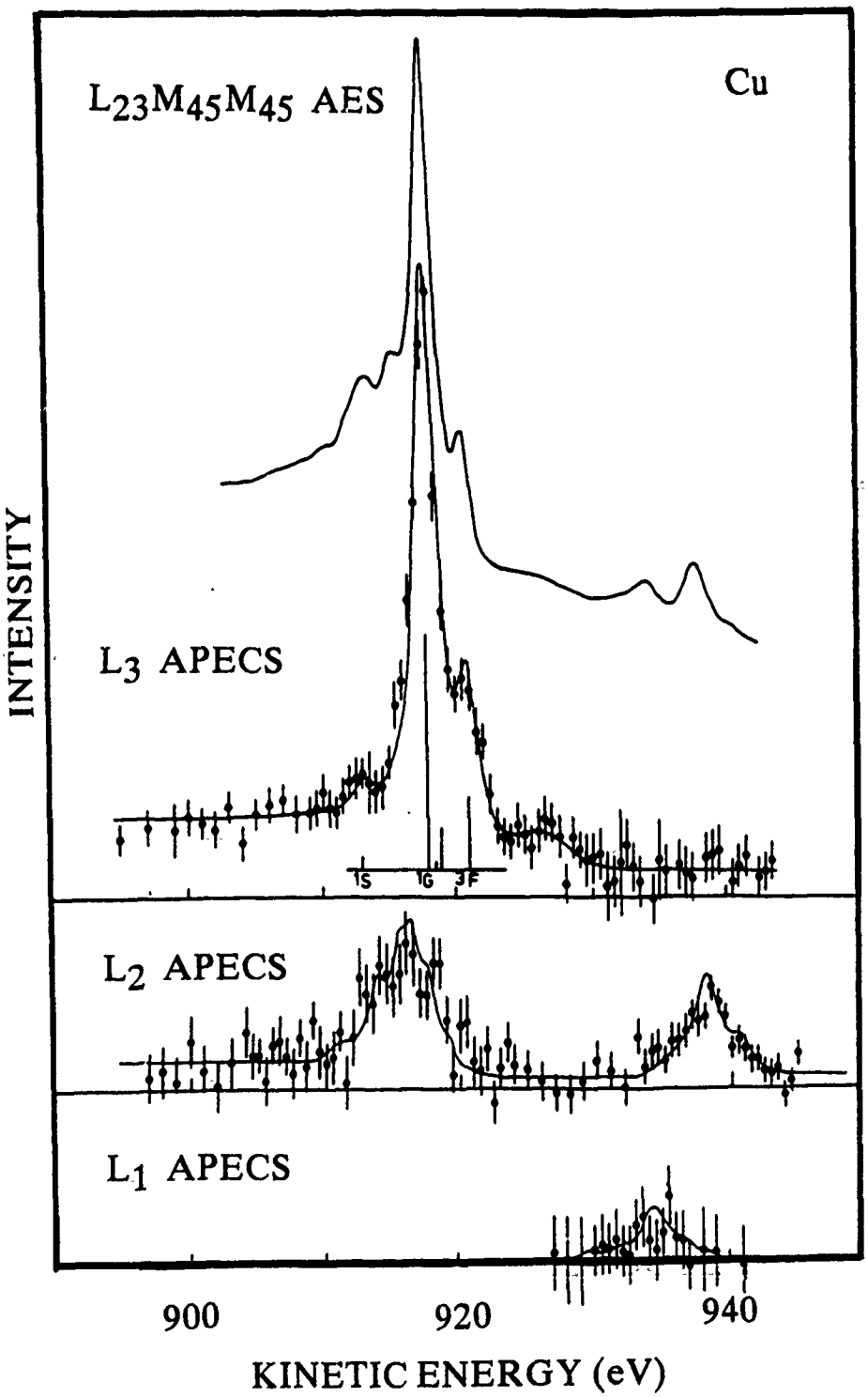
$L_{23}M_{45}M_{45}$ AES
Cu
INTENSITY
L_3 APECS
1S
1G
3F
L_2 APECS
L_1 APECS
900
920
940
KINETIC ENERGY (eV)

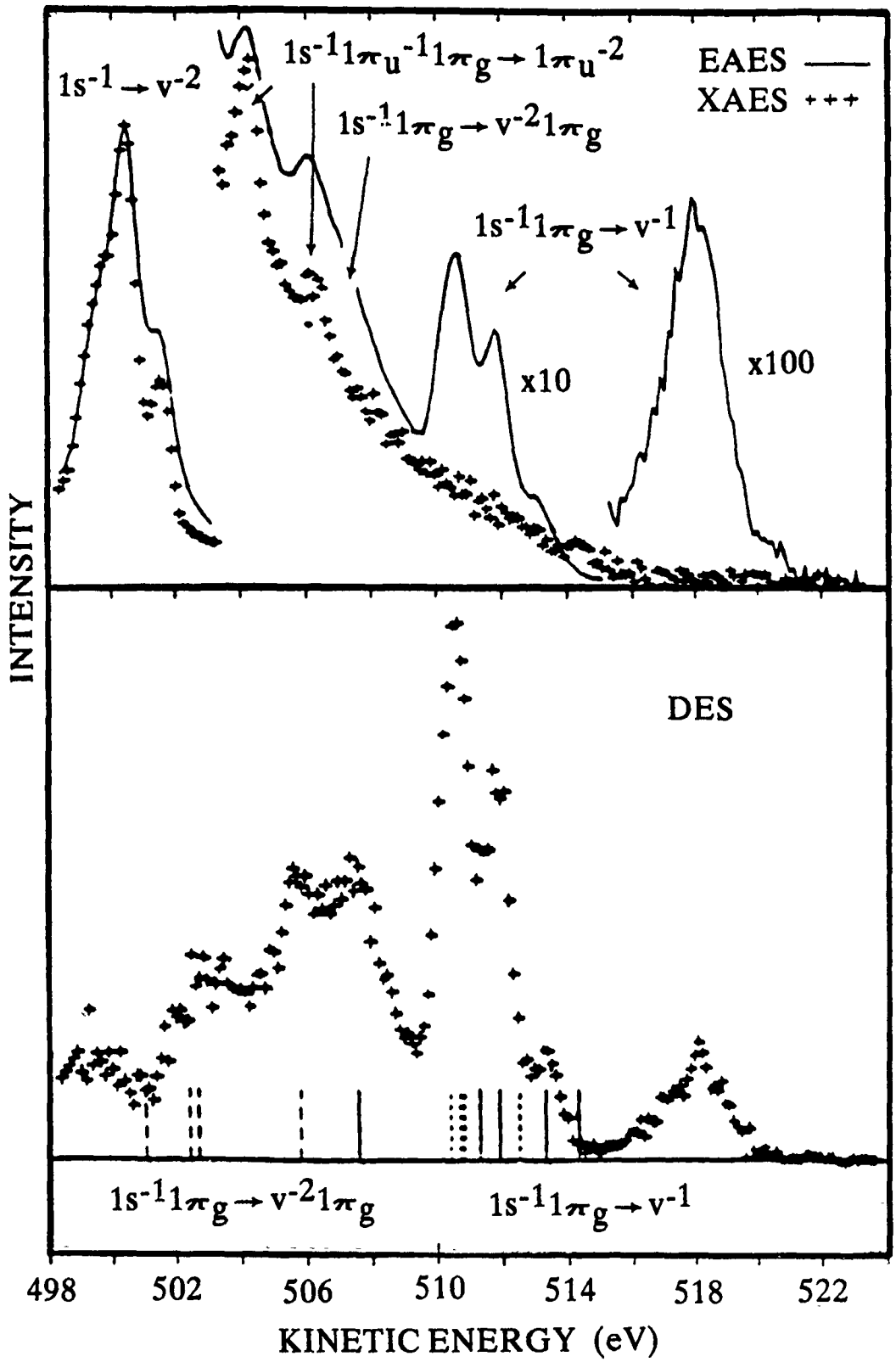
$1s^{-1} \rightarrow v^{-2}$
$1s^{-1}1\pi_u^{-1}1\pi_g \rightarrow 1\pi_u^{-2}$
$1s^{-1}1\pi_g \rightarrow v^{-2}1\pi_g$
$1s^{-1}1\pi_g \rightarrow v^{-1}$
EAES
XAES
x10
x100
DES
INTENSITY
$1s^{-1}1\pi_g \rightarrow v^{-2}1\pi_g$
$1s^{-1}1\pi_g \rightarrow v^{-1}$
498
502
506
510
514
518
522
KINETIC ENERGY (eV)

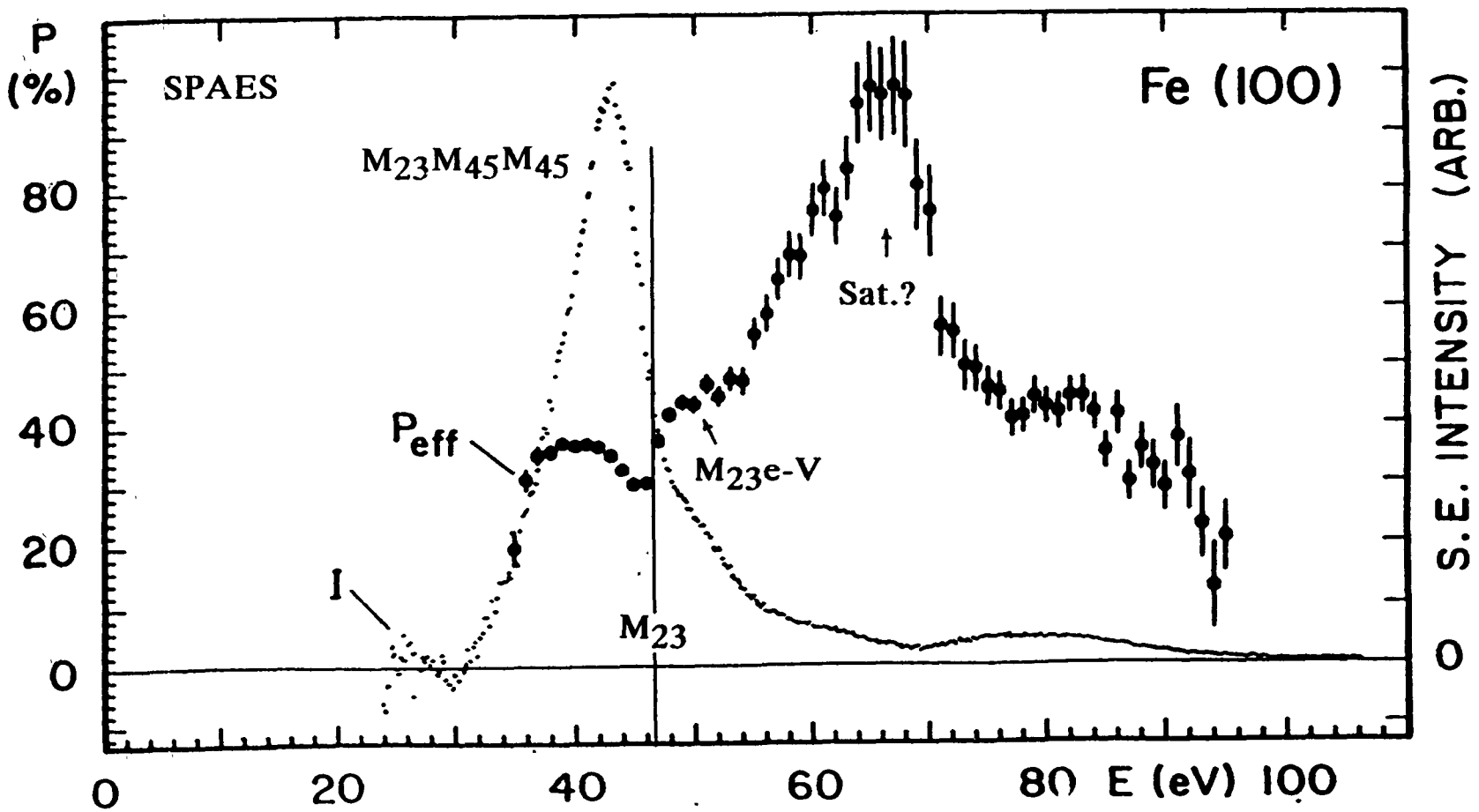
P
(%)
SPAES
Fe (100)
$M_{23}M_{45}M_{45}$
80
60
40
20
0
P_{eff}
I
M_{23}
M_{23}e-V
Sat.?
0
S.E. INTENSITY (ARB.)
0
20
40
60
80
E (eV)
100

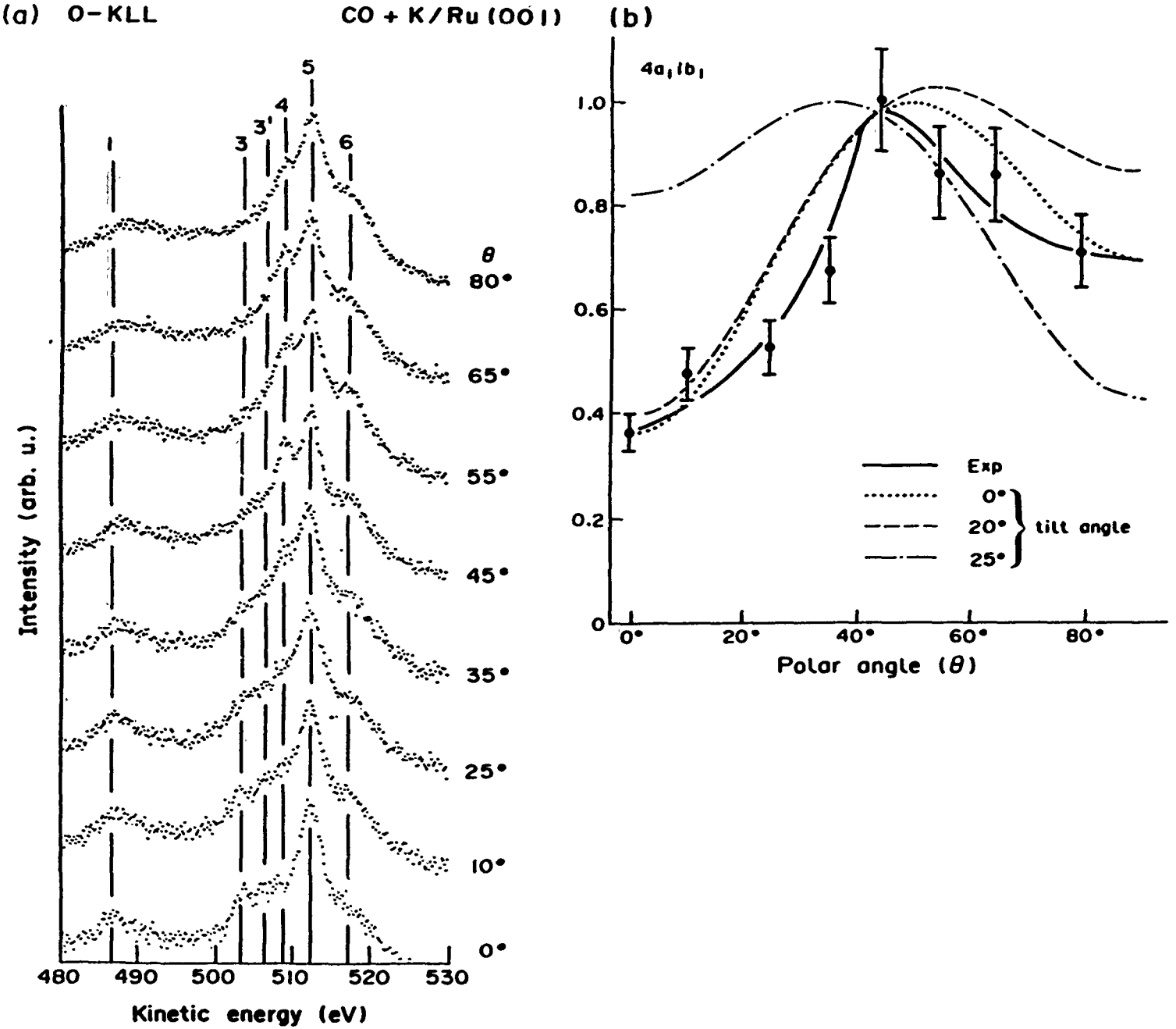
(a) O-KLL
CO + K/Ru(001)
(b)
1
3
3'
4
5
6
θ
80°
65°
55°
45°
35°
25°
10°
0°
Intensity (arb. u.)
480
490
500
510
520
530
Kinetic energy (eV)
4a1 1b1
1.0
0.8
0.6
0.4
0.2
0
0°
20°
40°
60°
80°
Polar angle (θ)
Exp
0°
20°
25°
tilt angle

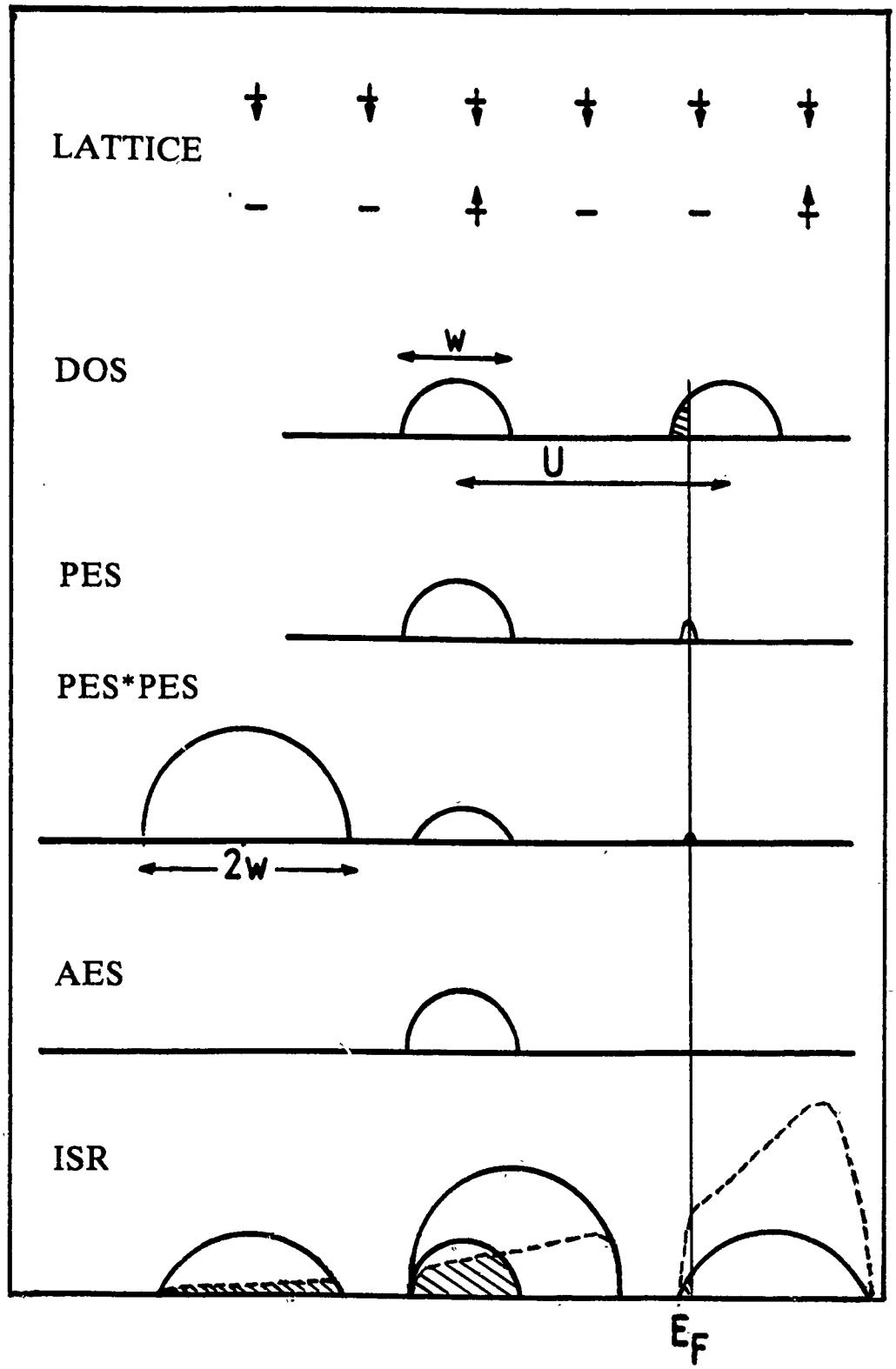
LATTICE
DOS
W
U
PES
PES*PES
2W
AES
ISR
E_F

FS Rule

(Band > 1/2 filled)

IS Rule

(Band ≤ 1/2 filled)

N(E)

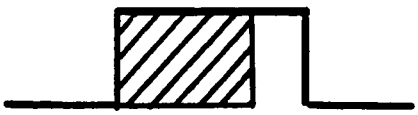

N * N

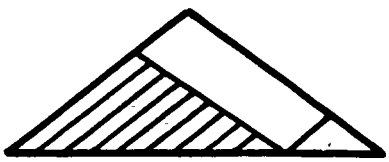

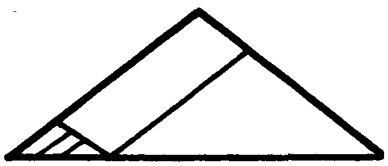

C(N * N)

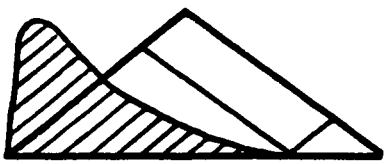

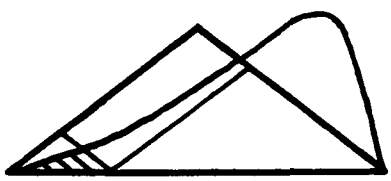

U > 0

U < 0

TECHNICAL REPORT DISTRIBUTION LIST - GENERAL

Office of Naval Research (2)
Chemistry Division, Code 1113
800 North Quincy Street
Arlington, Virginia 22217-5000

Commanding Officer (1)
Naval Weapons Support Center
Dr. Bernard E. Douda
Crane, Indiana 47522-5050

Dr. Richard W. Drisko (1)
Naval Civil Engineering Laboratory
Code L52
Port Hueneme, CA 93043

David Taylor Research Center (1)
Dr. Eugene C. Fischer
Annapolis, MD 21402-5067

Dr. James S. Murday (1)
Chemistry Division, Code 6100
Naval Research Laboratory
Washington, D.C. 20375-5000

Dr. Robert Green, Director (1)
Chemistry Division, Code 385
Naval Weapons Center
China Lake, CA 93555-6001

Chief of Naval Research (1)
Special Assistant for Marine Corps Matters
Code 00MC
800 North Quincy Street
Arlington, VA 22217-5000

Dr. Bernadette Eichinger (1)
Naval Ship Systems Engineering Station
Code 053
Philadelphia Naval Base
Philadelphia, PA 19112

Dr. Sachio Yamamoto (1)
Naval Ocean Systems Center
Code 52
San Diego, CA 92152-5000

Dr. Harold H. Singerman (1)
David Taylor Research Center
Code 283
Annapolis, MD 21402-5067

Defense Technical Information Center
Building 5, Cameron Station
Alexandria, VA 22314

ENCLOSURE(2)

FY90 Abstracts Distribution List for Solid State & Surface Chemistry

Professor John Baldeschwieler
Department of Chemistry
California Inst. of Technology
Pasadena, CA 91125

Professor Paul Barbara
Department of Chemistry
University of Minnesota
Minneapolis, MN 55455-0431

Dr. Duncan Brown
Advanced Technology Materials
520-B Danury Rd.
New Milford, CT 06776

Professor Stanley Bruckenstein
Department of Chemistry
State University of New York
Buffalo, NY 14214

Professor Carolyn Cassady
Department of Chemistry
Miami University
Oxford, OH 45056

Professor R.P.H. Chang
Dept. Matls. Sci. & Engineering
Northwestern University
Evanston, IL 60208

Professor Frank DiSalvo
Department of Chemistry
Cornell University
Ithaca, NY 14853

Dr. James Duncan
Federal Systems Division
Eastman Kodak Company
Rochester, NY 14650-2156

Professor Arthur Ellis
Department of Chemistry
University of Wisconsin
Madison, WI 53706

Professor Mustafa El-Sayed
Department of Chemistry
University of California
Los Angeles, CA 90024

Professor John Eyler
Department of Chemistry
University of Florida
Gainesville, FL 32611

Professor James Garvey
Department of Chemistry
State University of New York
Buffalo, NY 14214

Professor Steven George
Department of Chemistry
Stanford University
Stanford, CA 94305

Professor Tom George
Dept. of Chemistry & Physics
State University of New York
Buffalo, NY 14260

Dr. Robert Hamers
IBM T.J. Watson Research Center
P.O. Box 218
Yorktown Heights, NY 10598

Professor Paul Hansma
Department of Physics
University of California
Santa Barbara, CA 93106

Professor Charles Harris
Department of Chemistry
University of California
Berkeley, CA 94720

Professor John Hemminger
Department of Chemistry
University of California
Irvine, CA 92717

Professor Roald Hoffmann
Department of Chemistry
Cornell University
Ithaca, NY 14853

Professor Leonard Interrante
Department of Chemistry
Rensselaer Polytechnic Institute
Troy, NY 12181

Professor Eugene Irene
Department of Chemistry
University of North Carolina
Chapel Hill, NC 27514

Dr. Sylvia Johnson
SRI International
333 Ravenswood Avenue
Menlo Park, CA 94025

Dr. Zakya Kafafi
Code 6551
Naval Research Laboratory
Washington, DC 20375-5000

Professor Larry Kesmodel
Department of Physics
Indiana University
Bloomington, IN 47403

Professor Max Lagally
Dept. Metal. & Min. Engineering
University of Wisconsin
Madison, WI 53706

Dr. Stephen Lieberman
Code 522
Naval Ocean Systems Center
San Diego, CA 92152

Professor M.C. Lin
Department of Chemistry
Emory Univer[illegible]y
Atlanta, GA [illegible]

Professor Fred McLafferty
Department of Chemistry
Cornell University
Ithaca, NY 14853-1301

Professor Horia Metiu
Department of Chemistry
University of California
Santa Barbara, CA 93106

Professor Larry Miller
Department of Chemistry
University of Minnesota
Minneapolis, MN 55455-0431

Professor George Morrison
Department of Chemistry
Cornell University
Ithaca, NY 14853

Professor Daniel Neumark
Department of Chemistry
University of California
Berkeley, CA 94720

Professor David Ramaker
Department of Chemistry
George Washington University
Washington, DC 20052

Dr. Gary Rubloff
IBM T.J. Watson Research Center
P.O. Box 218
Yorktown Heights, NY 10598

Professor Richard Smalley
Department of Chemistry
Rice University
P.O. Box 1892
Houston, TX 77251

Professor Gerald Stringfellow
Dept. of Matls. Sci. & Engineering
University of Utah
Salt Lake City, UT 84112

Professor Galen Stucky
Department of Chemistry
University of California
Santa Barbara, CA 93106

Professor H. Tachikawa
Department of Chemistry
Jackson State University
Jackson, MI 39217-0510

Professor William Unertl
Lab. for Surface Sci. & Technology
University of Maine
Orono, ME 04469

Dr. Terrell Vanderah
Code 3854
Naval Weapons Center
China Lake, CA 93555

Professor John Weaver
Dept. of Chem. & Mat. Sciences
University of Minnesota
Minneapolis, MN 55455

Professor Brad Weiner
Department of Chemistry
University of Puerto Rico
Rio Piedras, Puerto Rico 00931

Professor Robert Whetten
Department of Chemistry
University of California
Los Angeles, CA 90024

Professor R. Stanley Williams
Department of Chemistry
University of California
Los Angeles, CA 90024

Professor Nicholas Winograd
Department of Chemistry
Pennsylvania State University
University Park, PA 16802

Professor Aaron Wold
Department of Chemistry
Brown University
Providence, RI 02912

Professor Vicki Wysocki
Department of Chemistry
Virginia Commonwealth University
Richmond, VA 23284-2006

Professor John Yates
Department of Chemistry
University of Pittsburgh
Pittsburgh, PA 15260